Thalamocortical Circuits and Visuospatial Attention

Submitted by Fang-Chi Yang

May, 2017

In fulfillment of the requirement for a Dissertation
In the Psychology Graduate Program
Brown University
Department of Cognitive, Linguistic, and Psychological Sciences

| | |
|---|---|
| Advisor: | Dr. Rebecca Burwell |
| Dissertation Committee: | Dr. Dima Amso |
| | Dr. Michael Frank |

This dissertation by Fang-Chi Yang is accepted in its present form
by the Department of Cognitive, Linguistic, and Psychological Sciences
as satisfying the dissertation requirement for the degree of Doctor of Philosophy.

Date_____ _____
Dr. Rebecca Burwell, Advisor

Recommended to the Graduate Council

Date_____ _____
Dr. Dima Amso, Reader

Date_____ _____
Dr. Michael Frank, Reader

Approved by the Graduate Council

Date_____ _____
Dr. Andrew Campbell, Dean of the Graduate School

**Fang-Chi Yang**
Curriculum Vitae

Brown University
Department of Cognitive, Linguistic & Psychological Sciences
Providence, RI, 02912
fang-chi_yang@brown.edu

## EDUCATION

Ph.D. Brown University, Providence, Rhode Island, 2016, Psychology Program,
Thesis title: Thalamocortical Circuits and Visuospatial Attention

M.S., Brown University, Providence, Rhode Island, 2012, Psychology Program,
Thesis title: Neuronal activity in the posterior parietal cortex during performance on a visuospatial attention task

M.A., National Taiwan University, Taipei, Taiwan, 2007, Psychology Program
Thesis title: Interaction among the hippocampus, medial prefrontal cortex and nucleus accumbens during formation of affective memory in two different tasks

B.S., National Chengchi University, Taipei, Taiwan, 2005, Psychology

## HONORS AND AWARDS

| | |
|---|---|
| 2003 | College Student Research Project Fellowship, National Science Council, Taiwan (R.O.C.) |
| 2013 Fall | BIBS Graduate Research Fellowship |
| 2015 Spring | BIBS Graduate Research Fellowship |

## PUBLICATIONS

**Yang, F-C.,** & Liang, K. C. (2014). Interactions of the dorsal hippocampus, medial prefrontal cortex and nucleus accumbens in formation of fear memory: Difference in inhibitory avoidance learning and contextual fear conditioning. *Neurobiology of Learning and Memory,* 112, 186-194.

Jacobson, T. K., Ho, J. W., Kent, B. W., **Yang, F-C**, Burwell R. D. (2014). Automated visual cognitive tasks for recording neural activity using a Floor Projection Maze, J. Vis. Exp., 84, e51316.

**Yang, F-C.,** Jacobson, T. K., Burwell, R. D. (under revision). Posterior parietal cells signal stimulus onset, spatial locations, and behavioral outcome during performance on a visuospatial attention task.

**Yang F-C,** Dokovna L.B., and Burwell R.D. (in preparation). Connections of the lateral posterior nucleus with the posterior parietal and postrhinal cortices in the rat.

## CONFERENCE PRESENTATIONS

**Yang, F. C.** & Burwell, R. D. (2015). Neuronal correlates in rat posterior parietal cortex and the lateral posterior thalamic nucleus during performance on a visuospatial attention task. *Society for Neuroscience,* Chicago, Poster session.

**Yang, F. C.** & Burwell, R. D. (2015). Neuronal correlates in rat posterior parietal cortex and the lateral posterior thalamic nucleus during performance on a visuospatial attention task. *The 38th Annual Meeting of the Japan Neuroscience Society,* Kobe, Japan, Poster session.

**Yang, F. C.,** Jacobson, T. K., & Burwell, R. D. (2014). Neuronal correlates in rat posterior parietal cortex and the lateral posterior thalamic nucleus during performance on a visuospatial attention task. *Society for Neuroscience*, DC, Poster session.

**Yang, F. C.,** Jacobson, T. K., & Burwell, R. D. (2013). Local field potential oscillations in rat posterior parietal cortex during performance on a visuospatial attention task. *Society for Neuroscience,* San Diego, Poster session.

**Yang, F. C.,** Jacobson, T. K., & Burwell, R. D. (2012). Neuronal correlates in the posterior parietal cortex during performance on a visuospatial attention task. *Society for Neuroscience,* New Orleans. Poster session.

Liao, R. M., Shen, Y. L., Chang, T. Y., Tien, H. H., **Yang, F. C.,** Chang, C. W., & Wang, P. Y. (2012). Expressions Of Bdnf in medial prefrontal cortex and the reinstatement of amphetamine induced conditioned place preference in the rat. *Forum of Neuroscience*. Poster session.

**Yang, F. C.** & Burwell, R. D. (2011). Neuronal correlates in the posterior parietal cortex during performance on a visuospatial attention task. *Society for Neuroscience*, DC. Poster session.

Liao, R.M., Chang Y. C., **Yang, F. C.,** & Shen, Y. L. (2011). Priming effects of dopamine D1 receptor agonist on the reinstatement of amphetamine induced conditioned placed preference. *Conference of the College on Problems of Drug Dependence,* Hollywood, FL. Poster session.

**Yang, F. C.,** & Liao, R. M. (2009). Adenosine receptor agonists infused into striatal subareas blocking the expression of conditioned place preference induced by amphetamine. *Society for Neuroscience*, Chicago, IL. Poster session.

Chiang, Y. H., Cheng, S. J., **Yang, F. C.,** Min, M. Y., Wen, C. C., Hwu, H. G., & Fu, W. M. (2009). Role of schizophrenia-related gene of neuregulin 1 in fear memory and depression. *Society for Neuroscience*, Chicago, IL. Poster session.

**Yang, F. C.,** & Liang, K. C. (2007). Posttraining intra-accumbal administration of lidocaine attenuated memory enhancing effects of norepinephrine infused into the hippocampus or medial prefrontal cortex in an inhibitory avoidance task. *Society for Neuroscience,* San Diego, CA. Poster session.

Liang, K. C., **Yang, F. C.,** & Chang, S. D. (2007). Posttraining infusion of norepinephrine modulated memory in contextual fear conditioning: Interaction between the dorsal hippocampus and medial prefrontal cortex. *Society for Neuroscience,* San Diego, CA. Poster session.

**Yang, F. C.,** & Liang, K. C. (2007). Suppressing the nucleus accumbens blocked memory enhancing effects of norepinephrine infused into the dorsal hippocampus or medial prefrontal cortex in an inhibitory avoidance task. *47th Taiwan Psychology Association annual Conference.* Poster session.

**Yang, F. C.,** Chen, D. Y., & Liang, K. C. (2006). Interaction between the medial prefrontal cortex and hippocampus on formation of affective memory in various tasks. *46th Taiwan Psychology Association annual Conference.* Poster session.

**Yang, F. C.,** & Liang, K. C. (2005). Lidocaine suppression of the medial prefrontal cortex blocked the enhancing effect of posttraining intra-hippocampal infusion of norepinephrine on retention of an inhibitory avoidance task. *45th Taiwan Psychology Association annual Conference.* Poster session.

## PREFACE

The guiding hypothesis for this body of work is that the PPC integrates sensory information from visual and somatosensory areas in order to plan appropriate actions. Such actions are modulated by attentional demands communicated to the PPC through its connections with the pulvinar in the primate brain and the lateral posterior nucleus of the thalamus in the rodent brain. I addressed this hypothesis using anatomical, behavioral, and electrophysiological techniques combined with optogenetic manipulation in a rodent behavioral model of visuospatial attention.

I first developed a novel behavioral task, the Visuospatial Attention (VSA) task, in which stimuli are limited to the visual and spatial domains. This task allows assessment of visuospatial attention and action selection. Versions of this task were used for the three electrophysiological studies. In the first study, I recorded single unit and local field potential activity in the dorsal limb of the PPC during performance on the VSA task. This experiment revealed cellular correlates of attention and action selection. In the second study, I inspected anatomical connections of the dorsal and caudal PPC with the LPO and the postrhinal cortex. This experiment showed that rodent-primate connectional homology of the PPC extends to the dorsal and caudal PPC subdivisions in the rat. In the third study, I simultaneously recorded different subdivisions of the rat PPC including both dorsal and caudal limbs as well as the LPO. This study addressed the question of whether the connectional homology across PPC subdivisions extends to the functions of the subdivisions. In the fourth and final study, I combined the electrophysiology and optogenetic manipulations to examine the influence of the LPO

input on the dorsal and caudal PPC. This final study provided additional evidence that these three regions are part of a functional circuit.

This series of studies advances our basic understanding of the role of the posterior parietal cortex in the circuitry that supports visuospatial attention and visually guided behavior and cognition. These studies further developed the rodent model of attention by elucidating the contributions of the caudal posterior parietal cortex and its role in these circuits. Finally, a more complete rodent model will be advantageous for understanding and treating human disorders relevant to the PPC, such as attention deficit disorder, hemispatial neglect, and attentional alterations in various mental disorders.

# Table of Contents

# List of Tables

**Table** **Pages**

# List of Figures

**Figure** **Pages**

**CHAPTER 4**



**CHAPTER 5**

**CHAPTER 6**

# CHAPTER 1

# INTRODUCTION

The posterior parietal cortex has been identified and anatomically described in primates and non-primate animals (Cavada & Goldman-Rakic, 1989a, 1989b; Kolb & Walkey, 1987; Krieg, 1946; Reep, Chandler, King, & Corwin, 1994). Early studies reported that patients with parietal injury often have visual neglect, which is considered to be an attention deficit (Mesulam, 1981; Posner, Walker, Friedrich, & Rafal, 1984). Consistent with this view, experimental lesion studies in animals implicate the region in spatial memory and visual attention (Crowne, Richardson, & Dawson, 1986; Gaffan & Hornak, 1997; King & Corwin, 1993). These findings show the importance of the PPC in visual perception, but there are open questions about the function of PPC and how it interacts with other brain structures to support memory.

The PPC is located between somatosensory cortex and visual cortex in both the monkey and the rat. As might be expected based on its proximity to occipital cortex, the PPC receives heavy inputs from visual areas (Cavada & Goldman-Rakic, 1989a; Kolb & Walkey, 1987). In monkey and rat, the PPC reciprocally connects with widespread areas of the visual cortex. The connection between visual cortex and the PPC is a part of the dorsal stream, a pathway that contributes to processing of visuospatial information as well as processing visual information for guiding movements in space (Goodale & Milner, 1992).

Another corticocortical connection of the PPC identified in monkey is the parahippocampal cortex (Cavada & Goldman-Rakic, 1989b). The rodent connectional and functional homologue of the parahippocampal cortex, the postrhinal cortex, also reciprocally connects with the PPC (Burwell & Amaral, 1998). There is evidence that the parahippocampal cortex and the postrhinal cortex contribute to both attention and to

representing context or contextual associations (Bar, Aminoff, & Schacter, 2008; Bucci, Phillips, & Burwell, 2000; Yi & Chun, 2005). The attentional and context processing functions of the parahippocampal/postrhinal cortex may depend on inputs from the PPC.

The anatomical location and neuronal connections of the PPC spawned research addressing its possible roles in a variety of behavioral functions, including visual perception as well as spatial learning, memory, and attention (Andersen, Snyder, Bradley, & Xing, 1997; Bucci, 2009; Calton & Taube, 2009; Ciaramelli, Grady, & Moscovitch, 2008; Kesner, 2009; Reep & Corwin, 2009). Although, it is clear that the PPC has some role in a variety of cognitive and behavioral functions, there is no agreement as to the core function of the PPC in processing visual and spatial information. In this thesis, I combine anatomical, behavioral, electrophysiological, and optogenetic methods in an animal model to address questions about the core function of the PPC.

The first part of this chapter reviews the anatomy of the PPC in human and other mammals, and evaluates the case for anatomical homology of the PPC between primates and rodents. The second part reviews the functions of this brain region including behavioral, imaging and electrophysiological studies in primates and rodents. At the end of this chapter presents the guiding hypotheses and approaches employed in each of a series of experiments designed to elucidate the function of PPC.

## The comparative anatomy of the posterior parietal cortex

According to Campbell and Hodos' criteria for inferring the homology of brain regions across species (Campbell & Hodos, 1970), there are several useful indexes. These indexes include neuronal connections, topology, topography, the location of sulci,

embryology, morphology of neurons, histochemistry, electrophysiology, and behavioral evidence. The more consistency among these indexes across species, the stronger homology exists in corresponding areas. Using these criteria, studies of the PPC in primates and rodents indicate strong homology of this area across species. This section will review evidence for homology based on neuronal connections and topology. The electrophysiological and behavioral evidence will be addressed in the following sections.

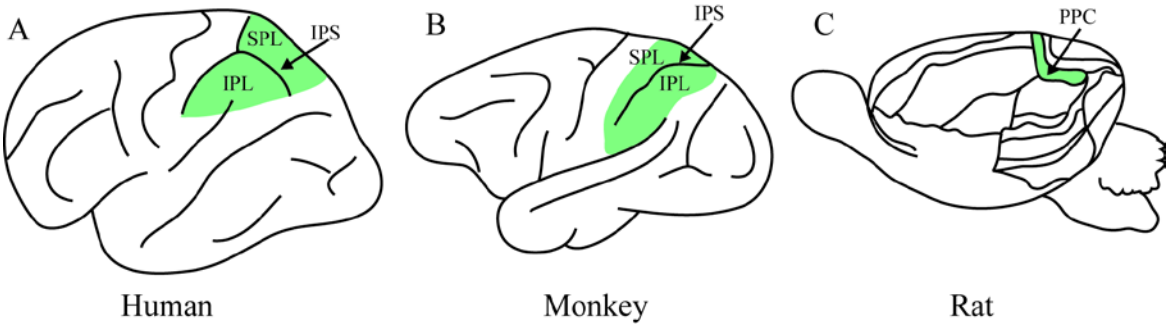


Figure 1. Surface views of brains showing the location of the posterior parietal cortex. A. The posterior parietal cortex (PPC) of human. The human PPC is divided by the intraparietal sulcus (IPS) into two parts: the superior parietal lobe (SPL) and the inferior parietal lobe (IPL). B. The PPC of monkey. The monkey PPC is also divided into SPL and IPL by IPS. C. The PPC of rat. Adapted from Husain & Nachev (2007) and Burwell (2001).

In humans, the PPC is traditionally divided by the intraparietal sulcus (IPS) into two parts: the superior parietal lobe (SPL) and inferior parietal lobe (IPL, Figure 1A). The SPL is usually considered to be Brodmann areas (BAs) 5 and 7 and locates in the upper part of the IPS (Cabeza, Ciaramelli, Olson, and Moscovitch, 2008). The IPL includes BAs 39 and 40, and lies in the lower portion of the IPS. Studies show that damage to the PPC in human causes visual neglect and other attention deficits (Corbetta, Kincade, Ollinger, McAvoy, & Shulman, 2000; Driver & Mattingley, 1998). Although anatomical evidence from humans is limited, available studies show that the human posterior parietal cortex has functionally important connections with other cortical regions, as well as the pulvinar nucleus of thalamus (Behrens et al., 2003; Kahn,

Andrews-Hanna, Vincent, Snyder, & Buckner, 2008; Mars et al., 2011). The most detailed anatomical knowledge of the primate PPC mainly comes from monkey studies. Although the PPC is thought to be more specialized in humans than nonhuman primates, the anatomy and physiology of this region in human and other primates are similar.

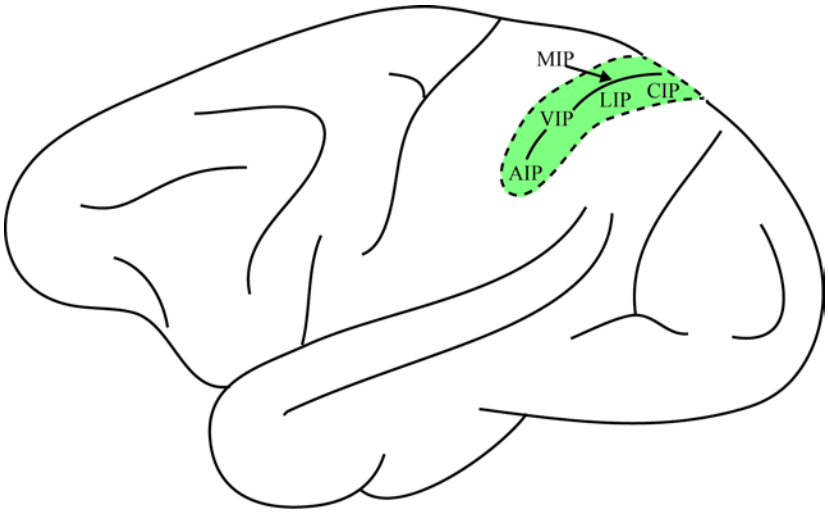


Figure 2. A monkey brain showing the intraparietal sulcus (IPS) opened up. The IPS is divided into five areas: the anterior intraparietal area (area AIP), the caudal intraparietal area (area CIP), the ventral intraparietal area (area VIP), the medial intraparietal area (area MIP), and the lateral intraparietal area (area LIP). This figure is adapted from Grefkes and Flink (2005).

As in the human brain, the monkey PPC is divided into SPL and IPL by the IPS (Figure 1B). The SPL and IPL correspond to BA 5 and BA 7, respectively. According to the nomenclature of Brodmann (Brodmann, 1909), Vogts (1919) first divided BA 5 and BA 7 into areas 5a, 5b, 7a and 7b, which correspond to areas PE, PG and PF of Von Bonin and Bailey's nomenclature (Cavada & Goldman-Rakic, 1989a; Hyvarinen, 1982; Vogt & Vogt, 1919; Von Bonin & Bailey, 1947). As shown in Figure 2, the monkey IPS has also been subdivided based on location into the anterior intraparietal area (area AIP), the caudal intraparietal area (area CIP), the ventral intraparietal area (area VIP), the

medial intraparietal area (area MIP), and the lateral intraparietal area (area LIP) (Grefkes & Fink, 2005).

The similarity of anatomical divisions of the PPC across human and monkey suggests that the behavioral functions could also be similar. In fact, many studies in monkeys have shown that the monkey PPC, like the human PPC, is involved in aspects of visual attention. For example, the AIP is involved in visually guided grasping movements (Sakata, Taira, Murata, & Mine, 1995). CIP neurons selectively respond to orientation of three dimensional surface representations (Taira, Tsutsui, Jiang, Yara, & Sakata, 2000). The VIP is involved in the direction of self-movement and object movement (Colby, Duhamel, & Goldberg, 1993). The MIP is associated with the coordination of movements and visual target (Eskandar & Assad, 1999). Finally, the LIP is preferentially active during signal detection and planned movement (Andersen & Buneo, 2002; Colby & Duhamel, 1996). These studies suggest there may be functional differentiation within the PPC; however, it is difficult to make this interpretation because few studies examine multiple areas using the same tasks and methods.

Anatomical studies of the PPC provide additional clues about its functions. For the cortical connections, the PPC receives inputs from visual cortex and somatosensory cortex (Cavada & Goldman-Rakic, 1989a, 1989b). These connections would be important for the translation of visual information into actions. The PPC also has reciprocal connections with prefrontal cortex and parahippocampal cortex (Cavada & Goldman-Rakic, 1989b). The parahippocampal cortex is important for contextual-related memory processes (Bar et al., 2008). Based on the anatomy, the parietal input could support parahippocampal contextual functions by providing visuospatial input.

Importantly, the predominant thalamic input to the PPC arises in the pulvinar nucleus of thalamus (Baleydier & Mauguiere, 1977; Baleydier & Mauguiere, 1987). The pulvinar nucleus is strongly implicated in visuospatial attention (Petersen, Robinson, & Morris, 1987; Saalmann, Pinsk, Wang, Li, & Kastner, 2012; Zhou, Schafer, & Desimone, 2016), but how the pulvinar connections support the functions of the PPC remains unclear. Although there are more than 35 anatomical studies of the primate PPC and pulvinar, to our knowledge there are only five functional studies, one monkey electrophysiology study and four human imaging studies. Clearly, more studies addressing the circuits in which the PPC participates.

A number of studies have provided evidence for a rodent homolog of the primate PPC (Kolb & Walkey, 1987; Reep et al., 1994; Reep & Corwin, 2009). The location and neuronal connections of this area in rodents are similar to those in primates. As in the primate brain, the PPC in the rat is located between somatosensory cortex and visual cortex (Figure 1C). The range of this cortical area is about 3.5-5.0 mm caudal to bregma and 1.5-5.0 mm lateral from the midline. The definition of the rat PPC was based on studies of its thalamic inputs from the lateral dorsal (LD) and lateral posterior (LPO) nuclei of the thalamus (Chandler, King, Corwin, & Reep, 1992; Reep et al., 1994). The LPO is thought to be the functional homolog of the primate pulvinar (Kamishina, Conte, Patel, Tai, Corwin, & Reep, 2009). Taken together, the connectional evidence provides a good case that the rodent PPC can provide a strong experimental model for understanding the functions of the primate PPC.

One issue with the rodent studies is that they largely focused on the part of the PPC that lies on the dorsal surface of the rat brain (Paxinos and Watson, 2005). There is

good evidence that the posterior border of the rat PPC extends farther laterally and caudally than previously thought (Agster & Burwell, 2009; Hughes, 1977; Olsen & Witter, 2016; Swanson, 1992). To our knowledge, there is not a single lesion or electrophysiology that included the caudal limb of the rat PPC.

The cortical connections of the PPC in the rat include the somatosensory, visual, postrhinal and prefrontal cortices (Agster & Burwell, 2009; Burwell & Amaral, 1998; Reep et al., 1994). Inputs from somatosensory cortex and visual cortex provide major sensory sources for the PPC. The connections between PPC and postrhinal cortex have also been described in anatomical studies (Agster & Burwell, 2009; Burwell & Amaral, 1998). All portions of the PPC project to the postrhinal cortex. The interesting finding of these studies is that the caudal limb of the PPC provides a sizeable projection to the postrhinal cortex. There is a topography such that the rostrodorsal part of the PPC is interconnected with the rostral postrhinal cortex, whereas the caudal part of the PPC connects with the caudal postrhinal cortex. It is possible that the PPC input to the postrhinal cortex supports a role for the postrhinal cortex in attentional monitoring of the current environmental context for changes.

The prefrontal connections with the PPC in rat are also well described (Reep et al., 1994). Numerous cells in the ventrolateral and medial orbital frontal areas were labeled when rats received injections of fluorescent tracers into the PPC. The AGm was also densely labeled. The AGm (area Fr2) receives heavy thalamic input from mediodorsal nucleus (MD), which is similar to the thalamice input of the dorsolateral prefrontal cortex (DLPFC) in monkeys. Although it is still an issue, the AGm has been proposed to be a

functional homologue area of the DLPFC in primates because of the similar MD inputs in the AGm and DLPFC (Uylings & van Eden, 1991).

Based on Campbell and Hodos' (1970) criteria for anatomical homology, the above evidence suggested strong homology of the PPC between primates and rodents. First, in both primate and rodent, the PPC is located between the somatosensory cortex and visual cortex in the brain. Second, the PPC in primates and rodents shares similar neuronal connections. In primates, the PPC receives heavy inputs from visual areas and pulvinar nucleus. It has reciprocal connections with the parahippocampal cortex and prefrontal regions. In rodents, the PPC obtains projections from visual areas and LPO, and connects with the postrhinal cortex and prefrontal regions. The LPO and postrhinal cortex in rodents are homologous areas of the pulvinar nucleus and parahippocampal cortex in primates.

## Visual processing for perception and action

In the 1990s, Goodale and Milner proposed that there are two separate pathways or information processing streams for visual information in the cerebral cortex (Goodale & Milner, 1992). The ventral stream originates from the primary visual cortex to the inferior temporal cortex. This pathway has been considered to represent visual information for identification or recognition and has known as a "What" pathway. The dorsal stream includes a dual pathway for visual information, one cortical and one subcortical. The cortical pathway visual cortical areas, but the subcortical pathway includes pulvinar nucleus input to the PPC. The dorsal stream was thought to be specialized for identifying where things are and was termed the "Where" pathway. Twelve years later, Goodale & Westwood (2004) proposed a reconceptualization of the functions of the ventral and

dorsal visual streams. By that view the ventral stream processes information for perception, and the dorsal stream processes visual information for guiding actions. Since this new conceptualization, the PPC has become an important cortical area for studying visually guided actions. It is surprising that there are so few studies addressing the functional implications of of the primate pulvinar and the rodent LPO input to the PPC.

A recent study further identified the dorsal stream as having three subpathways to contribute to visuospatial processing, which originate from the PPC. They include a parieto-prefrontal pathway, a parieto-premotor pathway, and a parieto-medial temporal lobe (MTL) pathway (reviewed in Kravitz, Saleem, Baker, and Mishkin, 2011). These three pathways have different anatomical connections and are thought to support different behavioral functions. The parieto-prefrontal pathway connects the parietal cortex and the prefrontal regions including BAs 8A and 46. This pathway is important for spatial working memory and control of eye movements. The parieto-premotor pathway links the parietal cortex and the premotor area. This pathway includes two parallel projections: the MIP projects to the dorsal premotor area and the VIP projects to the ventral premotor area. The MIP and VIP modulate responses based on the relative position of visual stimuli and the body, so the parieto-premotor pathway is involved in visually guided movements in peripersonal space.

The parieto-MTL pathway, the most complex one of the three pathways, connects the parietal cortex and the MTL through direct and indirect connections. Three direct projections from the PPC target the CA1 and subiculum, the pre-and parasubicular areas, and the parahippocampal cortex (areas TF and TH) in primates (postrhinal cortex in rodents). A set of indirect efferents connects the parietal cortex and the MTL through

retrosplenial cortex and posterior cingulate cortex. These two areas receive inputs from the PPC and project heavily to the presubiculum, parasubiculum, and parahippocampal cortex, which are subregions in the MTL. These subregions are involved in spatial information processing, including navigation. Taken together, the PPC is in good position to provide visuospatial information to other cortical areas for complex cognitive processing (Kravitz, Saleem, Baker, & Mishkin, 2011).

Studies using fMRI and electroencephalogram (EEG) found that the human PPC is activated during behaviors and tasks that require visuospatial attention. By using fMRI, Corbetta and his colleagues reported that different subregions of the PPC mediated different phases of attention. In their study, normal human subjects were given a stimulus detection task in which a visual precue indicating the most likely location of target stimuli. IPS activity increased bilaterally before target presentation, whereas the right temporoparietal junction was activated after target detection (Corbetta et al., 2000). Similar facilitation was found when subjects performed visual orienting to task-relevant cues (Corbetta, Kincade, & Shulman, 2002). Also, the IPS activation for target presentation could last through a delayed period when subjects were required to maintain attention (Corbetta et al., 2000). A human EEG study also reported that activity in the PPC changed during attention (Sauseng et al., 2005). Subjects were told to attend visual targets according to a visual cue in the same or different hemifield indicating valid or invalid trials. Event-related potential in the PPC was higher when the trial was valid. Further results showed that the alpha magnitude significantly decreased before visual target representation of invalid trial and this activity would maintain until the end of

target presentation. These findings indicated that the PPC not only participates in the initial phase of attention, but also is involved in maintaining sustained attention.

Available electrophysiological studies in monkeys show that neuronal activity in the PPC changes during task that require visuospatial attention. Early studies reported that posterior parietal activity increased when a monkey attended to a visual stimulus in the receptive field (M. C. Bushnell, Goldberg, & Robinson, 1981; Wurtz, Goldberg, & Robinson, 1980). Another study reported similar increasing activity when attention was overtly directed to a visual target (Robinson, Bowman, & Kertzman, 1995). Findings from Robinson and his colleagues revealed that neuronal activity in the PPC was evoked only when the monkey actively directed foveal attention to a visual target but not in a simple gaze situation. Also, when the monkey attended to a cued visual target, PPC activity was higher if the cue and target were located in different hemifields. In other words, PPC responded more when the monkey needed to shift its attention from one location to another.

These studies described above provide evidence for a role of the primate PPC in visuospatial attention, but strategies for studying detailed neuronal mechanism in primates are limited. One obvious disadvantage of primate studies is that, during attentional tasks, physical movement is generally limited. This is not a limitation of rodent studies in which it is possible to record from freely moving animals. Rodent studies of visuospatial attention have largely employed two tasks: the sustained attention task (SAT) and the five-choice serial reaction time task (5-CSRTT). The SAT was first developed by Bushnell and his colleagues and was modified by McGaughy and Sarter (P. J. Bushnell, Kelly, & Crofton, 1994; McGaughy & Sarter, 1995). In the SAT, visual

signals and blank trials are represented. There are four types of responses in this task: hit or miss in cued trials; correct rejection or false alarm in blank trials. A food reward follows after correct responses, and nothing happens after incorrect responses. Neuronal activity in rat PPC was observed to increase during detection of visual cues in a modified SAT (Broussard, Karelina, Sarter, & Givens, 2009; Broussard, Sarter, & Givens, 2006). Changes in low frequency oscillations in rat PPC were also observed in the same task (Broussard & Givens, 2010). The 5-CSRTT, was developed from the Continuous Performance task for humans (Rosvold, Mirsky, Sarason, Bransome, & Beck, 1956). In this task, animals are trained to monitor five locations with cued light in the operant chamber and respond with a nose-poking response. A food reward would be delivered after choosing correct location (Carli, Robbins, Evenden, & Everitt, 1983). Currently, there are no studies of single unit recording in the PPC reported with this behavioral paradigm. It should be noted that the vast majority of these studies using these tasks are experimental lesion studies. Only a few electrophysiological studies have examined the role of the rat PPC in visuospatial attention (Nitz, 2012; Whitlock, 2014; Wilber, Clark, Forster, Tatsuno, & McNaughton, 2014). Notably, all of these studies focused on the dorsal limb of the PPC.

A final issue with the available rodent literature on visuospatial attention is that the SAT and 5-CSRTT behavioral paradigms are employed in the operant chambers in which animals likely rely on multiple sensory modalities. Ideally, a task for examining the role of the rat PPC in visuospatial attention would require processing of information restricted to the visual and spatial domains.

## Conclusion

This review of existing evidence reveals several important points relevant to this thesis. First, the rodent PPC is a reasonable model of for understanding the functions of the primate PPC. It has already provided substantial insight from experimental lesion studies, but electrophysiological studies can enhance or understanding of how individual neurons contribute to parietal functions. Second, although the rodent PPC has provided a useful model, available studies have largely ignored the caudal limb, which requires further study. In the primate brain there is evidence for functional differentiation in PPC such that there is a subregional dissociation between top-down and bottom-up attention. Whether or not such a dissociation exists in the rat parietal areas is an open question that cannot be addressed without further study of the caudal limb. Third, there are few studies and many open questions about the role of the pulvinar input to the PPC. The rodent model is especially useful for this type of circuit analysis because of the capability for simultaneous multisite recording and for using optogenetics for manipulating circuits. The goal of this thesis is to use tools available in a rodent model of visuospatial attention to increase our understanding of how brain regions interact in the processing of visuospatial information under conditions of high attentional demands.

Our guiding hypothesis is that the PPC integrates sensory information from visual and somatosensory areas in order to plan appropriate actions. Such actions are modulated by attentional demands communicated to the PPC through its connections with the pulvinar/LPO. We addressed this hypothesis using anatomical, behavioral, and electrophysiological techniques combined with optogenetic manipulation in a rodent model.

We first developed a novel behavioral task, the Visuospatial Attention (VSA) task, in which stimuli are limited to the visual and spatial domains. This task allows assessment of visuospatial attention and action selection. Versions of this task were used for the three electrophysiological studies. In the first study, we recorded single unit and local field potential activity in the dorsal limb of the PPC during performance on the VSA task. This experiment revealed cellular correlates of attention and action selection. In the second study, we inspected anatomical connections of the dorsal and caudal PPC with the LPO and the postrhinal cortex. This experiment showed that rodent-primate connectional homology of the PPC extends to the dorsal and caudal PPC subdivisions in the rat. In the third study, we simultaneously recorded different subdivisions of the rat PPC including both dorsal and caudal limbs as well as the LPO. This study addressed the question of whether the connectional homology across PPC subdivisions extends to the functions of the subdivisions. In the fourth and final study, we combined the electrophysiology and optogenetic manipulations to examine the influence of the LPO input on the dorsal and caudal PPC. This study provided evidence that these three regions are part of a functional circuit.

This series of studies advanced our basic understanding the role of the PPC and the circuits that support visuospatial attention attention. In addition, these studies further developed the rodent model of attention by elucidating the contributions of the caudal PPC and its role in these circuits. Finally, a more complete rodent model will be advantageous for understanding and treating human disorders relevant to the PPC, such as attention deficit disorder, hemispatial neglect, and attentional alterations in various mental disorders.

## References


Agster, K. L., & Burwell, R. D. (2009). Cortical efferents of the perirhinal, postrhinal, and entorhinal cortices of the rat. *Hippocampus, 19*(12), 1159-1186. doi:10.1002/hipo.20578

Andersen, R. A., & Buneo, C. A. (2002). *Intentional maps in posterior parietal cortex.* Paper presented at the Annual Review of Neuroscience.

Andersen, R. A., Snyder, L. H., Bradley, D. C., & Xing, J. (1997). Multimodal representation of space in the posterior parietal cortex and its use in planning movements. *Annual Review of Neuroscience, 20*(1), 303-330.

Baleydier, C., & Mauguiere, F. (1977). *Pulvinar-latero posterior afferents to cortical area 7 in monkeys demonstrated by horseradish peroxidase tracing technique.* Paper presented at the Experimental Brain Research.

Baleydier, C., & Mauguiere, F. (1987). Network organization of the connectivity between parietal area 7, posterior cingulate cortex and medial pulvinar nucleus: a double fluorescent tracer study in monkey. *Experimental Brain Research, 66*(2), 385-393.

Bar, M., Aminoff, E., & Schacter, D. L. (2008). Scenes unseen: The parahippocampal cortex intrinsically subserves contextual associations, not scenes or places per se. *Journal of Neuroscience, 28*(34), 8539-8544.

Behrens, T., Johansen-Berg, H., Woolrich, M., Smith, S., Wheeler-Kingshott, C., Boulby, P., . . . Ciccarelli, O. (2003). Non-invasive mapping of connections between human thalamus and cortex using diffusion imaging. *Nature Neuroscience, 6*(7), 750-757.

Brodmann, K. (1909). *Vergleichende Lokalisationslehre der Grosshirnrinde.* Leipzig: Johann Ambrosius Bart.

Broussard, J. I., & Givens, B. (2010). Low frequency oscillations in rat posterior parietal cortex are differentially activated by cues and distractors. *Neurobiology of Learning and Memory, 94*(2), 191-198.

Broussard, J. I., Karelina, K., Sarter, M., & Givens, B. (2009). Cholinergic optimization of cue-evoked parietal activity during challenged attentional performance. *European Journal of Neuroscience, 29*(8), 1711-1722.

Broussard, J. I., Sarter, M., & Givens, B. (2006). Neuronal correlates of signal detection in the posterior parietal cortex of rats performing a sustained attention task. *Neuroscience, 143*(2), 407-417.

Bucci, D. J. (2009). *Posterior parietal cortex: An interface between attention and learning?* Paper presented at the Neurobiology of Learning and Memory.

Bucci, D. J., Phillips, R. G., & Burwell, R. D. (2000). Contributions of postrhinal and perirhinal cortex to contextual information processing. *Behavioral Neuroscience, 114*(5), 882-894.

Burwell, R. D. (2001). Borders and cytoarchitecture of the perirhinal and postrhinal cortices in the rat. *The Journal of Comparative Neurology, 437*(1), 17-41.

Burwell, R. D., & Amaral, D. G. (1998). Cortical afferents of the perirhinal, postrhinal, and entorhinal cortices of the rat. *The Journal of Comparative Neurology, 398*(2), 179-205.

Bushnell, M. C., Goldberg, M. E., & Robinson, D. L. (1981). Behavioral enhancement of visual responses in monkey cerebral cortex. I. Modulation in posterior parietal

cortex related to selective visual attention. *Journal of Neurophysiology, 46*(4), 755-772.

Bushnell, P. J., Kelly, K. L., & Crofton, K. M. (1994). Effects of toluene inhalation on detection of auditory signals in rats. *Neurotoxicology and Teratology, 16*(2), 149-160.

Cabeza, R., Ciaramelli, E., Olson, I. R., & Moscovitch M. (2008). The parietal cortex and episodic memory: an attentional account. *Nature Review of Neuroscience, 8*, 613-625.

Calton, J. L., & Taube, J. S. (2009). Where am I and how will I get there from here? A role for posterior parietal cortex in the integration of spatial information and route planning. *Neurobiology of Learning and Memory, 91*(2), 186-196.

Campbell, C. B. G., & Hodos, W. (1970). The concept of homology and the evolution of the nervous system. *Brain, Behavior and Evolution, 3*(5-6), 353-360.

Carli, M., Robbins, T. W., Evenden, J. L., & Everitt, B. J. (1983). Effects of lesions to ascending noradrenergic neurones on performance of a 5-choice serial reaction task in rats; implications for theories of dorsal noradrenergic bundle function based on selective attention and arousal. *Behavioural Brain Research, 9*(3), 361-380.

Cavada, C., & Goldman-Rakic, P. S. (1989a). Posterior parietal cortex in rhesus monkey: I. Parcellation of areas based on distinctive limbic and sensory corticocortical connections. *The Journal of Comparative Neurology, 287*(4), 393-421. doi:10.1002/cne.902870402

Cavada, C., & Goldman-Rakic, P. S. (1989b). Posterior parietal cortex in rhesus monkey: II. Evidence for segregated corticocortical networks linking sensory and limbic areas with the frontal lobe. *The Journal of Comparative Neurology, 287*(4), 422-445. doi:10.1002/cne.902870403

Chandler, H. C., King, V., Corwin, J. V., & Reep, R. L. (1992). Thalamocortical connections of rat posterior parietal cortex. *Neuroscience Letters, 143*(1-2), 237-242.

Ciaramelli, E., Grady, C. L., & Moscovitch, M. (2008). Top-down and bottom-up attention to memory: A hypothesis (AtoM) on the role of the posterior parietal cortex in memory retrieval. *Neuropsychologia, 46*(7), 1828-1851.

Colby, C. L., & Duhamel, J. R. (1996). Spatial representations for action in parietal cortex. *Cognitive Brain Research, 5*, 105-115.

Colby, C. L., Duhamel, J. R., & Goldberg, M. E. (1993). Ventral intraparietal area of the macaque: anatomic location and visual response properties. *Journal of Neurophysiology, 69*(3), 902-914.

Corbetta, M., Kincade, J. M., Ollinger, J. M., McAvoy, M. P., & Shulman, G. L. (2000). Voluntary orienting is dissociated from target detection in human posterior parietal cortex. *Nature Neuroscience, 3*(3), 292-297.

Corbetta, M., Kincade, J. M., & Shulman, G. L. (2002). Neural systems for visual orienting and their relationships to spatial working memory *Journal of Cognitive Neuroscience* (Vol. 14, pp. 508-523): MIT Press.

Crowne, D. P., Richardson, C. M., & Dawson, K. A. (1986). Parietal and frontal eye field neglect in the rat. *Behavioural Brain Research, 22*(3), 227-231.

Driver, J., & Mattingley, J. B. (1998). Parietal neglect and visual awareness. *Nature Neuroscience, 1*(1), 17-22.
Eskandar, E. N., & Assad, J. A. (1999). Dissociation of visual, motor and predictive signals in parietal cortex during visual guidance. *Nat Neurosci, 2*(1), 88-93. doi:10.1038/4594
Gaffan, D., & Hornak, J. (1997). Visual neglect in the monkey. Representation and disconnection. *Brain, 120*(9), 1647-1657.
Goodale, M. A., & Milner, A. D. (1992). Separate visual pathways for perception and action. *Trends in Neurosciences, 15*(1), 20-25.
Goodale, M. A., & Westwood, D. A. (2004). An evolving view of duplex vision: separate but interacting cortical pathways for perception and action. *Current Opinion in Neurobiology, 14*(2), 203-211.
Grefkes, C., & Fink, G. R. (2005). REVIEW: The functional organization of the intraparietal sulcus in humans and monkeys. *Journal of Anatomy, 207*(1), 3-17.
Hughes, H. C. (1977). Anatomical and neurobehavioral investigations concerning the thalamo-cortical organization of the rat's visual system. *The Journal of Comparative Neurology, 175*(3), 311-335.
Husain, M., & Nachev, P. (2007). Space and the parietal cortex. *Trends in Cognitive Sciences, 11*(1), 30-36.
Hyvarinen, J. (1982). Posterior parietal lobe of the primate brain. *Physiological reviews, 62*(3), 1060-1129.
Kamishina, H., Conte, W. L., Patel, S. S., Tai, R. J., Corwin, J. V., & Reep, R. L. (2009). Cortical connections of the rat lateral posterior thalamic nuclus. *Brain Research, 1264*, 39-56.
Kahn, I., Andrews-Hanna, J. R., Vincent, J. L., Snyder, A. Z., & Buckner, R. L. (2008). Distinct cortical anatomy linked to subregions of the medial temporal lobe revealed by intrinsic functional connectivity. *Journal of Neurophysiology, 100*(1), 129-139.
Kesner, R. P. (2009). The posterior parietal cortex and long-term memory representation of spatial information. *Neurobiology of Learning and Memory, 91*(2), 197-206.
King, V. R., & Corwin, J. V. (1993). Comparisons of hemi-inattention produced by unilateral lesions of the posterior parietal cortex or medial agranular prefrontal cortex in rats: Neglect, extinction, and the role of stimulus distance. *Behavioural Brain Research, 54*(2), 117-131.
Kolb, B., & Walkey, J. (1987). Behavioural and anatomical studies of the posterior parietal cortex in the rat. *Behavioural Brain Research, 23*(2), 127-145.
Kravitz, D. J., Saleem, K. S., Baker, C. I., & Mishkin, M. (2011). A new neural framework for visuospatial processing. *Nature Reviews Neuroscience, 12*(4), 217-230.
Krieg, W. J. S. (1946). Connections of the cerebral cortex. I. The albino rat. A. Topography of the cortical areas. *The Journal of Comparative Neurology, 84*(2), 221-275.
Mars, R. B., Jbabdi, S., Sallet, J., O'Reilly, J. X., Croxson, P. L., Olivier, E., . . . Rushworth, M. F. S. (2011). Diffusion-weighted imaging tractography-based parcellation of the human parietal cortex and comparison with human and

macaque resting-state functional connectivity. *The Journal of Neuroscience, 31*(11), 4087-4100.
McGaughy, J., & Sarter, M. (1995). Behavioral vigilance in rats: task validation and effects of age, amphetamine, and benzodiazepine receptor ligands. *Psychopharmacology, 117*(3), 340-357.
Mesulam, M. M. (1981). A cortical network for directed attention and unilateral neglect. *Annals of Neurology, 10*(4), 309-325.
Nitz, D. (2012). Spaces within spaces: rat parietal cortex neurons register position across three reference frames. *Nature Neuroscience, 15*(10), 1365-1367.
Olsen, G. M., & Witter, M. P. (2016). The posterior parietal cortex of the rat: architectural delineation and thalamic differentiation. *Journal of Comparative Neurology*, n/a-n/a.
Paxinos, G., & Watson, C. (2005). The rat brain in stereotaxic coordinates: Amsterdam;. Elsevier Academic Press.
Petersen, S. E., Robinson, D. L., & Morris, J. D. (1987). Contributions of the pulvinar to visual spatial attention. *Neuropsychologia, 25*(1, Part 1), 97-105.
Posner, M. I., & Dehaene, S. (1994). Attentional networks. *Trends in Neurosciences, 17*(2), 75-79.
Posner, M. I., Walker, J. A., Friedrich, F. J., & Rafal, R. D. (1984). Effects of parietal injury on covert orienting of attention. *The Journal of Neuroscience, 4*(7), 1863-1874.
Reep, R. L., Chandler, H. C., King, V., & Corwin, J. V. (1994). Rat posterior parietal cortex: topography of corticocortical and thalamic connections. *Experimental Brain Research, 100*(1), 67-84.
Reep, R. L., & Corwin, J. V. (2009). Posterior parietal cortex as part of a neural network for directed attention in rats. *Neurobiology of Learning and Memory, 91*(2), 104-113.
Robinson, D. L., Bowman, E. M., & Kertzman, C. (1995). Covert orienting of attention in macaques. II. Contributions of parietal cortex. *Journal of Neurophysiology, 74*(2), 698-712.
Rosvold, H. E., Mirsky, A. F., Sarason, I., Bransome, E. B., & Beck, L. H. (1956). A continuous performance test of brain damage. *Journal of consulting psychology, 20*(5), 343-350.
Saalmann, Y. B., Pinsk, M. A., Wang, L., Li, X., & Kastner, S. (2012). The pulvinar regulates information transmission between cortical areas based on attention demands. *Science, 337*(6095), 753-756.
Sakata, H., Taira, M., Murata, A., & Mine, S. (1995). Neural mechanisms of visual guidance of hand action in the parietal cortex of the monkey. *Cerebral Cortex, 5*(5), 429-438.
Sauseng, P., Klimesch, W., Stadler, W., Schabus, M., Doppelmayr, M., Hanslmayr, S., . . . Birbaumer, N. (2005). A shift of visual spatial attention is selectively associated with human EEG alpha activity. *European Journal of Neuroscience, 22*(11), 2917-2926.
Swanson, L. W. (1992). Brain maps: Structure of the rat brain: Elsevier (Amsterdam and New York).

Taira, M., Tsutsui, K. I., Jiang, M., Yara, K., & Sakata, H. (2000). Parietal Neurons Represent Surface Orientation From the Gradient of Binocular Disparity. *Journal of Neurophysiology, 83*(5), 3140-3146.

Uylings, H. B. M., & van Eden, C. G. (1991). Chapter 3 Qualitative and quantitative comparison of the prefrontal cortex in rat and in primates, including humans. In H. B. M. Uylings (Ed.), *Progress in Brain Research; The Prefrontal Its Structure, Function and Cortex Pathology* (Volume 85 ed., pp. 31-62): Elsevier.

Vogt, C., & Vogt, O. (1919). *Allgemeine Ergebnisse unserer Hirnforschung*. Leipzig: J.A. Barth.

Von Bonin, G., & Bailey, P. (1947). *The neocortex of Macaca mulatta,* . Urbana: Univ. of Illinois Press.

Whitlock, J. R. (2014). Navigating actions through the rodent parietal cortex. *Frontiers in Human Neuroscience, 8*.

Wilber, A. A., Clark, B. J., Forster, T. C., Tatsuno, M., & McNaughton, B. L. (2014). Interaction of egocentric and world-centered reference frames in the rat posterior parietal cortex. *The Journal of Neuroscience, 34*(16), 5431-5446.

Wurtz, R. H., Goldberg, M. E., & Robinson, D. L. (1980). Behavioral modulation of visual responses in the monkey: Stimulus selection for attention and movement. *Progress in Psychobiology and Physiological Psychology, 9*, 43-83.

Yi, D. J., & Chun, M. M. (2005). Attentional modulation of learning-related repetition attenuation effects in human parahippocampal cortex. *The Journal of Neuroscience, 25*(14), 3593-3600.

Zhou, H., Schafer, Robert J., & Desimone, R. (2016). Pulvinar-cortex interactions in vision and attention. *Neuron, 89*(1), 209-220.

# CHAPTER 2

# POSTERIOR PARIETAL CELLS SIGNAL STIMULUS LOCATION AND BEHAVIORAL OUTCOME DURING PERFORMANCE ON A VISUOSPATIAL ATTENTION TASK

## Abstract

The posterior parietal cortex (PPC) is implicated in directing and maintaining visual attention to locations in space. We hypothesized that the PPC also engages other cognitive processes in the transformation of behaviorally relevant visual inputs into appropriate actions, e.g. monitoring of multiple locations, selection of responses to locations in space, and monitoring the outcome of response selections. We recorded single cells and local field potentials in the rat PPC during performance on a novel visuospatial attention (VSA) task, which entails visually monitoring locations in space in order to make appropriate stimulus-guided locomotor responses. Rats attended to four locations on the floor of a maze. A randomly chosen location was briefly illuminated. Approach to the correct target location was followed by food reward. We observed that PPC activity correlated with multiple phases of the VSA task, including monitoring for stimulus onset, detection of a target, and spatial location of the target. Activity was also correlated with target selection, behavioral response, and outcome. About a third of PPC neurons were phase locked to theta. Peak theta power was higher in superficial layers than deep layers providing evidence against volume conduction from the hippocampus. In addition, theta power correlated with outcome. After an incorrect choice, theta increased, possibly providing a prediction error signal. Our study shows that the rat PPC has multiple roles in the translation of perception to appropriate actions.

## Introduction

Studies in humans and animal models suggest the posterior parietal cortex (PPC) supports a variety of cognitive processes. The bulk of available research in rodents, monkeys, and humans addresses the contributions of the PPC to spatial functions, navigation, and attention (Bucci, 2009; Colby & Goldberg, 1999; Corbetta & Shulman, 2002). Other work, however, suggests additional roles in perception, decision making, and visually-guided actions (Dijkerman & de Haan, 2007; Harvey, Coen, & Tank, 2012).

The role of the PPC in attention is well established, especially for spatial attention (Colby & Goldberg, 1999; Corbetta, Kincade, Ollinger, McAvoy, & Shulman, 2000; Posner, Walker, Friedrich, & Rafal, 1984; Reep & Corwin, 2009). In rats, PPC activity increased during detection of visual cues in a sustained attention task (Broussard, Karelina, Sarter, & Givens, 2009; Broussard, Sarter, & Givens, 2006). Other studies show that the primate and rat PPC are involved in navigation and representation of routes (Nitz, 2006, 2009; Rodriguez, 2010; Wilber, Clark, Forster, Tatsuno, & McNaughton, 2014). The activity of PPC neurons in rats also correlates with turning direction (McNaughton et al., 1994).

Electrophysiological and experimental lesion studies show that the rat PPC provides a good animal model of primate posterior parietal function, and indeed, anatomical studies support this view. The PPC has been anatomically defined in both rodents and primates (Cavada & Goldman-Rakic, 1989a, 1989b; Kolb & Walkey, 1987; Krieg, 1946). The thalamic input provides a good case for establishing connectional homology (Campbell & Hodos, 1970). The primate PPC is reciprocally connected with the pulvinar in the thalamus (Baleydier & Mauguiere, 1977). In the rodent, the lateral

posterior nucleus of the thalamus (LPO) is the likely homolog of the pulvinar. As in the monkey, the rat PPC is reciprocally connected with the LPO (Chandler, King, Corwin, & Reep, 1992; Reep, Chandler, King, & Corwin, 1994). Although a number of studies confirm that the PPC functions in navigation and visuospatial attention, other evidence obtained from monkeys in a tactile task suggests the PPC also contributes to perception and action (Dijkerman & de Haan, 2007). If the PPC is involved planning and executing perceptually-guided actions, this interpretation could explain the great variety of functions attributed to the PPC. In the present study, we addressed the hypothesis that, in addition to directing and maintaining visual attention to locations in space, the PPC engages other cognitive processes in the transformation of behaviorally relevant visual inputs into appropriate behavioral actions. We examined neuronal correlates in the rat PPC during performance on a novel visuospatial attention (VSA) task developed from the five-choice serial reaction time task (Carli, Robbins, Evenden, & Everitt, 1983). We used the VSA task to probe electrophysiological correlates of other cognitive processes, including perception, decision-making, and reward learning. We were able to show that the rat PPC has functions that go beyond stimulus detection and navigation, including monitoring locations in space, selection of appropriate visually-guided responses, and monitoring of the outcome of selected actions.

## Methods

### *Subjects*

Subjects were five male Long-Evan rats (Charles Rivers Laboratories, Wilmington, MA). They were individually housed in a temperature-regulated colony maintained on a

12:12 h light:dark cycle. Experiments were carried out in the light phase. All procedures followed the NIH guidelines and were approved by the Brown University animal care and use committee.

***Apparatus***

The task was run on the Floor Projection Maze, an apparatus that exploits the natural tendency of rats to attend to items located on or close to the ground and permits automated control over visual stimuli (Furtak et al., 2009; Jacobson, Ho, Kent, Yang, & Burwell, 2014). Essentially, the maze is a horizontal rear projection screen positioned to allow back-projection of visual stimuli and to the floor of any shaped arena (Figure 1A). The apparatus has a clear Plexiglas subfloor (147.32 × 111.80 × 1.25 cm) covered by Dual Vision Fabric (Da-Lite Screen Company, Warsaw, IN), a unity gain flexible fabric designed for rear screen projection. A thin Plexiglas sheet (0.32 cm) covers the fabric for protection. Visual stimuli were projected onto the unity gain fabric from below the subfloor using a short-throw LCD projector (WT610 projector, NEC Corporation). In this experiment, the arena comprised a linear runway at one end and a fan-shaped region for presentation of stimuli at the other (Figure 1B). Food reward (milk with various flavors) was delivered by an automated pump (Med Associates, Inc, St. Albans, VT) to a stainless steel food port located at the end of the runway opposite the fan-shaped presentation region. Auditory stimuli were controlled by an automated auditory stimulus generator (ANL926, Med Associates, Inc.) and delivered through a speaker located above the maze.

The Floor Projection Maze was interfaced with three Windows XP systems, for location tracking, behavioral control, and neuronal data acquisition. A CinePlex V2 Digital Video Recording and Tracking System (Plexon Inc., Dallas, TX) with an Imaging

Source ™ camera (640 x 480 resolution, 30 frames per sec) was used for tracking animals' location during behavioral performance. A custom Matlab program (Mathworks Inc., Natick, MA) translated XY coordinates from CinePlex into behavioral event flags for online control of behavior using Med Associates (Burlington, VT) software and hardware (MED PC IV software environment, DIG-700P2 PCI Interface Connection Card, a DIG-716P2 Smart Control Output Module). Based on the location of the rat, this system presented stimuli, collected behavioral data, and controlled delivery of reward. A Multichannel Acquisition Processor (MAP, Plexon Inc) and SortClient (Plexon, Inc) recorded real-time neuronal activity and behaviorally relevant event timestamps for later analysis. The MAP system was interfaced with the Med Associates system (DIG-713A SuperPort TTL Input Module and a DIG-726 SuperPort TTL Output module).

***Behavioral training***

Rats were put on food schedules to maintain body weight at 85-90% of free feeding weight. After handling for at least 7 days, rats were habituated to the behavioral room for 10 min/day for three days. Rats were then shaped and trained in the VSA task. In the shaping sessions, rats first were trained in a 30-minute session to approach a visual target stimulus for a food reward (a drop of flavored milk). In the initial shaping sessions, we adopted an errorless shaping procedure such that when the rat moved toward one of the four locations, the visual stimulus at that location would illuminate and a tone would signal a correct choice. After this initial shaping phase, rats were trained to stop in the ready position zone located at the end of the stem of the maze facing the fan-shaped area (Figure 1Bi). After a variable delay, a visual stimulus would illuminate in one of four randomly chosen locations (Figure 1Bii). There was a short response window for rats to

approach the location of the visual stimulus (Figure 1Biii). Approach to the correct location was signaled by a brief tone and presentation of a drop of flavored milk as a food reward (Figure 1Biv). If the rat approached an incorrect location, no reward was given, the trial was terminated, and a new trial would begin immediately. Rats were gradually trained in a series of steps culminating in the final parameters of the task. The duration for rats to stay in the ready position was gradually increased from 0.1 seconds to 1.2 seconds. Visual stimulus duration was gradually decreased from 20 seconds to 0.5 seconds. The response time window was decreased from 20 seconds to 5 seconds. In the final task, rats were required to stay in the ready position for stimulus onset for a variable interval (0.9-1.2 seconds).

The behavioral performance criterion for the end of training was 60% accuracy on the VSA task (chance is 25%). Behavior was well controlled on correct trials. Figure 1D shows an example of the path taken on correct trials to each target location. Rats in this study required 2-4 months of training to reach the behavioral criterion on the final stage of the task. When a rat reached criterion for 5 of 7 consecutive days, the hyperdrive was implanted.

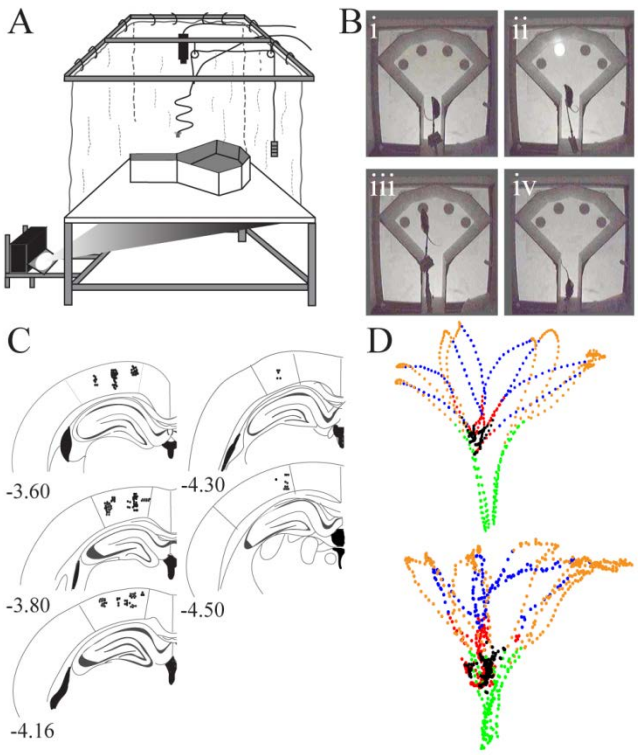


Figure 1. The VSA task and estimated location of recorded cells. A. Schematic of the Floor Projection Maze with the fan-shaped enclosure used for the task. B. Top down views of a rat in the maze. Trials were initiated when the animal stopped in the ready position (Bi). After a variable period, the target location was briefly illuminated (Bii). The animal made a selection by approaching one of the four locations (Biii), and then returned to the food port for a food reward (Biv). C. Estimated location of recorded posterior parietal cells in coronal sections between -3.60 to -4.50 mm relative to bregma. D. Example paths during performance of correct trials for two rats. Position data were from eight correct trials of two well-trained rats. Different colors represent task-relevant behavioral durations: ready position is black, after stimulus onset is red (light grey), approach for selection I orange (dark grey), after selection is blue (middle grey), and approach to reward is green (open circles).

### *Surgery*

Animals were premedicated with diazepam (2-5 mg/kg; i.p.), glycopyrrolate (0.05 mg/kg; s.c.), carprofen (5 mg/kg; s.c.), and butorphanol tartrate (0.5 mg/kg; s.c.) to counteract respiratory effects of anesthesia, to control pain, and to decrease risk of seizures. They were brought to a surgical level of anesthesia with isofluorane (1.0 – 2.5%). Using a stereotaxic apparatus (Kopf, Tujunga, CA), rats were implanted with a Harlan hyperdrive (Neuralynx, Tucson, AZ) into the left dorsal PPC (AP – 4.2 mm, ML

+ 3.0mm, DV -0.1mm). The Harlan hyperdrive had eight microdrives, each consisting of a drivable screw with guide tubing containing one tetrode. Tetrodes were made of four 12 μm twisted, formvar-insulated nichrome wires (A-M systems, Sequim, WA). A full turn of the screw advanced the tetrode by 160 μm. Two silver ground wires were wrapped around anchor screws in the skull. The hyperdrive was secured to the skull by the ground screws, small anchor screws, grip cement (Dentsply Caulk, Milford, DE), and dental cement (Coltene/Whaledent Inc., Cuyahoga Falls, OH).

***Histology***

After the last recording session, the rats were deeply anesthetized with an overdose of Beuthanasia-D (100 mg/kg, i.p.) and the final recording site was marked with an electrolytic lesion. The rats were then perfused with normal saline, followed by 4% formalin. The brains were post-fixed for 24 hours in 4% formalin and then transferred to a 30% sucrose solution until the time for sectioning. The brains were sectioned at 40 μm and stained for Nissl material with thionin.

***Electrophysiology***

Neuronal activity recorded from tetrodes, was amplified with a gain of 20 at the head stage (HST/32V-G20, Plexon, Inc., Dallas, TX). Signals from the preamplifier were then amplified with a gain of 50 (PBX2, Plexon, Inc.). Single-unit activity was filtered between 154–8,800 Hz and LFPs were filtered between 0.7–170 Hz. The signal was then digitized at 40 kHz for single-unit activity and 1 kHz for LFP activity, and further amplified for a total gain of 10,000 (MAP system, Plexon, Inc.). These signals were extracted through real-time thresholding (Sort Client, Plexon, Inc). The final waveforms were stored with timestamps of relevant events and position information for later analysis.

***Single neuron activity analysis***

Spikes associated with putative individual cells were isolated offline based on waveform characteristics and using a variety of partially automated and manual techniques (Offline Sorter, Plexon, Inc.). To ensure good quality of analyzed units, three raters gave each isolated unit a confidence rating of "Good", "Moderate", or "Poor" quality based on waveform characteristics, amplitude relative to noise, and auto correlations. Only units rated as "Good" quality by at least two of three independent raters were retained for the following analyses. The result was a dataset for each cell containing timestamps corresponding to spike times and behaviorally relevant event markers. These datasets were further analyzed using Neuroexplorer (NEX, Nex Technologies, Madision, AL) and SPSS.

Each cell was analyzed for behavioral correlates using factorial analysis of variance (fANOVA). Firing rate was the dependent variable for the fANOVAs. For each neuron, we first computed the mean firing rate (spikes/sec) for each of five epochs on each trial. The five epochs included the following: the pre-stimulus and post-stimulus epochs were the 500 msec periods immediately before and after stimulus onset; the pre-selection and post-selection epochs were the 500 msec periods immediately before and after the rat selected a target by approaching the location; and the reward-approach epoch was the first 500 msec after the animal reentered the stem of the maze to collect a food reward. The stimulus event was the onset of the target stimulus. The selection time event was the moment the rat entered a zone just in front of a stimulus location. On correct trials, this would be the zone in front of the location in which the target stimulus had appeared. Reentry of the stem of the maze triggered the next trial. Rats invariably approached and

checked the food port even after incorrect trials (Figure 1Biv). Although the post-stimulus and pre-selection epochs could have overlapped, latencies were always over 1 second, and so there was no overlap in time between different epochs.

In the first set of analyses, we examined whether cells signaled the onset of the target stimulus and the selection of the target location. We also assessed selectivity for stimulus onset, selection, and reward approach were modulated by outcome. The dependent variable was firing rate. For stimulus onset, the within trial variable was epoch (pre-stimulus epoch vs. post-stimulus epoch) and the between-trial variable was outcome (correct response vs. incorrect response). Similarly, for selection time the within trial variable was epoch (pre-selection epoch vs. post-selection epoch) and the between-trial variable was outcome. Only outcome was analyzed for the reward-approach epoch. The criteria for analysis were at least 10 complete trials and at least 30 total spikes in the analyzed epochs.

In a second set of analyses, we examined neural correlates associated with the location of the target stimulus. Because of number of possible target locations and the low numbers of trials, we pooled trials in which the target stimulus was at one of the two left locations and trials in which the target was at one of the two right locations. Location was analyzed separately for the post-stimulus, pre-selection, and post-selection epochs. The pre-stimulus and reward-approach epochs were not analyzed for location correlates because there was no information about the location of the target during these two epochs. Criterion for analysis was at least three trials on each of four trial types (Correct-Left, Correct-Right, Incorrect-Left, Incorrect-Right) and at least 30 spikes. A fANOVA was computed on each PPC cell meeting the stated criterion. We included outcome as a factor

because preliminary analyses indicated some cells showed location selectivity only for correct trials. Thus, between trial variables were choice location (left vs right) and outcome (correct vs incorrect). Location cells were cells that showed a main effect of location or an interaction with location.

One possibility is that location correlates might be explained by spatial selectivity or spatial tuning of PPC neurons unrelated to task demands. To address this question, we conducted a place field analysis using the xy coordinates of the animal and spike timestamps for each cell (Burwell & Hafeman, 2003). Prior to the analysis, the occasional missing position coordinates were estimated by averaging the last good coordinates with the subsequent good coordinates. For each neuron, a firing rate map was created by calculating the total number of spikes divided by total occupancy time for each pixel. Pixels that were not visited at least 3 times were eliminated from the analysis. Place fields were defined as at least five adjacent and contiguous pixels in which the firing rate of the cell was 3x greater than the grand mean.

Finally, we examined whether neuronal correlates were related to cortical laminar location. Cells were classified as belonging to superficial layers or deep layers. Cells for which the laminar location could not be determined were eliminated from this analysis. A Chi-square test was used to examine the distribution of superficial- and deep layer cells with respect to neuronal correlates.

All analyses were conducted using Offline Sorter (Plexon Inc, Dallas, Texas), NeuroExplorer (Nex Technologies, Littleton, MA), Matlab (Mathworks, Natick, MA), or SPSS (IBM Corporation, Somers, NY). Level of significance for statistical analyses was $p < 0.05$.

***Population analyses***

In addition to correlates of individual PPC neurons, we were also interested in representations of neural populations of cells. To examine whether PPC ensembles code for task-relevant behavior, we employed a representational similarity analysis (Kriegeskorte, Mur, & Bandettini, 2008; McKenzie et al., 2014). In the VSA task, two task components are pertinent to the animals' behavioral responses: outcome (correct vs. incorrect) and trial location (left vs. right). These two components were used to categorize trials into four trial types: Correct-Left (CL), Correct-Right (CR), Incorrect-Left (IL), Incorrect-Right (IR) for each of the three behavioral epochs that contained location information (post-stimulus, pre-selection, post-selection epochs).

To examine neural population coding in PPC in the VSA task, we first calculated z-score normalized firing rates for each cell using the mean and standard deviation among all events. The normalized firing rates were used to construct a population vector for each trial type (CL, CR, IL, IR) and epoch (post-stimulus, pre-selection, and post-selection) for a total of 12 vectors (3 behavioral epochs × 4 trial types). Pearson's correlation coefficients were calculated for every pair of vectors yielding a 12 x 12 similarity matrix (Figure S1)(McKenzie et al., 2014). We then calculated the average correlations for same and different conditions. First, we asked whether the ensemble of PPC cells differentiated same side trials from different side trials, regardless of trial outcome. We compared the average correlation of same side trials (R vs. R and L vs. L) to the average correlation for different side trials (R vs. L). If the ensemble is coding for location, we would expect that vector correlations across same side trials would be significantly higher than correlations across different side trials. Next, we asked whether

the ensemble of PPC cells differentiated the different outcome trials and same outcome trials, regardless of location. We compared the average correlation of same outcome trials (C vs. C and I vs. I) to the average correlation of different outcome trials (C vs. I). Our prediction was that correlations for same outcome trials would be significantly higher than correlations for different outcome trials.

To test for statistical significance, we used a bootstrapping test in which we randomly shuffled the event conditions for mean firing rates 10,000 times and performed the above correlation analyses, obtaining correlation differences in the same way for each resampled data set. We then compared the observed difference from the original data set to the differences calculated from the resampled data. Statistical significance was defined as an observed difference greater than the 95% of the distribution of correlation differences obtained from the bootstrapped datasets.

***LFP and phase locking analyses***

Files were first corrected for an identified issue of time alignment between spike data and field potential data using FPAlignV2 (Plexon, Inc.) (Nelson, Pouget, Nilsen, Patten, & Schall, 2008). Continuous data (LFPs), timestamps for behaviorally relevant event markers, and spike times were extracted and exported to Matlab (Mathworks, Natick, MA) from Neuroexplorer (NEX, Plexon, Inc.). For analysis of speed, XY coordinates for the animals were collected at a rate of 30Hz. The coordinates were first smoothed using a moving average filter then low pass filtered to remove any jitter caused by reflection against the floor projection maze arena walls. Instantaneous speed was then calculated as the rate of change in position of the pixels.

We used the Chronux toolbox for Matlab (chronux.org) for the multitaper spectral

analysis of the LFP. For each session the spectrum was calculated for the entire session and separately for each of the behaviorally relevant epochs used in the single unit analysis. To assess the effect of speed on power, we split the session into 500 ms windows. For each window, we calculated average speed and the power spectra. Power was extracted for specific frequency ranges (theta power was calculated between 6 and 10 Hz, low gamma power between 30 and 50 Hz, high gamma power between 70 and 100 Hz) and normalized for comparisons by dividing the power in each epoch by the power of the entire session. Repeated measures analysis of covariance (RM-ANCOVA) was used to assess differences in normalized power across the five epochs (within factor) with speed as the covariate, and outcome (correct vs. incorrect trial) as the between-subjects factor.

For spike-LFP phase relationships, LFP data were filtered for theta (6 - 10 Hz), low (30 - 50 Hz) and high gamma (70 - 100 Hz) using a 4-pole symmetrical butterworth filter. Instantaneous phase was calculated using the Hilbert transform of the filtered signal yielding values ranging from 0 - 360° (where 180° corresponds to the trough) and thus providing an indication of the current phase position of the oscillation over time. The instantaneous phase of the LFP at each individual spike time was extracted for each cell. Circular statistics were used to analyze these spike-phase distributions and significant phase-locking was determined using a Rayleigh's Z test, where the null hypothesis is that the distribution of spikes across was uniform at all phases.

## Results

### *Histology*

Examination of Nissl-stained coronal brain sections from each of the five animals indicated electrode tips for all but one tetrode were located in PPC between 3.6 and 4.5 mm posterior to bregma and between 2.0-4.0 mm lateral to the midline (Figure 1C). The remaining tetrode was located in the adjacent visual association cortex. In addition, later recordings were obtained from some tetrodes located in the underlying dorsal hippocampal CA1 cell layer. No cells from visual cortex or hippocampus (HIP) were analyzed, but some CA1 LFPs were examined as noted below.

### *PPC cells were selective for stimulus onset and predicted behavioral outcome*

All five animals reached criterion within several weeks (Figure 1D). After training the rats were implanted with eight driveable tetrodes. Each rat yielded isolated units. A total of 147 PPC cells rated as "good by at least two of three raters were used in the following analyses. Each cell was recorded for a single session. The mean firing rate for all cells was 3.86 ± 0.30 Hz (range, 0.30- 22.56 Hz). Of these PPC cells, 125 cells met the criteria for analysis for at least one epoch. The majority of these criterion cells, 63 (50%), exhibited behavioral correlate(s) during at least one of the task epochs as indicated by main effects or interactions of stimulus onset, target selection time, location, or outcome.

To investigate whether PPC cells signaled attention to visual stimuli, we first analyzed neuronal responses to stimulus onset by comparing firing rates for the 500 ms before vs 500 ms after the onset of the 500 ms illumination of the target stimulus for correct vs incorrect trials. A total of 121 cells met the criteria for this analysis. We found

two types of selectivity. Seventeen cells (14%) showed significant increases or decreases in firing rate associated with stimulus onset (Table 1). The behavior of 15 of these cells could be categorized in the following ways. The firing rates of five cells decreased after stimulus onset. The firing rates of two cells ramped up during the pre-stimulus epoch suggesting vigilance. The firing rates of five cells increased after stimulus onset in a sensory-driven manner. Three cells increased firing rates after onset, but not until later in the post-stimulus epoch, e.g. the cell shown in Figure 2A. This later category of cells may be signaling detection rather than stimulus onset. Nine cells (7%) were sensitive to stimulus onset and outcome; eight of those exhibited a significant interaction between stimulus onset and outcome, and one cell showed main effects of stimulus and outcome without an interaction. For example, the cell shown in Figure 2B fired more in the pre-stimulus epoch than the post-stimulus epoch when the rat as about to make a correct selection and less in the pre-stimulus epoch and when the animal was about to make an incorrect. Of 121 cells, 26 (21%) showed selectivity for stimulus onset, and nine of those cells were also sensitive to outcome. Six cells (5%) exhibited a main effect of outcome, alone during the peri-stimulus interval (Figure 2C). Those six cells with the nine cells that exhibited an interaction with outcome yields a total of 15 of 121 cells (12%) that fired differentially depending on the outcome of the trial. This pattern of results was similar across animals (Table 1, right two columns).

***PPC cells signaled target selection and behavioral outcome***

The activity of PPC cells also correlated with target selection. A total of 122 cells met criterion for this analysis. Eight cells (7%) signaled selection by firing more during either the pre-selection or the post-selection epoch (Table 1 and Figure 2D). A total of 10

cells (8%) signaled selection and outcome. Seven of those exhibited an interaction effect showing differential firing patterns depending on whether the animal made a correct vs. an incorrect selection, and 3 cells displayed main effects of both selection and outcome without a significant interaction. For example, the cell shown in Figure 2E fired more in the pre-selection epoch on correct trials and more in the post-selection epoch on incorrect trials. Nine cells (7%) responded to outcome alone during the peri-selection interval (Table 1 and Figure 2F). Thus, 18 of 122 cells (15%) differentiated pre- and post-selection epochs, and 19 of 122 cells (16%) displayed differential firing patterns related to behavioral outcome.

For the reward-approach epoch, in which the animal had just reentered the stem of the maze after selecting a target location, 104 cells met the criteria for analysis. Seven cells (7%) displayed selectivity for different outcomes in the reward-approach epoch (Table 1). A representative cell, shown in Figure 2G, fired more in correct trials than incorrect trials. Again, the pattern of results was similar across individual animals (Table 1).

Table 1. Behavioral correlates of posterior parietal cells

| **Epoch (criterion cells)** | **Correlate** | **Cells** | **% Total** | **#66** | **#112** |
|---|---|---|---|---|---|
| Peri-Stimulus (121) | Stimulus Only | 17 | 14.05 | 13.64 | 14.47 |
| | Stimulus and Outcome | 9 | 7.44 | 6.82 | 7.89 |
| | Outcome Only | 6 | 4.96 | 2.27 | 6.59 |
| Total | | 32 | 26.45 | 22.72 | 28.94 |
| Peri-Selection (122) | Selection Only | 8 | 6.56 | 6.98 | 6.49 |
| | Selection and Outcome | 10 | 8.20 | 6.98 | 9.09 |
| | Outcome Only | 9 | 7.38 | 4.65 | 7.79 |
| Total | | 27 | 22.13 | 18.61 | 23.38 |
| Reward-Approach (104) | Outcome | 7 | 6.73 | 6.01 | 7.04 |

Numbers of the criterion cells for each analysis and numbers/percentages of cells that displayed significant main effect or interactions during selective behavioral relevant epochs. On the right we show percentages for the two rats with the most cells (n=56 and 84, respectively). The results are remarkably similar to the total findings. The categories of “Stimulus and Outcome” and “Selection and

Outcome" include cells exhibiting interactions of the two variables and main effects for both variables. Most cells exhibited a single main effect or interaction, but some cells showed multiple significant effects and/or interactions across analyses. So, for example, the number of cells that showed a Stimulus correlate in the Peri-Stimulus epoch is 26, with 17 showing only the Stimulus correlate and 9 showing both Stimulus and Outcome correlates

### *PPC cells signaled left vs. right trial types*

We predicted that PPC cells would display selectivity for the location of the target stimulus, as demonstrated by differential firing patterns on left vs. right trials (Figure 1D). We analyzed the post-stimulus, pre-selection, and post-selection epochs because spatial location was relevant during these epochs. As expected, for each epoch we found cells that showed a main effect or interaction with location. In all three epochs the majority of location selective cells showed a main effect of location. Eight of 66 criterion cells (12%) in the post-stimulus epoch, 14 of 67 (22%) in the pre-selection epoch, and 10 of 68 (15%) in the post-selection epoch showed trial location selectivity as indicated by a significant difference in firing rate between left and right trials (Figure 2H, I, J; Table 2).

After selecting a target location, rats must necessarily make a turn to return to the stem of the maze for a food reward and/or to start the next trial. Thus, one possibility is that trial location selectivity during the post-selection epoch was due to some aspect of turning behavior (left turn vs. right turn) as has been previously reported (Chen, Lin, Green, Barnes, & McNaughton, 1994; McNaughton et al., 1994). To evaluate whether the activity of the cells that showed location selectivity in the post-selection epoch correlated with turning behavior, we compared neuronal activity for left and right turn trials using a t-test. For eight of ten cells there was no effect of turning behavior (all *p values* > 0.05). Two cells may have been modulated both by trial location and turning behavior. One cell showed significantly higher firing to right trials and right turns; however, the animal

always turned right on right trials. On the left side of the maze, firing rates for that cell were no difference between left and right turns ($t_8 = 0.03$, $p > 0.05$). The other cell showed significantly higher firing to left trials and left turns. The animal turned left mostly on left trials, except one right turn. On the right side of the maze, firing rates were not different between left and right turns ($t_{24} = 1.4$, $p > 0.05$). Taken together, our results provide evidence that turning behavior does not explain location selectivity for PPC cells.

Another possibility is that overall spatial tuning accounts for location selectivity. To address this issue, we analyzed all PPC neurons (n=147) to determine whether task-relevant location selectivity can be explained by task-irrelevant firing fields. Of the 147 cells, eight cells (5%) exhibited spatial firing fields based on established criteria for identifying place fields (Burwell & Hafeman, 2003). When the eight spatially selective cells were compared with the 24 location selective cells, three cells showed both spatial and location selectivity. In one cell the spatial tuning was consistent with location selectivity, and in two cells the firing field was inconsistent with location selectivity. The main difference between the spatially selective cells and location selective cells is the relevance of the behavior. The spatially selective cells showed a general spatial tuning regardless of the behavior whereas the location selective cells displayed specific task-relevant location preference during different epochs of the VSA task. According to our results, the location selectivity can be explained by spatial tuning in only one of 24 location cells suggesting that most of the location cells in the PPC were selective to specific task-relevant epochs during the VSA task.

Table 2. Location correlates of posterior parietal cells

| **Epoch (criterion cells)** | **Cells** | **% Total** | **#66** | **#112** |
|---|---|---|---|---|
| Post-Stimulus (66) | 8 | 12.12 | 21.05 | 8.51 |

| | | | | |
|---|---|---|---|---|
| Pre-Selection (67) | 14 | 20.89 | 22.23 | 20.40 |
| Post-Selection (68) | 10 | 14.70 | 26.32 | 10.20 |

Numbers of the criterion cells for each epoch and numbers/percentages of cells that displayed significant main effect of location or and interaction between location and outcome. On the right we show percentages of location cells for the two rats with the most cells (n=56 and 84, respectively).

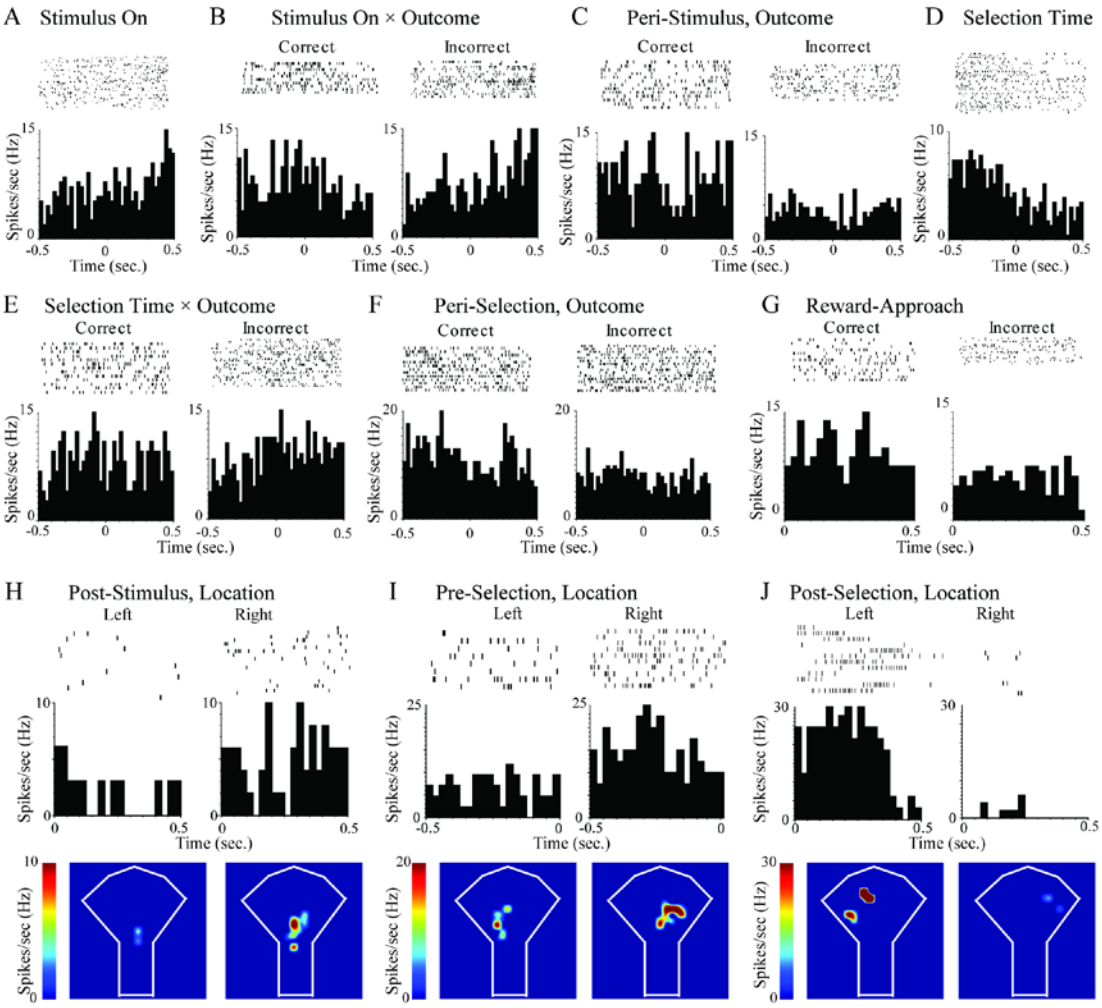


Figure 2. Example neuronal correlates for posterior parietal cells. Perievent raster plots and histograms are shown for example cells with behaviorally relevant firing patterns. For the stimulus epoch, time 0 is stimulus onset (A, B, C, H). For the selection epoch, time 0 is selection (D, E, F, I, J). For the reward-approach epoch, time 0 is when the animal entered the stem of the maze (G). For the cells that displayed a main effect or interaction of outcome, plots for correct and incorrect trials are shown separately (B, C, E, F, G). For example cells with location correlates, firing fields are shown below (H-J). The cell in H fired more on right trials during the post-stimulus epoch. The cell in I fired more in right trials during the pre-selection epoch. The cell in J fired more on left trials during the post-selection epoch.

***Summary of PPC single unit correlates***

Of the 147 cells recorded, 125 cells met the criterion for analysis in at least one epoch. Of those criterion cells, 63 exhibited some type of selectivity in at least one epoch or analysis. Of the selective cells, 12 showed selectivity only for location, 26 showed selectivity only for outcome, and 12 showed selectivity for both location and outcome. The remaining 13 cells were selective for either stimulus onset or selection time without location or outcome selectivity. Note that we performed multiple analyses to confirm cell selectivity of location and outcome, so the numbers of selective cells came from all analyses. Thus, of the 63 selective cells, 24 (38%) signaled location and 38 (60%) signaled outcome in at least one analysis.

We also compared the percentages of all types of selectivity from two animals that contributed majority of the PPC units and observed a significantly highly positive correlation ($r = 0.97$, $p < 0.0001$) between the two animals showing the stability of the selective effects across animals.

***Cells located in deep layers were more likely to signal stimulus onset***

We examined whether behavioral correlates of PPC cells differ according to laminar position. Results showed that behavioral correlates did not differ for cells located in deep and superficial layers, except for selectivity for stimulus onset (Table S1). Out of 121 cells that met criteria for the stimulus onset analysis, 90 cells were in superficial layers and 31 cells were in deep layers. Forty-five percent of cells in deep layers were more likely to signal stimulus onset as compared with 20% of cells in superficial layers ($\chi^2_{(1)} = 7.504$, $p < 0.006$). This finding is consistent with the anatomical evidence that the deep layers of the PPC receive more inputs from visual areas than do the superficial layers

(Miller & Vogt, 1984). Behavioral correlates did not differ by laminar location for the selection ($\chi^2_{(1)} = 0.186$, $p > 0.05$) and reward-approach epochs ($\chi^2_{(1)} = 0.459$, $p > 0.05$) or for location selectivity of cells ($\chi^2_{(1)} = 0.138$, $p > 0.05$).

***PPC ensembles code for location and outcome***

To examine how PPC neural populations represent trial location and outcome across epochs, we employed a representational similarity analysis to understand the encoding patterns from the PPC ensemble. We created population vectors of normalized mean firing rates for four trial types (CL, CR, IL, and IR) and for three epochs (post-stimulus, pre-selection, and post-selection). We then computed correlation coefficients for every pair of population vectors yielding a 12 x 12 similarity matrix. Finally, we randomly shuffled the conditions and compared the observed difference to the difference generated from shuffled data (see details in methods) to test the statistical significance. This analysis allowed us to determine whether the population codes for different task-relevant events.

As suggested by the single unit patterns of activity, we predicted that ensemble activity would code for location. Accordingly, correlations of pairs of population vectors on trials in which the stimulus was on the same side would be higher than correlations of pairs of population vectors on trials in which the stimulus was on the different sides. We found that neuronal firing patterns in PPC showed significantly higher correlations in same side trials than the correlations obtained from different side trials (same side mean r = 0.71; different side mean r = 0.54, $p < 0.0001$).

Based on single unit patterns of activity, we also predicted that ensemble activity would code for outcome. If this is the case, then correlations of pairs of population

vectors on trials in which the outcome was the same would be higher than correlations of pairs of population vectors on trials in which the outcome was different. We found significantly higher correlations in same outcome trials than the correlations obtained from different outcome trials (same outcome mean r = 0.66; different outcome mean r = 0.58, $p < 0.022$).

Taken together, our population analyses showed that, during the VSA task, the PPC ensemble differentiated different side trials and different outcome trials providing further evidence that the PPC, indeed, codes both location and outcome components during visuospatial attention processing. Coding for location, however, did appear to be more robust than coding for outcome.

***Oscillatory activity in PPC signals behavioral relevant epochs.***

Local field potentials were recorded along with single unit data in each session. A total of 14 sessions were eliminated from analyzes of power due to clipping or interference at 6 Hz likely arising from nearby building construction. Thus, we analyzed 29 recording sessions from 2 rats. Example PSDs are shown in Figure S3A. In 79% of sessions, theta power correlated significantly with running speed (Figure 3A). RM-ANCOVA controlling for speed revealed a significant main effect of epoch on theta power ($F_{4,290}=12.12$, $p < 0.001$) and a marginally significant interaction between epoch and outcome ($F_{4,290}=2.33$, $p < 0.056$). In order to further investigate how trial outcome affected theta power, we compared theta power for correct vs incorrect trials by ANCOVA controlling for speed. During the reward-approach epoch theta power was higher following an incorrect selection than following a correct selection ($F_{1,57}=3.88$, p =

0.05). Note that this epoch occurs when rats enter the stem of the maze and not when they are at the end of the maze consuming reward.

An important issue regarding theta oscillations in PPC is whether these oscillations reflect volume conduction from the underlying hippocampal region. We recorded LFPs simultaneously from two pairs of electrodes in the PPC and dorsal to CA1 cell layer (Figure S2A). Filtered theta in both regions indicates that theta oscillations in the two regions were out of phase. In addition, we showed PPC coherency in the theta frequency band across different PPC electrodes, but coherency was not evident across PPC and HIP electrodes (Figure S2B). In addition, peak normalized theta power was overall higher in superficial than deep layers of PPC ($t_{32}$=4.17, $p < 0.001$), further arguing against volume conduction (Figure 3B-D).

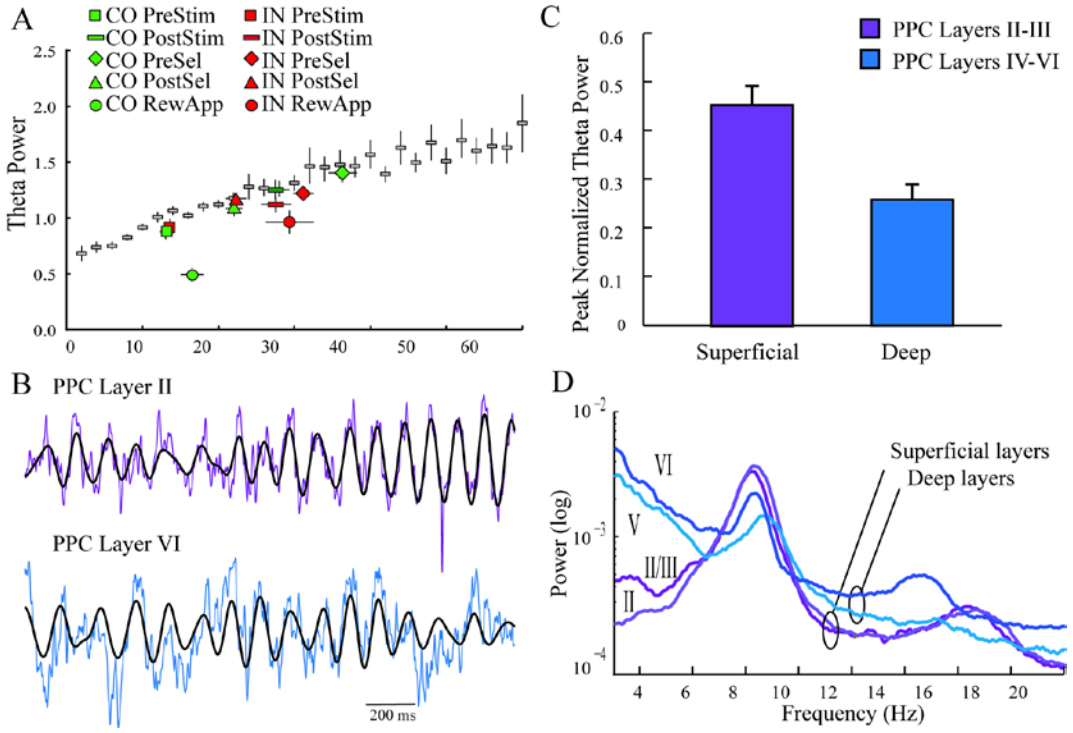


Figure 3. Theta power by running speed and cortical layer. A. Power in the theta frequency band (6-12 Hz). The overall speed-power relationship is shown by grey rectangles. To calculate this overall relationship, each session was binned into 500 ms time windows and the mean speed and mean power were computed

for each window. Vertical error bars are for the normalized power (SEM) over all sessions; horizontal error bars represent variability in speed (SEM) for that epoch. Theta was strongly correlated with running speed. Theta power was obtained for task-relevant epochs, including pre-stimulus (PreStim), post-stimulus (PostStim), pre-selection (PreSel), post-selection (PostSel), reward-approach (RewApp). Theta power tended to be lower than predicted by speed, especially when rats were approaching the reward locations. With a few exceptions, theta was not different for correct and incorrect trials. For the post-stimulus and pre-selection epochs theta was significantly higher prior to correct trial outcome, suggesting that theta is modulated by attention. For the reward-approach epoch, theta power was higher following incorrect trials than correct trials, suggesting correlation with prediction error for the expected reward. B. Examples of raw theta are shown in purple and blue (grey) and filtered power is shown in black in superficial and deep PPC. C. Peak normalized theta in the 6-10 frequency band was higher in LFPs recorded in superficial PPC than in deep PPC. E. Examples of power spectral densities in superficial and deep PPC.

For low gamma, there was no systematic relationship between power and speed (Figure S3B, left); there was a significant negative correlation between speed and power in 14% of sessions and a significant positive correlation in 43%. Nevertheless, low gamma power in the reward epoch was higher than the speed-power correlation would predict. RM-ANCOVA of power across different epochs controlling for speed reveal a significant effect of epoch ($F_{4,290}$=8.04, $p < 0.001$), but no significant effect of behavioral outcome and no interaction (all $p > 0.1$).

High gamma power was positively correlated with speed in 39% of sessions. RM-ANCOVA of power across different epochs reveal a significant main effect of epoch ($F_{4,290}$=3.66, $p < 0.006$) and a small trend toward an effect of outcome ($F_{1,290}$=3.09, $p$ = 0.08) but no interaction ($p > 0.1$)(Figure S3B, right). Again to explore how trial outcome affected high gamma power across epochs, paired t-tests in each of the five behavioral epochs were conducted for correct vs incorrect trials. High gamma power was significantly higher only in the post-selection epoch ($F_{1,57}$=5.41, $p < 0.02$).

An examination of neuronal synchrony revealed that a proportion of PPC cells fired in phase to theta, low gamma, and high gamma (Figures 4, S3C, and S3D, respectively). A total of 137 cells were analyzed for phase locking to local theta and

gamma oscillations; 107 (78%) cells showed phase locking to at least one of the designated frequency ranges. Of the 137 cells, 42 (31%) were significantly phase locked to local theta oscillations (Figure 4). Seven of those we considered putative interneurons comprised based on spike width. The preferred phase of most cells phase locked to theta was just prior to the trough. The putative interneurons tended to be phaselocked to the peak.

A total of 43 (31%) were significantly phase locked to local low gamma oscillations, and 69 (50%) were significantly phase locked to local high gamma oscillations. Each isolated unit was further distinguished as either a putative interneuron or pyramidal cell based on the waveform shape and the spike half-width (time from trough - peak of the averaged waveform). Putative interneurons comprised 7 of the 42 cells were phase locked to theta, 2 of 43 were phase locked to low gamma, and 4 of 69 were phase locked to high gamma. The distribution cells firing in phase to theta (Figure 5C), low gamma (Figure S3C, right) and high gamma (Figure S3D, right).

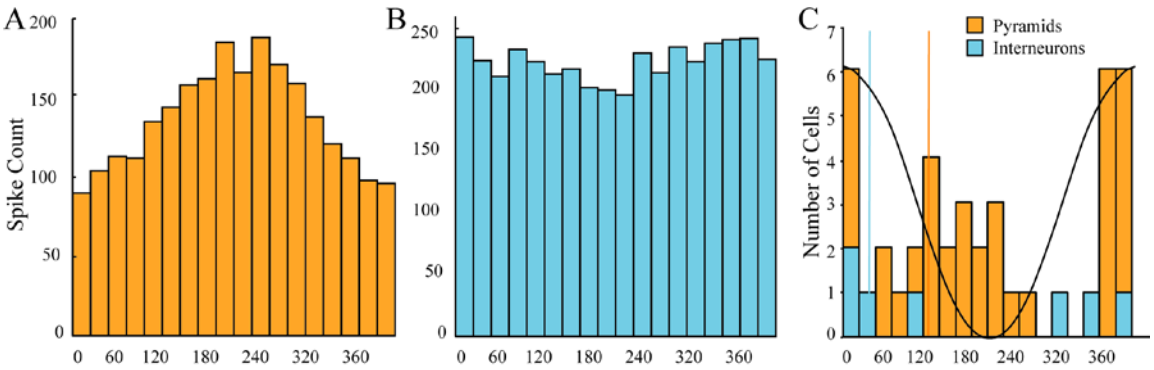

Figure 4. PPC phase locking to theta oscillations. Spike phase locking to theta in the 6-10 frequency band is shown for a putative pyramidal cell (A) and a putative interneuron (B). C. Distribution of preferred phases is shown for all significantly phase locked cells. The mean preferred phase in orange for pyramidal cells and in blue for putative interneruons. Phase locking was observed in 30.66% of the 137 cells recorded simultaneously with the corresponding LFPs from the same electrode.

## Discussion

We used our novel VSA task to address hypotheses about PPC function. As expected, based on prior studies of signal detection and spatial tasks, we found evidence consistent with the view that the PPC is engaged in stimulus-driven attention and in the processing of spatial information. We also found evidence for our hypothesis that the PPC engages multiple cognitive processes in the transformation of behaviorally relevant visual inputs into appropriate actions. In the VSA task, rats are required to monitor multiple locations for a brief presentation of a target stimulus and then indicate a choice by approaching the correct target location for a food reward. Consistent with our hypothesis, we found PPC correlates of visually guided selection of locomotor responses and we found correlates of choice outcome. In the peri-stimulus time window, over 12% of criterion cells (half of the selective cells) fired differentially depending on whether the animal was about to make a correct choice, suggesting that the animal had detected stimulus onset and thus was more likely to make a correct selection. Similarly, in the peri-selection time window, 15% of criterion cells (more than half of selective cells) fired differentially to outcome. Other studies have found that PPC neuronal activity changes differentially in response to behavioral outcomes in detection and navigation tasks (Broussard & Givens, 2010; Broussard et al., 2006; Harvey et al., 2012), but our study is the first to report that PPC neuronal activity correlates with response outcome in a task in which the animal must choose between multiple responses.

Our task tapped multiple types of attention and we observed that PPC cells correlated with all types. Some PPC neurons fired more during the pre-stimulus epoch when the animal was monitoring locations in which the target stimulus might appear.

Other cells increased or decreased firing rates with the onset of the target, suggesting sensory-driving attention. Still others fired later in the stimulus on epoch. These cells may reflect detection of the stimulus if the stimulus was not detected immediately at onset. We also observed PPC neurons in the stimulus on epoch that signaled when the target appeared in particular locations. Thus we saw evidence for vigilance, detection, and visuospatial attention.

We also observed evidence that the PPC is important for visually-guided action. Nearly 21% of cells fired selectively as rats approached a particular target location. Another 15% were selective for particular locations after the rat had made a selection. These cells were unlikely to be selective for particular places unrelated to task parameters. Overall, spatial tuning assessed by analysis of spatial firing fields in the PPC was relatively weak as has been previously reported (Whitlock, Pfuhl, Dagslott, Moser, & Moser, 2012). Location selectivity also could not be explained by turning or self-motion behaviors associated with turning.

One concern is the small numbers of cells in some categories of selectivity for the epochs analyzed. This concern is mitigated by the observation that patterns of selectivity are observed for the individual rats with the most cells (two right most columns of Table 1). Results of location analyses were also similar for individual rats. It should also be noted that, in Table 1, we made a separate category for cells showing an interaction or two main effects. For example, in the peri-stimulus epoch, 17 cells showed stimulus selectivity only, but an additional 9 cells showed stimulus selectivity along with outcome selectivity. Thus 26 cells (21%) showed stimulus selectivity. By the same calculation, then, 12% of cells showed outcome selectivity in the peri-stimulus epoch. In the peri-

selection epoch, 15% showed selectivity for the time of selection, and 15.6% showed outcome selectivity.

Population analyses provided evidence that ensembles of PPC cells coded for task relevant locations and outcomes, providing further evidence to support the role of PPC in visuospatial attention and visually-guided actions. Ensemble activity was more similar for pairs of trials in which the target stimulus was on the same side (left-left or right-right) than for pairs of trials in which the target stimulus was on different sides (left-right), suggesting that the ensemble coded for location. As our single-unit data indicated, individual cells in the ensemble had preferred sides (left or right) and were more likely to fire similarly on the trials in which the target was on the preferred side. Presumably the ensemble includes cells with left and right location selectivity. The implication is that the ensemble can code for location more reliably than individual neurons that show variability across trials. Likewise, ensemble activity is more similar for pairs of trials in which the outcome was the same (correct-correct or incorrect-incorrect) than for pairs of trials in which the outcome was different (correct-incorrect), suggesting that the ensemble also codes for outcome. Taken together, our results from both single unit and PPC ensemble supported our hypothesis about the role of PPC in visuospatial attention that the PPC involved in multiple cognitive processes to transform visual attention inputs for appropriate responses.

Our study provides the first evidence that theta and gamma brain oscillations in the rat PPC are modulated by task demands in a visuospatial attention task. Both theta and gamma oscillations have been observed across a range of species; these oscillations are proposed to provide discrete windows for spikes to occur in order to enhance

processing of inputs within a region and the transmission of information across regions (Buzsaki & Draguhn, 2004; Buzsaki, Logothetis, & Singer, 2013; Fries, Reynolds, Rorie, & Desimone, 2001). In our study, a substantial proportion of PPC cells were phase locked to theta, low gamma, and high gamma suggesting that PPC oscillatory activity is coordinating spiking activity.

PPC power in the theta frequency band was correlated with running speed, as has been observed in hippocampus and postrhinal cortex (Furtak, Ahmed, & Burwell, 2012; Hinman, Penley, Long, Escabi, & Chrobak, 2011). Theta power, however, was different across task epochs, controlling for speed. During the reward-approach epoch, theta was higher on incorrect trials than correct trials, consistent with signaling prediction error. A similar finding has been observed in frontal theta in a human EEG study (Cavanagh, Frank, Klein, & Allen, 2010) and in postrhinal theta in rats (Furtak et al., 2012). Surprise generated by prediction error results in enhanced attention and learning. Holland and colleagues have shown that the neural circuitry underlying this enhancement depends on the PPC and its cholinergic inputs (Bucci, Holland, & Gallagher, 1998; Chiba, Bucci, Holland, & Gallagher, 1995). The observation that some PPC cells are phaselocked to local theta suggests PPC theta may be the mechanism for this enhancement. Notably, increased phase-locking to theta has been observed in other cortical regions during expectancy, for example, the orbitofrontal cortex (van Wingerden, Vinck, Lankelma, & Pennartz, 2010).

Other studies show increased gamma synchronization between the parietal and visual regions during visually guided attention in primates (Engel, Fries, & Singer, 2001; Fries et al., 2001). Our study showed that high gamma, but not low gamma, power was

significantly correlated with running speed, however, low gamma power was higher than expected based on speed during the reward epoch. Both theta and low gamma power may then provide some sort of error feedback after correct or incorrect trials.

The primate PPC is functionally differentiated such that dorsal PPC is more involved in top-down attention and ventral PPC is involved in bottom-up attention (Shomstein, 2012). In other words, dorsal PPC may be guiding behavior based on intention whereas neuronal responses in ventral PPC may reflect stimulus salience. An open question is whether there is functional differentiation in the rat PPC with regard to top-down and bottom-up attention. In the present study, we targeted dorsal PPC, and we found substantial evidence that this region is important for more than stimulus detection, consistent with guiding behavior based on intention or top-down control. To our knowledge, all rat electrophysiology and experimental lesion studies, including the present study, have targeted dorsal PPC. Yet, there is an understudied subregion of the rat PPC. In addition to the dorsal aspect, the rat PPC has a caudal limb (Swanson, 1992). Interestingly, it is the caudal PPC that is more closely connected with visual and spatial processing regions, including the postrhinal cortex (Agster & Burwell, 2009; Burwell & Amaral, 1998). Thus, it may be that dorsal PPC in the rat is biased toward top-down attention and caudal PPC is biased toward salience-based, stimulus-guided responses. Future studies will address whether there is functional differentiation between dorsal and caudal aspects of the rat PPC.

We have shown that, in addition to directing and maintaining visual attention to locations in space, the PPC also engages other cognitive processes to transform behaviorally relevant visual information into appropriate actions. We used a novel

visuospatial attention task to provide evidence that the PPC is engaged in monitoring of multiple locations, selection of responses to locations in space, and monitoring the outcome of response selections. PPC cells exhibited correlates of stimulus onset, stimulus detection, target selection, and the outcome of behavioral responses. We also showed that a proportion of PPC cells are phase locked to theta, and that theta power correlates with outcome. These findings are consistent with a role for PPC in top-down control in the translation of perception to action.

## References


Agster, K. L., & Burwell, R. D. (2009). Cortical efferents of the perirhinal, postrhinal, and entorhinal cortices of the rat. *Hippocampus, 19*(12), 1159-1186.

Baleydier, C., & Mauguiere, F. (1977). Pulvinar-latero posterior afferents to cortical area 7 in monkeys demonstrated by horseradish peroxidase tracing technique. *Experimental Brain Research, 27*(5), 501-507.

Broussard, J. I., & Givens, B. (2010). Low frequency oscillations in rat posterior parietal cortex are differentially activated by cues and distractors. *Neurobiology of Learning and Memory, 94*(2), 191-198.

Broussard, J. I., Karelina, K., Sarter, M., & Givens, B. (2009). Cholinergic optimization of cue-evoked parietal activity during challenged attentional performance. *European Journal of Neuroscience, 29*(8), 1711-1722.

Broussard, J. I., Sarter, M., & Givens, B. (2006). Neuronal correlates of signal detection in the posterior parietal cortex of rats performing a sustained attention task. *Neuroscience, 143*(2), 407-417.

Bucci, D. J. (2009). Posterior parietal cortex: An interface between attention and learning? *Neurobiology of Learning and Memory, 91*(2), 114-120.

Bucci, D. J., Holland, P. C., & Gallagher, M. (1998). Removal of cholinergic input to rat posterior parietal cortex disrupts incremental processing of conditioned stimuli. *The Journal of Neuroscience, 18*(19), 8038-8046.

Burwell, R. D., & Amaral, D.G. (1998). Cortical afferents of the perirhinal, postrhinal, and entorhinal cortices of the rat. *The Journal of Comparative Neurology, 398*(2), 179-205.

Burwell, R. D., & Hafeman, D. M. (2003). Positional firing properties of postrhinal cortex neurons. *Neuroscience, 119*(2), 577-588.

Buzsaki, G., & Draguhn, A. (2004). Neuronal oscillations in cortical networks. *Science, 304*, 1926-1929.

Buzsaki, G., Logothetis, N., & Singer, W. (2013). Scaling brain size, keeping timing: Evolutionary preservation of brain rhythms. *Neuron, 80*(3), 751-764.

Campbell, C.B.G., & Hodos, W. (1970). The concept of homology and the evolution of the nervous system. *Brain Behav. Evol., 3*, 353-367.

Carli, M., Robbins, T. W., Evenden, J. L., & Everitt, B. J. (1983). Effects of lesions to ascending noradrenergic neurones on performance of a 5-choice serial reaction task in rats; implications for theories of dorsal noradrenergic bundle function based on selective attention and arousal. *Behavioural Brain Research, 9*(3), 361-380.

Cavada, C., & Goldman-Rakic, P. S. (1989a). Posterior parietal cortex in rhesus monkey: I. Parcellation of areas based on distinctive limbic and sensory corticocortical connections. *The Journal of Comparative Neurology, 287*(4), 393-421.

Cavada, C., & Goldman-Rakic, P. S. (1989b). Posterior parietal cortex in rhesus monkey: II. Evidence for segregated corticocortical networks linking sensory and limbic areas with the frontal lobe. *The Journal of Comparative Neurology, 287*(4), 422-445.

Cavanagh, J. F., Frank, M. J., Klein, T. J., & Allen, J. J. B. (2010). Frontal theta links prediction errors to behavioral adaptation in reinforcement learning. *NeuroImage, 49*(4), 3198-3209.

Chandler, H. C., King, V., Corwin, J. V., & Reep, R. L. (1992). Thalamocortical connections of rat posterior parietal cortex. *Neuroscience Letters, 143*(1), 237-242.

Chen, L. L, Lin, L., Green, E. J , Barnes, C. A., & McNaughton, B. L. (1994). Head-direction cells in the rat posterior cortex. *Experimental Brain Research, 101*(1), 8-23.

Chiba, A. A., Bucci, D. J., Holland, P. C., & Gallagher, M. (1995). Basal forebrain cholinergic lesions disrupt increments but not decrements in conditioned stimulus processing. *The Journal of Neuroscience, 15*(11), 7315-7322.

Colby, C. L., & Goldberg, M. E. (1999). Space and attention in parietal cortex. *Annual Review of Neuroscience, 22*(1), 319-349.

Corbetta, M., Kincade, J. M., Ollinger, J. M., McAvoy, M. P., & Shulman, G. L. (2000). Voluntary orienting is dissociated from target detection in human posterior parietal cortex. *Nature Neuroscience, 3*(3), 292-297.

Corbetta, M., & Shulman, G. L. (2002). Control of goal-directed and stimulus-driven attention in the brain. *Nature Reviews Neuroscience, 3*(3), 201-215.

Dijkerman, H. C., & de Haan, E. H. F. (2007). Somatosensory processing subserving perception and action: Dissociations, interactions, and integration. *Behavioral and Brain Sciences, 30*(02), 224-230.

Engel, A. K., Fries, P., & Singer, W. (2001). Dynamic predictions: Oscillations and synchrony in top-down processing. *Nature Reviews Neuroscience, 2*(10), 704-716.

Fries, P., Reynolds, J. H., Rorie, A. E., & Desimone, R. (2001). Modulation of oscillatory neuronal synchronization by selective visual attention. *Science, 291,* 1560-1563.

Furtak, S. C., Ahmed, O., & Burwell, R. D. (2012). Single neuron activity and theta modulation in postrhinal cortex during visual object discrimination. *Neuron, 76*(5), 976-988.

Furtak, S. C., Cho, C. E., Kerr, K. M., Barredo, J. L., Alleyne, J. E., Patterson, Y. R., & Burwell, R. D. (2009). The Floor Projection Maze: A novel behavioral apparatus for presenting visual stimuli to rats. *Journal of Neuroscience Methods, 181*(1), 82-88.

Harvey, C. D., Coen, P., & Tank, D. W. (2012). Choice-specific sequences in parietal cortex during a virtual-navigation decision task. *Nature, 484*, 62-68.

Hinman, J. R., Penley, S. C., Long, L. L., Escabi, M. A., & Chrobak, J. J. (2011). Septotemporal variation in dynamics of theta: speed and habituation. *Journal of Neurophysiology, 105*(6), 2675-2686.

Jacobson, T. K., Ho, J. W., Kent, B. W., Yang, F. C., & Burwell, R. D. (2014). Automated visual cognitive tasks for recording neural activity using a Floor Projection Maze. *Journal of Visual Experimentation*.

Kolb, B., & Walkey, J. (1987). Behavioural and anatomical studies of the posterior parietal cortex in the rat. *Behavioural Brain Research, 23*(2), 127-145.

Krieg, W. J. S. (1946). Connections of the cerebral cortex. I. The albino rat. B. Structure of the cortical areas. *The Journal of Comparative Neurology, 84*(3), 277-323.

Kriegeskorte, N., Mur, M., & Bandettini, P. (2008). Representational similarity analysis–connecting the branches of systems neuroscience. *Frontiers in systems neuroscience, 2*.

McKenzie, S., Frank, A. J., Kinsky, N. R., Porter, B., Riviere, P. D., & Eichenbaum, H. (2014). Hippocampal representation of related and opposing memories develop within distinct, hierarchically organized neural schemas. *Neuron, 83*(1), 202-215.

McNaughton, B. L., Mizumori, S. J. Y., Barnes, C. A., Leonard, B. J., Marquis, M., & Green, E. J. (1994). Cortical representation of motion during unrestrained spatial navigation in the rat. *Cerebral Cortex, 4*(1), 27-39.

Miller, M. W., & Vogt, B. A. (1984). Direct connections of rat visual cortex with sensory, motor, and association cortices. *The Journal of Comparative Neurology, 226*(2), 184-202.

Nelson, M. J., Pouget, P., Nilsen, E. A., Patten, C. D., & Schall, J. D. (2008). Review of signal distortion through metal microelectrode recording circuits and filters. *Journal of Neuroscience Methods, 169*(1), 141-157.

Nitz, D. (2006). Tracking route progression in the posterior parietal cortex. *Neuron, 49*(5), 747-756.

Nitz, D. (2009). Parietal cortex, navigation, and the construction of arbitrary reference frames for spatial information. *Neurobiology of Learning and Memory, 91*(2), 179-185.

Posner, M. I., Walker, J. A., Friedrich, F. J., & Rafal, R. D. (1984). Effects of parietal injury on covert orienting of attention. *The Journal of Neuroscience, 4*(7), 1863-1874.

Reep, R. L., Chandler, H. C., King, V., & Corwin, J. V. (1994). Rat posterior parietal cortex: topography of corticocortical and thalamic connections. *Experimental Brain Research, 100*(1), 67-84.

Reep, R. L., & Corwin, J. V. (2009). Posterior parietal cortex as part of a neural network for directed attention in rats. *Neurobiology of Learning and Memory, 91*(2), 104-113. doi:

Rodriguez, P. F. (2010). Human navigation that requires calculating heading vectors recruits parietal cortex in a virtual and visually sparse water maze task in fMRI. *Behavioral Neuroscience, 124*(4), 532-540.

Shomstein, S. (2012). Cognitive functions of the posterior parietal cortex: top-down and bottom-up attentional control. *Frontiers in integrative neuroscience, 6*, 38.

Swanson, L.W. (1992). Brain maps: Structure of the rat brain: Elsevier (Amsterdam and New York).

van Wingerden, M., Vinck, M., Lankelma, J., & Pennartz, C. M. A. (2010). Theta-band phase locking of orbitofrontal neurons during reward expectancy. *The Journal of Neuroscience, 30*(20), 7078-7087.

Whitlock, J. R., Pfuhl, G., Dagslott, N., Moser, M.B., & Moser, E. I. (2012). Functional split between parietal and entorhinal cortices in the rat. *Neuron, 73*(4), 789-802.

Wilber, A. A., Clark, B. J., Forster, T. C., Tatsuno, M., & McNaughton, B. L. (2014). Interaction of egocentric and world-centered reference frames in the rat posterior parietal cortex. *The Journal of Neuroscience, 34*(16), 5431-5446.

## SUPPLEMENTARY MATERIALS

## Supplemental Tables

Table S1. Laminar difference in patterns of selectivity.

| | Type of Selectivity | | | | | | | |
|---|---|---|---|---|---|---|---|---|
| | Stimulus | | Selection | | Reward-approach | | Location | |
| **Layer** | **Selective** | **Not Selective** | **Selective** | **Not Selective** | **Selective** | **Not Selective** | **Selective** | **Not Selective** |
| **Superficial** | 18 (20%) | 72 (80%) | 21 (23%) | 70 (77%) | 6 (8%) | 72 (92%) | 17 (34%) | 33 (66%) |
| **Deep** | *14 (45%) | 17 (55%) | 6 (19%) | 25 (81%) | 1 (4%) | 25 (96%) | 7 (39%) | 11 (61%) |

Shown are numbers and percentages of selective and non-selective cells that met criterion for three epochs and for the location analysis by layer. For the three epochs, selectivity is for any combination of main effects and interactions. Laminar distributions of behavioral selectivity cells were similar with the exception of stimulus-related selectivity. Cells in deep layers were more likely than cells in superficial layers to exhibit stimulus-related correlates. * Proportion of selective cells in deep layers than cells in superficial layer ($p < 0.05$).

## Supplemental Figures

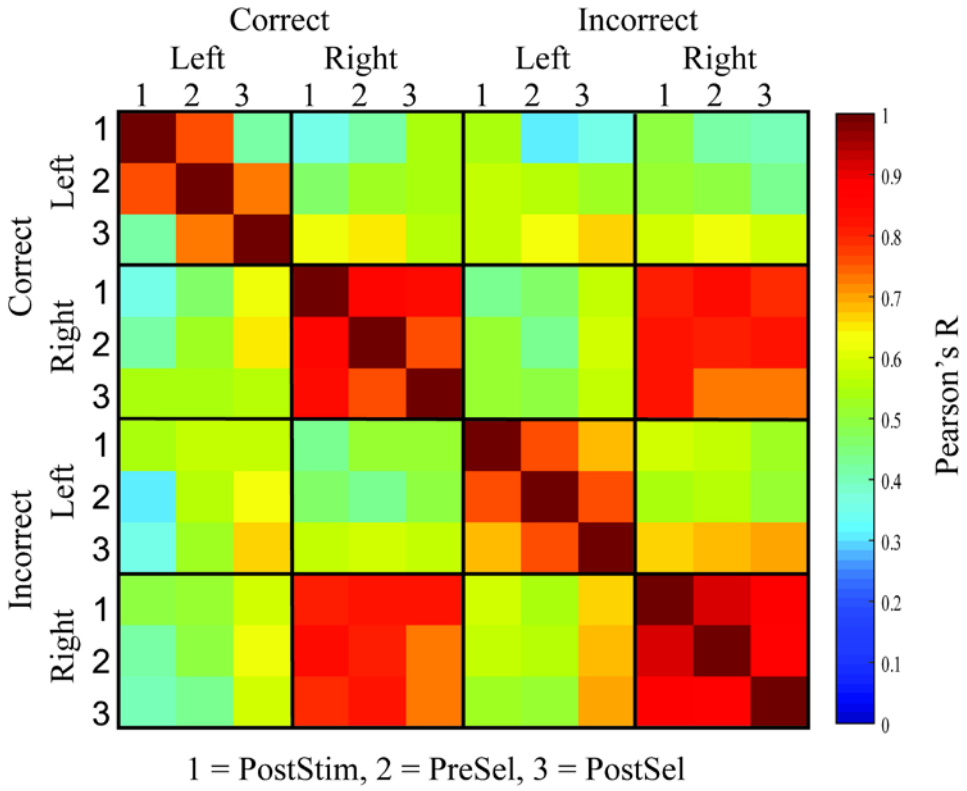


Figure S1. Similarity matrix to assess ensemble coding for location and outcome. Firing rates for each cell were z-score normalized using the mean and standard deviation among all events. The normalized firing rates were used to construct a population vector for each trial type (correct left and right, incorrect left and right) and epoch (post-stimulus, pre-selection, and post-selection, shown as 1, 2, and 3 respectively). This resulted in a total of 12 vectors (3 behavioral epochs × 4 trial types). Pearson's correlation coefficients were calculated for every pair of vectors yielding a 12 x 12 similarity matrix.

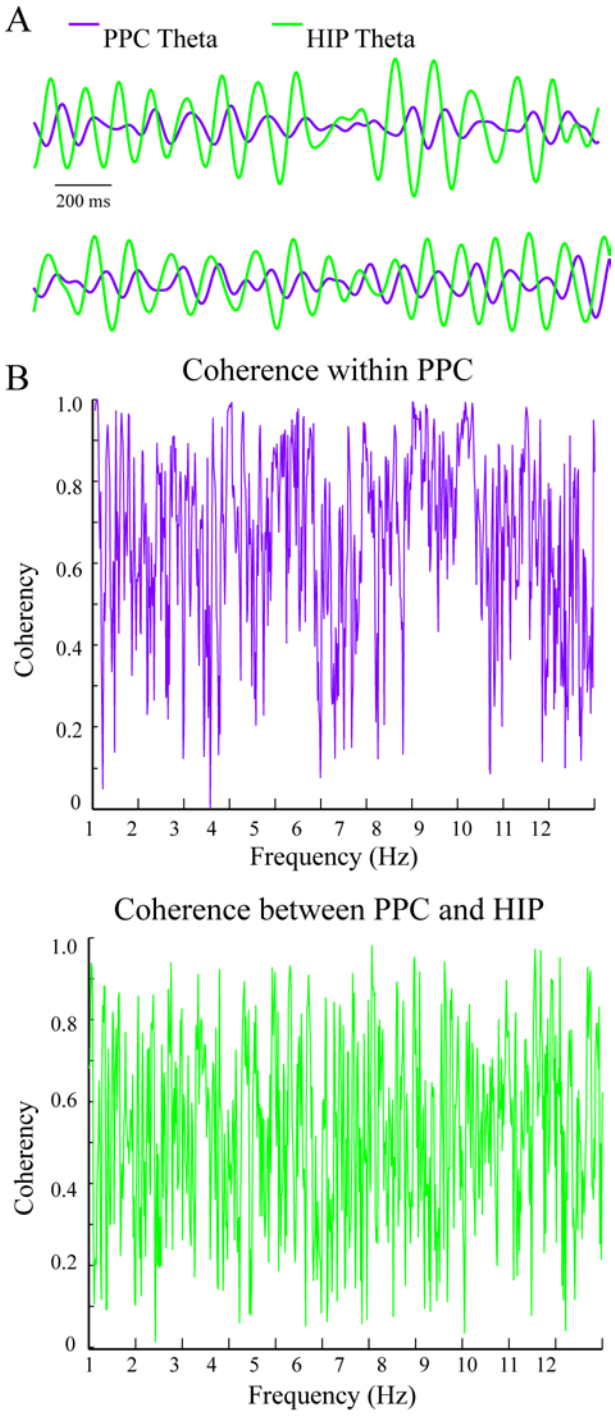


Figure S2. Simultaneously recorded local field potentials in PPC and CA1. A. Filtered theta power is higher in the PPC than the hippocampus (HIP) for two sessions with simultaneously recorded LFPs. B. Examples of coherence within PPC (upper) and between PPC and HIP. C. Peak normalized theta in the 6-10 frequency band was higher in LFPs recorded in superficial PPC than in deep PPC. These examples suggest that theta is unlikely to be volume conducted from CA1.

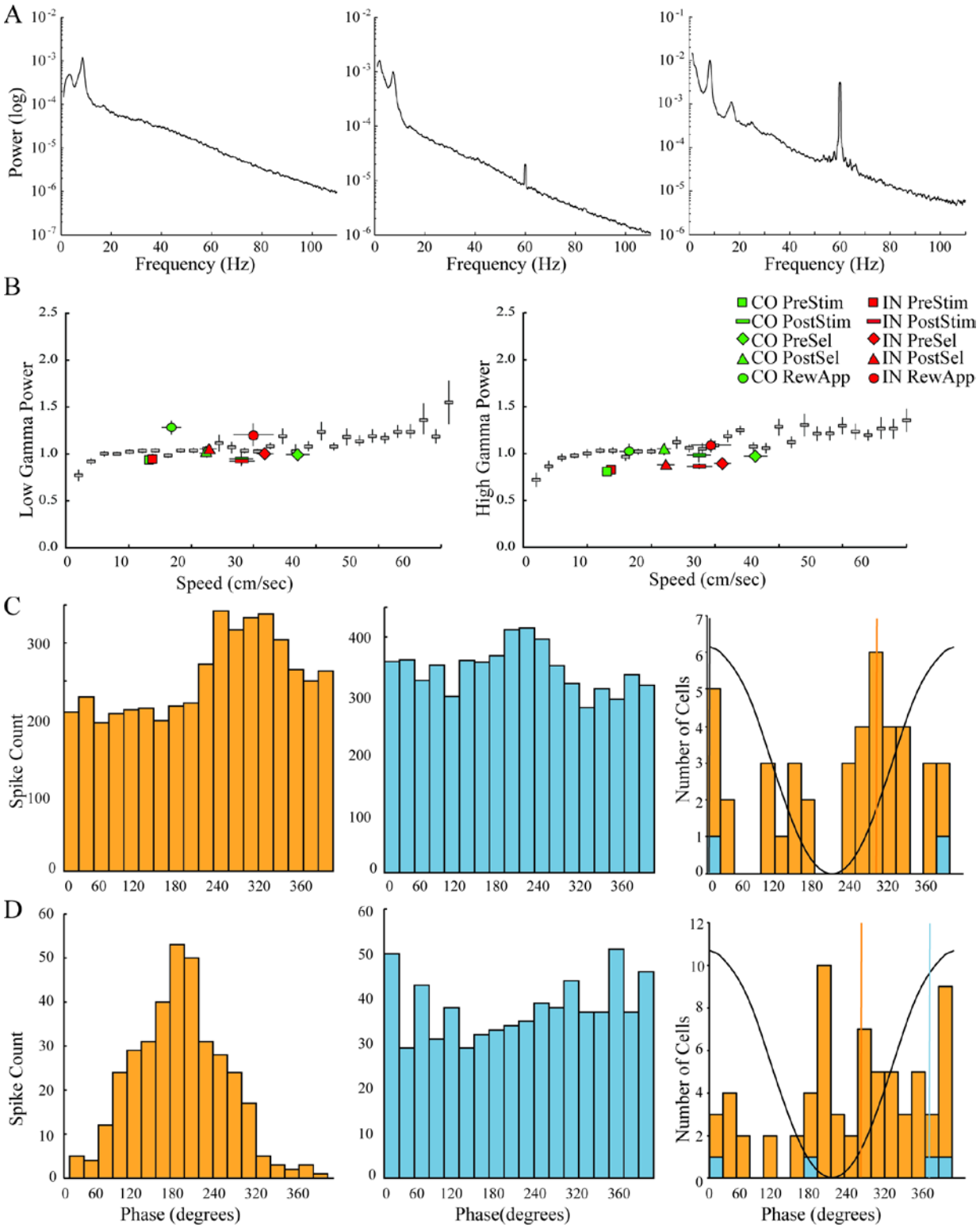


Figure S3. Analysis of gamma power, modulation by running speed, and phaselocking. A. Examples of power spectral density plots. Many local field potentials were characterized by 60 Power in the low gamma frequency band (30-50 Hz) and high gamma frequency band (70-100 Hz) was not increased relative to the 1/f power function. B. Speed-power relationship is shown by grey rectangles for low gamma (left) and high gamma (right). To calculate this overall relationship, each session was binned into 500 ms time windows and the mean speed and

mean power was computed for each window. Vertical error bars are for the normalized power (SEM) over all sessions; horizontal error bars represent varibility in speed (SEM) for that epoch. Only high gamma power was significantly positively correlated with speed. Theta power was obtained for task-relevant epochs, including pre-stimulus (PreStim), post-stimulus (PostStim), pre-selection (PreSel), post-selection (PostSel), reward-approach (RewApp). With the exception of correct reward approaches, power in all frequency bands was higher during task-relevant epochs than non-task relevant epochs. C. Phase locking to low gamma for pyramidal cells and putative interneurons. An example of distribution of spikes are shown for a pyramid (left) and a putative interneuron (right). Spike phase locking for low gamma at 30-50 was observed in 31.39% of the cells. Distribution of preferred phases for pyramids and interneurons on shown on the right. Mean phase preferences is indicated by vertical lines in matched colors. C. The same information is shown for high gamma. Spike phase locking for high gamma at 70-100 was observed in 50.36% of the cells.

# CHAPTER 3

# INTERCONNECTIONS OF THE POSTERIOR PARIETAL CORTEX, POSTRHINAL CORTEX, THE LATERAL POSTERIOR NUCLEUS OF THE THALAMUS IN THE RAT

## Abstract

In this chapter, we characterized the connections among the rat lateral posterior nucleus of thalamus (LP), postrhinal cortex (POR) and posterior parietal cortex (PPC). We analyzed 16 anterograde tract-tracing experiments and 6 retrograde tract-tracing experiments across these regions. For the anterograde experiment, anterograde tracers were injected into LP or POR and the density of fiber labeling was quantified. For the retrograde experiment, retrograde traces were injected in subdivisions of POR. The density and percentages of labeled cells were estimated across LP and PPC. Overall, the LP, POR and PPC interconnect with each other intensely. All subdivisions of the LPO project to both POR and PPC, especially to more caudal portions of these two cortical areas, whereas the rostral portions of the POR and PPC still have moderate LP inputs. We observed that the medial subnuclei of the LP have project more heavily to the POR than the lateral subnuclei do. The POR and PPC also have returned projections to the LP. In addition, reciprocal connections between the POR and PPC were observed. The POR receives heavy inputs from the PPC, especially from the caudal PPC. The POR also provides stronger inputs to the PPC. Specifically, the caudal POR has more intense inputs to the parietal areas.

## Introduction

The posterior parietal cortex (PPC) in humans, monkeys, and rodents is implicated in attention, particularly visuospatial attention (Bucci, 2009; Colby & Goldberg, 1999; Petersen & Posner, 2012; Posner & Dehaene, 1994). A primary target of the PPC is the medial temporal lobe, including the hippocampal formation and the parahippocampal cortex (Kamishina et al., 2009; Kravitz, Saleem, Baker, & Mishkin, 2011). The rodent homology of the primate parahippocampal cortex is the postrhinal cortex (POR) (Burwell, Witter, & Amaral, 1995). Some evidence suggests the POR, which has reciprocal connections with the PPC, supports attentional monitoring for the purpose of detecting changes in the environmental context (Bucci & Burwell, 2004; Furtak, Ahmed, & Burwell, 2012). Both the POR and PPC are interconnected with the lateral posterior nucleus of the thalamus (LP) (Furtak, Wei, Agster, & Burwell, 2007).

A number of anatomical studies have addressed connections among the PPC, POR and LP in rats (Chandler, King, Corwin, & Reep, 1992; Furtak et al., 2007; Nakamura, Hioki, Furuta, & Kaneko, 2015; Reep, Chandler, King, & Corwin, 1994). None of these studies, however, reported the detailed connections among different subdivisions of these structures. In addition, most focused entirely on the dorsal portion of the PPC (3.5-5.0 mm posterior to bregma and 1.5-5.0 mm lateral from the midline). Thus, the connections of the caudal PPC have not been described. A more thorough understanding of these connections in rats would inform studies of the neural bases of visuospatial attention. In the present study, we used anterograde and retrograde tract tracing methods in rats to characterize the topography of the anatomical connections among the PPC, POR and LP.

Table 1. Nomenclature and Abbreviations

| Regions | Abbreviations |
|---|---|
| nucleus lateralis dorsale pars dorsomedialis | LD |
| lateral posterior nucleus | LP |
| nucleus lateralis posterior pars rostromedialis | LPMR |
| nucleus lateralis posterior pars caudomedialis | LPMC |
| nucleus lateralis posterior pars lateralis | LPL |
| nucleus lateralis posterior pars rostralis | LPLR |
| nucleus lateralis posterior pars caudalis | LPLC |
| posterior parietal cortex | PPC |
| medial parietal association cortex | MPtA |
| lateral parietal association cortex | LPtA |
| parietal cortex, posterior area, dorsal part | PtPD |
| parietal cortex, posterior area, rostral part | PtPR |
| parietal cortex, posterior area, caudal part | PtPC |
| the parietal region, posterior association area | PtLp |
| the parietal region, posterior association area, dorsal part | DPtLp |
| the parietal region, posterior association area, caudal part | CPtLp |
| entorhinal cortex | EC |
| perirhinal cortex | PER |
| postrhinal cortex | POR |
| ventral postrhinal cortex | PORv |
| dorsal postrhinal cortex | PORd |
| dorsal posthinal cortex, rostral part | rPORd |
| dorsal postrhinal cortex, caudal part | cPORd |

Nomenclature is from Paxinos and Watson (2005) and Swanson (1992).

## Methods

### *Subjects*

Ten Sprague-Dawley rats (Harlan Laboratories, Houston, TX) weighing from 300-400 grams received tracer injections in the POR. Data from these rats were previously reported (Agster & Burwell, 2009, 2013; Burwell & Amaral, 1998a). An additional six Sprague-Dawley rats (Charles River Laboratories, Wilmington, MA)

weighing 250-350 grams received injections in the LP. Prior to surgery rats were housed individually or in pairs with ad libitum access to food and water. Pair housed rats were separated following surgery. All methods involving the use of live animals conformed to NIH guidelines and were approved by the appropriate Institutional Animal Care and Use Committee.

***Surgery***

Subjects that received POR injections were anesthetized by a 50 mg/kg intraperitoneal (i.p.) injection of sodium pentobarbital (n=10; Nembutal©, Abbott Laboratories, North Chicago, IL). Subjects that received LP injections (n=6) were anesthetized with isoflurane (Isothesia, Butler Schein Animal Health, Dublin, OH). Anesthesia was induced with 3% isoflurane. One hour prior to surgical induction, these subjects received preoperative medications to control for possible respiratory problems, minimize stress from surgery, and as a prophylactic measure against seizures. These medications included a 2 mg/kg intraperitoneal injection of Diazepam (Hospira, Inc., Lake Forest, IL), and the following subcutaneous (s.q.) injections of 5 mg/kg Carprofen (Pfizer Animal Health, New York, NY), 0.5 mg/kg Butorphanol tartrate (Fort Dodge Animal Health, Fort Dodge, IO), and 0.05 mg/kg Glyocpyrrolate (West Ward, Eatontown, NJ). Following anesthesia induction, rats were secured in a Kopf stereotaxic apparatus in the flat skull position, after which isoflurane was reduced to 1-2.5% for the remainder of the surgery. Body temperature was maintained during surgery at 37° C with a calibrated heating pad. The scalp was shaved and cleaned with a betadine swab, and the subject then received a s.q. injection of 0.1 ml lidocane (Hospira, Inc., Lake Forest, IL). An incision was then made after a brief waiting period to expose the skull, with bregma and lambda

readily visible. A craniotomy was made dorsal to the intended injection site and a small incision was made in the dura to allow smooth entry of the glass micropipette. Coordinates for target areas were according to Paxinos and Watson(Paxinos & Watson, 2005) and Swanson (Swanson, 1992).

Retrograde tracers used were either Fast Blue (FB; Dr. Illing, Gmbh and Co. Gross Umstadt, Germany) or Diamidino Yellow (DY; Dr. Illing, Gmbh and Co. Gross Umstadt, Germany). FB and DY were pressure injected through a glass micropipette with tip diameter ranging from 60 to 90 µm, with an approximate injection rate of 30 nl/min. The FB injections were approximately 150 nl of a 3% solution in distilled $H_2O$, and the DY injections were approximately 200 nl of a 2% solution in distilled H2O. Following the injection of the retrograde tracer, the micropipette was raised 100 µm, and then after a 10-min waiting period, was slowly raised 500 µm/min before being removed (Burwell & Amaral, 1998a, 1998b).

Anterograde tracers used were either a 2.5% solution of Phaseolus vulgaris-leucoagglutinin (PHA-L; Vector Laboratories, Burlingame, CA) in 0.1 M phosphate-buffered saline (PBS), or a 10% solution of biotinylated dextran amine (BDA, 10K MW, Molecular Probes, Inc., Eugene, OR) in 0.1 M PBS. Anterograde tracers were delivered through glass micropipettes with tip diameter ranging from 5 µm to 15 µm by iontophoresis, with 4 µA of positive direct current (7 seconds on and 7 seconds off) for 8 -10 minutes. Similar to the retrograde injections, there was a 10 minute wait period following the injection, during which the micropette remained stationary. The micropipette was then slowly raised and removed from the injection site. Upon completion of the injections, the craniotomy was filled with gel foam, and the scalp was

sutured along the incision. Rats were observed for 1-2 hours following surgery, and were kept warm with a heating pad during recovery. After the rats could demonstrate the righting reflex, they were returned to the colony. Rats received 6 mg of Rimadyl in chow (Rodent MD'sTM, BioServ, Hudson, NH) for three days following surgery.

***Tissue Processing***

Rats recovered for 7 to 14 days following surgery to allow for optimal transport of the tracers. After the survival period, subjects with POR injections were deeply anesthetized prior to perfusion with a 35% solution of chloral hydrate. Subjects with LP injections were anesthetized prior to perfusion with 1.0 ml Beuthanasia-D (Schering-Plough Animal Health Corp, Union, NJ). All rats for this study were transcardially perfused following a pH-shift procedure to maximize visualization of tracers, as described previously in Burwell and Amaral (1998a, 1998b). Rats were perfused at a flow rate of 30-35 ml/minute. Each subject's head was packed with ice for the duration of the procedure. Rats were perfused with room temperature saline for approximately 2 minutes, followed by 4% paraformaldehyde in 0.1 M sodium acetate buffer, pH= 6.5, at 4oC for 10 minutes. Perfusion solution was then switched to a 4% paraformaldehyde in 0.1 M sodium borate buffer, pH=9.5, for 15 minutes. Brains were immediately removed from the skull, and post-fixed in 4% paraformaldehyde in 0.1 sodium borate buffer for 6-24 hrs at $4^{o}$C. Brains were then cryoprotected in 20% glycerol in 0.02 M potassium PBS (KPBS) solution, pH=7.4, for at least 24 hrs prior to sectioning. Brains were coronally sectioned at 30 µm on a freezing microtome and collected in five series for processing and storage. For each brain, one 1:5 series was collected in formalin for Nissl staining with 0.25 % thionin, one series was collected in KPBS for immunohistochemical

processing for visualization of the anterograde tracer, and one series was collected in KPBS for fluorescent visualization of the retrograde tracer. Spare series were either collected in PBS and stored at 4$^{o}$ C or in tissue collecting solution (30% ethylene glycol, 25% glycerine, 25% PBS, and 20% dH2O) and stored at -20$^{o}$C.

PHA-L anterograde cases were visualized using a biotinylated secondary antibody with an avidin-biotin reaction, and intensified using osmium tetroxide and thiocarbohydrazide. Free floating sections were first blocked in 0.5% Triton-X (TX) with 5% normal goat serum (NGS) in 0.02 M potassium phosphate buffered saline (KPBS) for 2 hours at room temperature on a rotating plate. This was followed by a primary antiserum incubation for two days in rabbit anti-PHA-L (1:12000; Dako, Carpenteria, CA) with 0.3% TX-100 in 2% NGS in KPBS at 4$^{o}$ C on a rotating plate. Free-floating sections were then washed 3 × 10 minutes in 2% NGS in KPBS prior to incubation in the biotinylated secondary solution. Afterwards, sections were then incubated for one hour in biotinylated goat-anti-rabbit IgG (1:227; Vector Laboratories, Burlingame, CA) in 0.3% TX-100 with 2% NGS in KPBS. Sections then washed 2 × 10 minutes in 2% NGS in KPBS, and then incubated in the avidin-biotin complex (Super ABC Kit; Biomedia Corporation, Foster City, CA) for 45 mins. Following the ABC incubation, sections were washed 2 × 10 minutes in 0.02M KPBS and then returned to the biotinylated secondary solution for an additional 45 minutes. Next, sections were washed 2 × 10 minutes in 0.02M KPBS, and then returned to the ABC solution for an additional 30 minutes. Sections were washed 3 × 10-minutes in 0.02M KPBS prior to the visualization step. For this step, tissue was incubated in 0.05% diaminobenzidine (DAB; Pierce, Tacoma, WA) and 0.04% $H_2O_2$ in KPBS for 5-10 min. Sections were then washed 3 × 10 minutes in

0.02 M KPBS prior to being mounted on gelatin-coated slides. After slides were allowed to dry, they were defatted in a 50% chloroform in 100% ethanol solution for one hour. Slides were then hydrated through graded alcohols for 2 minutes each, prior to 10-20 minute incubation in 0.005% Osmium tetroxide in ddH2O. Slides were then washed for 30 minutes in running tap water, and then incubated for 5-15 minutes in 0.05% thiocarbohydrazide in $ddH_2O$. Following a 30-minute rinse in running tap water, slides were transferred back to the original osmium solution for 10-30 minutes, with background staining determining the length of time for the incubation. Finally, slides were rinsed for 30-minutes in running tap water, dehydrated through graded alcohols, cleared in xylene, and coverslipped with DPX.

BDA anterograde cases were visualized using an avidin-biotin reaction with either the osmium tetroxide and thiocarbohydrazide protocol described above, or a gold chloride procedure for intensification. Free-floating sections were first washed 3 × 10 min in KPBS and pretreated with a 1% solution of TX-100 in KPBS for 1 hr. The sections were then incubated overnight at $4^oC$ in a solution of avidin reagent and stabilizer (1:25 and 1:50 dilutions, respectively; Super ABC Kit; Biomeda Corporation; Foster City, CA) in KPBS plus 0.1% solution of TX. Following 3 × 10 minute washes in KPBS, sections were visualized using a 0.05% DAB with 0.04% H2O2 in KPBS procedure for 5-30 minutes at room temperature depending on the speed of the reaction. Afterwards, sections were washed in KPBS and mounted on gelatin coated or charged slides. Slides were allowed to dry overnight, were defatted in a 50% chloroform in 100% ethanol solution for one hour, and then were hydrated for two minutes each in a series of graded alcohols. BDA was visualized with a 45-minute incubation at $56^oC$ in 1% silver

nitrate in dH2O in the dark. Silver nitrate was neutralized with a 30% ammonium hydroxide in dH2O, and then slides were rinsed with running water for two minutes prior to a 10-minute incubation in 0.2% Gold chloride in $dH_2O$ in the dark. Slides were again washed in running water for two minutes before the silver-gold complex was stabilized in a 5% solution of sodium thiosulfate in dH2O for 10 minutes at 56$^{o}$C. Finally, slides were rinsed for two minutes in running water, dehydrated through graded alcohols, cleared in xylene, and coverslipped with DPX.

Sections to be analyzed for fluorescent retrogradely labeled cells were mounted on gelatin-coated slides. Slides were then dried for 2-4 hrs in a vacuum desiccator at room temperature. Slides were dehydrated 2 × 10 minutes in 100% ethanol, cleared in xylene for 3 × 2 minutes, and coverslipped with DPX or Vectashield (Vector labs, Burlingame, CA).

***Data Analysis***

**Quantification of Anterograde Labeling.** Location of the injection site for the anterograde cases was identified using both bright-field and dark-field optics (Table 2). Some of these cases were previously used to describe the cortical, hippocampal, parahippocampal, and subcortical connections of the PER, POR and EC (Agster & Burwell, 2009, 2013; Agster, Tomás Pereira, Saddoris, & Burwell, 2016; Burwell & Amaral, 1998b). For each case, a 1:5 series of 30 µm sections were examined using darkfield optics on a Nikon Optiphot-2 microscope (Tokyo, Japan) at a magnification of 4x and 10x. Using a methodology described in previous studies (Agster & Burwell, 2009, 2013), for each section, density of fiber labeling for each region of interest was rated on a scale of 0-5: A score of zero indicated no fibers were present; 1, very weak fiber labeling;

2, weak; 3, moderate; 4, dense; and 5, very dense fiber labeling. The ratings were adjusted for each animal such that the full scoring range was used. A final estimate of anterograde label density was made for each target region and for each injection site by averaging across all sections.

**Quantification of Retrograde Labeling.** Location of the injection site for the retrograde cases was identified using bright-field optics (Table 2). These cases were previously used to describe the cortical, hippocampal, and parahippocampal connections of the PER, POR and EC (Agster & Burwell, 2013; Burwell & Amaral, 1998a, 1998b; Tomás Pereira, Agster, & Burwell, 2016). Using a methodology described in previous studies (Agster & Burwell, 2013), the distribution of fluorescently labeled cells was plotted for a 1:10 series in the hemisphere ipsilateral side to the injection using Neurolucida 10 software (Microbrightfield Inc., Colchester, VT) interfaced with either a Nikon Optiphot-2 microscope or a Nikon E600 microscope (Tokyo, Japan) at a total magnification of 100X. For quantification, contours of the subcortical areas of interest and POR were drawn using Nissl-stained sections aligned with the brain contour drawn from the fluorescent retrograde sections. Neuroexplorer 10 analysis software (Microbrightfield Inc., Colchester, VT) was used to analyze each region of interest and the total number of labeled cells identified in the region of interest. Total cell numbers were first normalized for each section using a correction factor derived from the total number of labeled subcortical cells for each case. These cell counts were then multiplied by 10, to account for the 1:10 series, to estimate the total cell count in the region of interest. The volume of the region of interest was estimated by multiplying the total area of each section by 10 to account for the 1:10 series. The density of labeled cells for the region of interest was then

calculated by dividing the estimated total number of cells by the estimated volume of the region of interest. Total cell counts were also used to calculate the percent of cells labeled in a subdivision, out of total number of cells in the region of interest.

Table 2. Description of injection sites for cases included in analyses

| case | Type | | Location | Layers | Size (μm) |
|---|---|---|---|---|---|
| 13-052 | anterograde | BDA | LPMR/LPLR | n/a | 200 |
| 13-053 | anterograde | BDA | LPLR | n/a | 300 |
| 13-054 | anterograde | BDA | LPMR/LPMC | n/a | 300 |
| 13-089 | anterograde | BDA | LPLR | n/a | 100 |
| 13-090 | anterograde | BDA | LPLR | n/a | 200 |
| 13-091 | anterograde | BDA | LPLR | n/a | 100 |
| 102* | retrograde | FB | Rostral POR | V | 200 |
| 97* | retrograde | FB | Rostral POR | V | 400 |
| 98* | retrograde | FB | Middle POR | I-VI | 600 |
| 95* | retrograde | DY | Caudal POR | III-VI | 400 |
| 99* | retrograde | FB | Caudal POR | I-V | 500 |
| 100* | retrograde | FB | Caudodorsal POR | I-VI | 500 |
| 83* | anterograde | BDA | Rostral Dorsal POR | V-VI | 500 |
| 39* | anterograde | PHA-L | Rostral POR | I-IV | 400 |
| 134* | anterograde | BDA | Dorsal POR | I-VI | 500 |
| 40* | anterograde | PHA-L | Caudal POR | III-VI | 500 |

*Animals previously reported in Burwell and Amaral, 1998a, 1998b. Size of injection is reported as the diameter of the injection site dye core. Abbreviations list: BDA: biotinylated dextran amined, DY: diamidino yellow, FB: fast blue, PHA-L: *Phaseolus vulgaris*-leucoagglutinin. All abbreviations for this and the following tables can be found in the list of abbreviations.

**Nomenclature**

Definition of the POR borders were from a previous study (Burwell, 2001). The POR usually begins at the caudal end of the angular bundle, just caudal to the end of the PER, area 36. The POR is bordered ventrally by the medial EC and lies dorsal to the rhinal sulcus. The most rostral extent of the POR can be divided into two subfields, a dorsal POR (PORd) and ventral POR (PORv) based on the cytoarchitecture (Burwell, 2001). Our analysis also included a rostral/caudal division of the POR for the purpose of observing a topographic map of interconnections with the LP and the PPC.

For nomenclature and coordinates of the LP, we used Paxinos and Watson, adapted in Figure 1A-F (Paxinos & Watson, 2005). The definition of the LP and its subdivisions are taken from Takahashi (1985), shown in Figure 1G. Three subdivisions of the LP were first identified on the basis of cytoarchitecture — the nucleus lateralis posterior pars rostromedialis (LPMR), nucleus lateralis posterior pars caudomedialis (LPMC), and the nucleus lateralis posterior pars lateralis (LPL). Six coronal levels are shown in Figure 1A-F, with an overhead view of the nuclei shown in Figure 1G. The rostral end of the LPMR appears medial to the nucleus lateralis dorsale pars dorsomedialis (LD) and lateral to centrolateral nucleus (Takahashi, 1985). The LPMR is bordered laterally by the LPL and dorsally by the emerging LPMC. The LPMC emerges dorsal to the caudal tail of the LPMR, and is bordered medially by the anterior pretectal nucleus and laterally by the LPL. The caudal portion of LPMC is bordered dorsal-medially by the nucleus of the optic tract and ventral medially by the olivary pretectal nucleus. The LPL lies medial to the intramedullary thalamic area and lateral to the LPMR and LPMC. The LPL is further subdivided into the pars rostralis (LPLR) and pars caudalis (LPLC) based on its connectivity. LPLC, a narrower caudal portion of the LPL, receives input from the superficial layers of the ipsilateral SC, whereas LPLR receives no collicular input, but does receive input from cortical areas 17 and 18 (Takahashi, 1985). This border, however, is not distinct based off of cytoarchitecture, but a working division can be used, where LPLR ends with the appearance of the rostral limit of LPMC. Subnuclei were identified and confirmed by comparing the gold intensified BDA sections with the corresponding Nissl stained sections. The subnuclei of the LP are known to have

a differential neuronal morphology, which is identifiable using cytoarchitecture (Takahashi, 1985).

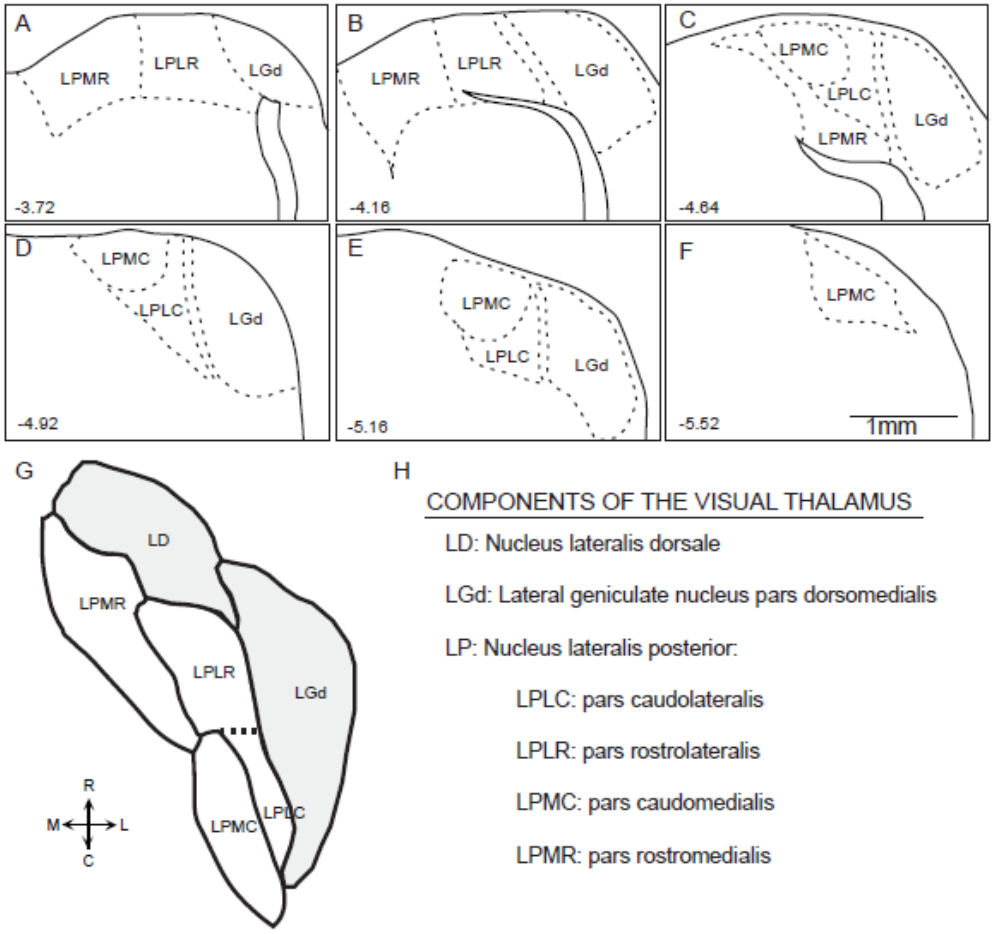


Figure 1. Subdivisions of the lateral posterior nucleus of the thalamus. A-F. The subdivisions of the LP shown as coronal sections through the rat brain, adapted from Paxinos and Watson (2005). The dorsal part of the lateral geniculate nucleus (LGd) is included for reference. G. Subdivisions of the LP shown from a superior view, looking down on the rat brain from above, which is adapted from Takahashi (1985) and provides an important visual aid in distinguishing the alignment of the subdivisions of the LP. The lateral dorsal nucleus (LD) is shown with the LGd for reference. H. Components of the visual thalamus.

The PPC in the rat is a long strip of cortex located between somatosensory cortex and visual cortex that can be divided into dorsal and caudal limbs (Figure 2). The dorsal limb extends from close to the midline and then turns caudally becoming the caudal limb of this brain area (Paxinos & Watson, 2005; Swanson, 1992). The dorsal limb, which is

about 3.5-5.0 mm caudal to bregma and 1.5-5.0 mm lateral from the midline is much better studied, as fewer investigators have recognized the demarcation of the caudal limb. This may have resulted because two prominent atlases agree more on the dorsal portion of the PPC than the caudal portion. We thought it important to include both limbs because of different connection patterns. The dorsal portion of the PPC is known to be interconnected with frontal regions (Reep et al., 1994). The caudal limb is more robustly interconnected with the POR than the dorsal limb (Burwell & Amaral, 1998a).

For the PPC, we used nomenclature and borders from both Paxinos and Watson (2005) and Swanson (1992). Paxinos and Watson (2005) subdivided the parietal regions into the medial parietal association cortex (MPtA), lateral parietal association cortex (LPtA), and the posterior parietal association cortex. The posterior region was further subdivided into the dorsal posterior parietal posterior area (PtPD), the rostral posterior parietal posterior area (PtPR), and the caudal posterior parietal posterior area (PtPC). In Swanson (1992), the parietal region, posterior association area (PtLP) is a cortical area ranging from 3.9-6.9 mm caudal to bregma and 1.0-5.0 mm from the midline. The border of caudal limb of the PtLp in Swanson's definition is more extended (to 6.9 mm posterior to bregma) than the PtPC (the limit is about 6.1 mm posterior to bregma) in Paxinos & Watson (2005). Because both atlases are widely used, we quantified our data using both sets of borders and nomenclatures.

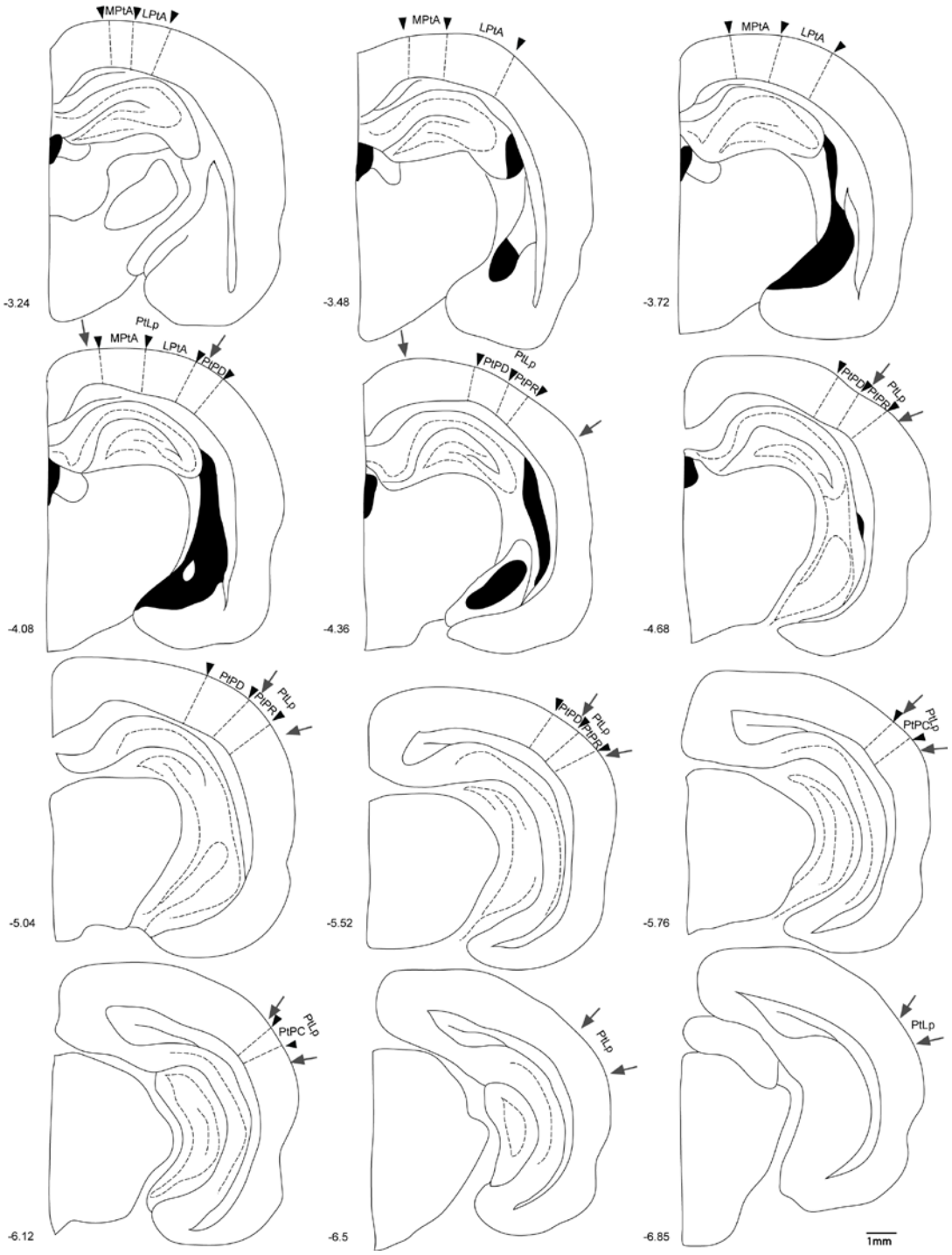


Figure 2. Subdivisions of the posterior parietal cortex (PPC). Black texts were medial parietal association cortex (MPtA), lateral parietal association cortex (LPtA), and parietal cortex, posterior area, caudal part (PtPC); dorsal part (PtPD); rostral part (PtPR) (Paxinos & Watson, 2005) . Gray texts were parietal region, posterior association area (PtLP) (Swanson, 1992).

## Results

### *Identification of Injection Sites*

The site of a retrograde injection was defined as the area that encompassed the dye core and the region of necrosis surrounding it. The site of an anterograde injection was defined as the area containing the most labeled cell bodies. The estimated size of the injection sites and laminar location of the injection sites for each case are provided in Table 2. The locations of all injection sites analyzed are shown in Figure 3.

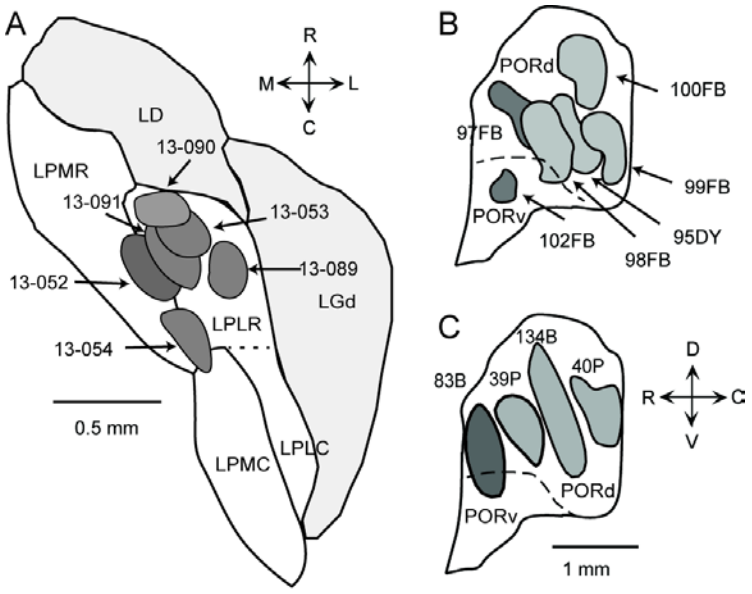


Figure 3. Injection sites. A. Location of anterograde sites in the LP. B. location of retrograde sites in the POR. C. Location of anterograde sites in the POR. See Table 1 for abbreviations.

### *Projections from LP to POR*

Anterograde injections from six LP cases were analyzed. A distinct pattern of labeling was seen as a result of each injection, depending on the location of the injection site (Figure 3A). One injection site involved LPMR and LPLR, one involved LPMR and LPMC, and four sites were confined to LPLR.

Overall, the four cases restricted to LPLR resulted in the weakest labeling in the POR. Cases 13-053 and 13-091 resulted in weak fiber labeling in the rostral portions of both dorsal and ventral POR. Labeling in the POR from both more rostral LPLR injection site was observed in the most caudal sections of POR, with only moderate labeling in layer IV (Figure 4D-F). The other two LPLR cases, 13-089 and 13-090 resulted in slightly different patterns of labeling in the POR.For case 13-089 with injection site in the caudal LPLR, labeled fiber was observed in dorsal POR, especially heavier in the caudal portion, and there is only poor labeling in the ventral POR. In case 13-090 with injection site in the most rostral LPLR, no labeling was observed in either POR subdivision. These results suggest that the LPLR projects only weakly to the POR, limited to caudal levels of PORd.

Case 13-052 had an injection site that involved both the LPMR and LPLR (see Figure 3A and Table 2). This more rostral injection site in the LP resulted in strong fiber labeling in all aspects of the POR. The density of labeled fibers was consistent throughout dorsal POR. Most of the labeled fibers were in the deep layers of POR, which is consistent with thalamic nuclei innervation of layer IV of cortex. Because POR has a poorly differentiated layer IV, this pattern of labeling would be seen as a modified feed forward projection. The density of labeling was greatest in the caudal parts of POR (Table 3, Figure 4A-C). Because LPLR injection sites result in weaker and more restricted labeling, we can conclude that the LPMR projects to all.

Case C13-054 (Figure 4G-I), had an injection site a little more caudal than the other cases, and was located on the midline between the LPMR and LPMC. This injection site produced poor labeling in the rostral sections of POR. Labeled fibers were

observed mostly in the caudal of POR. Labeling in the caudal part of POR was very strong, and restricted to the deep layers of POR. This pattern of labeling shows that the midline nuclei of the LP have strong projections to the caudal portion of the POR. It is difficult to determine whether the labeling in the POR is from LPMC or LPMR given the midline placement of the injection. However, comparing this site with 13-052 suggests that the LPMC projects weakly to the POR and most likely only to the caudal part of PORd.

The labeling patterns varied across different LP anterograde injections indicating that the nuclei of the LP differentially project to the POR in a topographic manner, shown in Figure 4. In summary, LPMR provides strong input throughout the POR, whereas the LPLR projects weakly to the POR primarily to the caudal portion of the POR. The caudal portions of the LPMR and the LPMC mainly project to the caudal portions of the POR.

Table 3. LP input to POR: Density of anterogradely labeled fibers in POR

| | LP Injection Sites | | | | | |
|---|---|---|---|---|---|---|
| Target Region | C13-052 LPMR/LPLR | C13-054 LPMR/LPMC | C13-053 LPLR | C13-089 LPLR | C13-090 LPLR | C13-091 LPLR |
| PORv | +++ | + | - | + | - | - |
| rPORd[†] | +++ | + | - | ++ | - | + |
| cPORd[†] | +++++ | +++++ | +++ | ++++ | - | ++ |

Densities are shown using a quantitative scale of 0-5 to capture the density of anterograde labeled fibers in the region of interest. The averages were then translated into the following symbol scale: (-) 0-0.5; (+) 0.5-1.5; (++) 1.5-2.5; (+++) 2.5-3.5; (++++) 3.5-4.5; (+++++) 4.5-5.0. [†]The PORd has been divided into the rostral portion (rPORd) and a caudal portion (cPORd). See list of abbreviations.

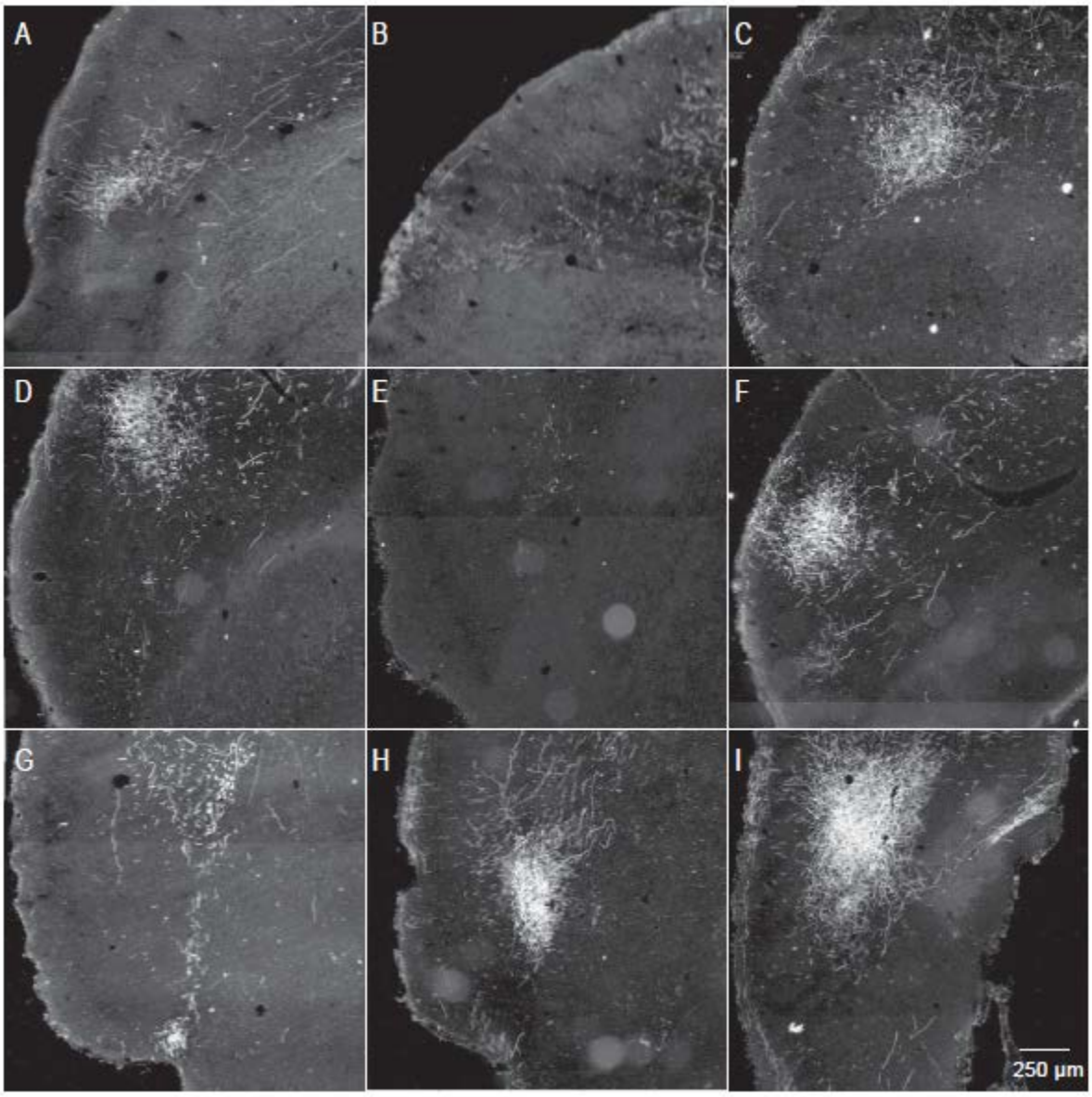


Figure 4. Anterograde labeling in the POR arising from injections in the LP. A-C, case 13-052 whose injection site was located in the LPMR showed the densest labeling in the caudal PORd, with some minor labeling in PORv. D-F, case 13-053 whose injection site was located in LPLR showed poor labeling throughout the POR, except in the most caudal sections, F. G-I, case 13-054 whose injection site was located in the caudal part of LPMR and most rostral part of LPMC. The labeling was found to be the most dense in the more caudal portions of PORd, with less labeling in the rostral portion of POR. Distance from Bregma is about -7.8 in A,D,E; -8.3 in B,E,G; and -8.8 in C,F, I. Scale bar shown is 250 µm.

Retrograde tracer injections in POR resulted in fluorescently labeled cells in the LP for all cases, regardless of the location of the injection site in the POR. The specific

location and size of these injection sites are provided in Table 2 and Figure 3. Case 102 was located in the middle of PORv in layer V. Case 100 was located in the caudal and dorsal part of PORd. The remaining cases (97, 98, 95, and 99) were in the ventral PORd and ranged from rostral to caudal levels, respectively.

All cases resulted in labeled cells in all four subdivisions of the LP. The relative density of labeled cells in the LP subdivisions, however, varied according to the placement of the injection site in the POR (Figure 3B and Table 4). Rostral POR injections (102 in PORv and 97 in rostral and ventral PORd) resulted in overall lower density, but relatively higher density of labeling in the LPMC compared to other subdivisions of the LP. These injection sites were restricted to layer V. Although both injections were restricted to the deep layers of POR, case 102 showed relatively denser labeling in the LP compared to case 97. The densest labeling was found in LPMC (Figure 5A-C).The next lowest density of labeling resulted from case 100, located in dorsal and caudal PORd. Case 100 resulted in relatively more labeled cells in the LPMR, followed by the LPMC with lower densities in the other subdivisions. Injection sites in cases 98, 95, and 99 were located in all layers of ventral PORd and ranged from midrostrocaual to caudal levels. In case 98 labeled cells were observed throughout the LP, especially in the LPMR and LPMC (Figure 5D-F). The adjacent injection site, case 95, showed a similar pattern, with the heaviest densities of labeled cells in the LPMR and LPLR (Figure 5G-I). The caudally located injection site in case 99 resulted in the overall highest density of labeled cells, with the relatively highest densities located in the LPMC, followed by the LPLC.

To summarize, the more caudal and ventral cases produced the highest densities of labeled cells in the LP (Table 4). Injection sites that spanned layer IV, which thalamic projections usually target, resulted in a higher densities of labeled cells. Finally, the medial subnuclei of the LP are more densely labeled than the lateral subnuclei.

Table 4. LP input to POR: Density of retrogradely labeled cells in the LP

| | POR Injection Sites and Laminar Location | | | | | |
|---|---|---|---|---|---|---|
| Target Region | C102 V | C97 V | C98 I-VI | C95 III-VI | C100 I-VI | C99 I-V |
| LPMR | 95 | 96 | 183 | 315 | 573 | 59 |
| LPLR | 83 | 95 | 84 | 280 | 115 | 46 |
| LPMC | 323 | 126 | 252 | 168 | 360 | 551 |
| LPLC | 161 | 82 | 79 | 131 | 168 | 285 |

For each injection site the density of labeled cells (cells/mm$^3$) is shown for each LP target region. The laminar location of the injection site in the POR is shown for each case. See list of abbreviations

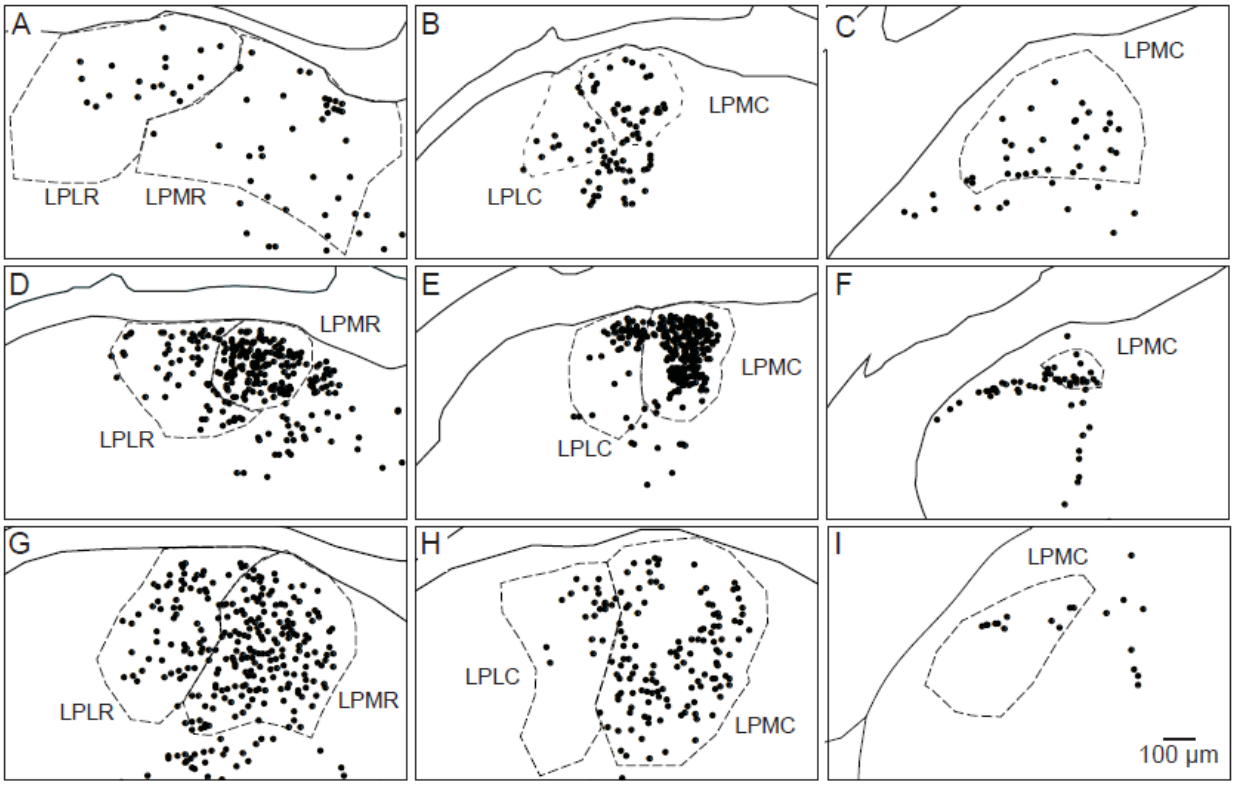


Figure 5. Schematic of the retrograde labeled cells in the LP arising from injections in the POR. A-C. Representative case 102FB, whose injection site was located in the deep layers of rostral POR shows very little labeling throughout the LP. Labeled cells are predominantly seen in medial subdivisions of the LP. D-

F. Representative case 98, whose injection site was located in all layers of mid rostral-caudal POR.Labeled cells are seen throughout the LP, with dense labeling in the medial subdivisions, LPMR (D) and LPMC (E,F). G-I. Representative case 95, whose injection site was located in caudal POR spanning all layers, this injection resulted in labeling throughout the LP, with dense labeling in the medial subdivisions, LPLR and LPMR. Estimated distance from Bregma is -4.0 in A; -4.3 in D,G; -5.0 in B, E, H; -5.5 in C,I; and -5.6 in F. Scale bar shown is 100 μm.

Table 5 shows the percentages of labeled cells in each LP subnucleus resulting from the six POR injection sites. This table provides a different view in that it shows the distribution of labeled cells across the subnuclei of the LP. Here one can see that for every case, the percentage of labeled cells is higher in the medial subnuclei than its associated lateral subnuclei. In other words, for every case the percentage of labeled cells is higher in the LPMR than in the LPLR, and the percentage of labeled cells is higher in the LPMC than in the LPLC. Moreover, for the more rostral injection sites, the caudal subnuclei exhibit a higher percentage of labeled cells than the rostral subnuclei. For the more caudal POR injection sites, the pattern is different. Except for C99, the rostral subnuclei exhibit a higher percentage of labeled cells than the caudal subnuclei.

Table 5. LP input to POR: Percentage of retrogradely labeled cells in LP subnuclei

| | | POR Injection Sites and Laminar Location | | | | | |
|---|---|---|---|---|---|---|---|
| Target Region | Mean | C102 V | C97 V | C98 I-VI | C95 III-VI | C100 I-VI | C99 I-V |
| LPMR | 37.88 | 16.62 | 29.65 | 34.91 | 44.97 | 61.43 | 24.91 |
| LPLR | 14.58 | 8.83 | 13.32 | 12.64 | 24.60 | 12.78 | 11.52 |
| LPMC | 34.16 | 52.47 | 39.20 | 42.21 | 25.55 | 18.39 | 39.87 |
| LPLC | 13.31 | 22.08 | 17.84 | 10.24 | 4.88 | 7.40 | 23.34 |

Total number of estimated cells were calculated by first correcting the number of cells for each case, by multiplying by its correction factor. The correction factor was calculated based off of the total number of subcortical cells labeled, averaged across each case. The corrected numbers of cells were then multiplied by 10 (given that we used a 1:10 series for analysis) to estimate the total number of cells in each region, which was then divided by the estimated total number of labeled cells in the LP to yield the following percentages.

Taken together, our observations suggest that the LP projects more strongly to caudal POR than to rostral POR. In addition, the medial subnuclei project to POR more strongly than the lateral subnuclei. These projections terminate more strongly in layer IV and subgranular layers that in supergranular layers. The density of labeling seen in the LP increased, as the POR injection sites were more caudal in origin, which suggests caudal POR receives the strongest projections from LP, a conclusion that is confirmed by the LP anterograde injections.

***Projections from POR to LP***

All anterograde injection sites in the POR resulted in labeling in the LP, regardless of rostral or caudal placement of the injection (Table 2). The density of labeling in the subdivisions of the LP did vary according to the placement of the injection in POR. The location of injection sites for the four cases was distributed along the rostrocaudal axis of the POR (Table 2 and Figure 3C). During analysis, the density of labeling was quantified in each of the four subdivisions of the LP and the density estimates for each case are shown in Table 6.

Injections located in rostral POR showed a great density of labeled fibers throughout the LP (case 83, Table 6, Figure 6A-C). The patters were similar for the two rostral injection sites, despite differences in the laminar location of the injection sites. Specifically, a greater density of labeled fibers was observed in LPMC and LPLC. The density of labeling in the caudal subdivisions was greater than that observed in the LPMR and LPLR. Labeled fibers were still observed in these rostral subdivisions. Similar labeled pattern was observed in case 39, which also had injections located in rostral POR

(Table 6). These results suggest that rostral POR does project to all regions of the LP, but that the projection to the caudal regions is heavier.

Injections located in caudal POR resulted in a different pattern of labeling. Caudal sites gave rise to a heavier density of labeling in the rostral subdivisions of the LP (case 40, Table 6, Figure 6D-F). Specifically, a dense pattern of anterograde labeling was observed in the LPMR and LPLR. The density of labeling in the LPMR as a result of caudal POR injections was greater than the labeling in any other subnucleus of the LP. Density of labeled fibers was also higher in LPLR than in LPMR. This pattern of labeling likely reflects that case 40 was both a deep and ventral injection site. The other caudal POR injection, case 134, also showed relatively higher density of labeled fibers in the LPMR compared to the other LP subdivisions.

Overall, it appears that rostral POR projects to the caudal subdivisions of the LP, whereas caudal POR projects to the rostral subdivisions of the LP.

Table 6. POR input to LP: Density of anterogradely labeled fibers in LP

| | POR Injection Sites | | | |
|---|---|---|---|---|
| Target Region | 83 V-VI | 39 I-IV | 134 I-VI | 40 III-VI |
| LPMR | ++ | +++ | +++ | ++++ |
| LPLR | +++ | +++ | + | +++ |
| LPMC | +++++ | +++++ | + | + |
| LPLC | +++++ | +++++ | + | ++ |

Densities are shown using a quantitative scale of 0-5 to capture the density of anterograde labeled fibers in the region of interest. The averages were then translated into the following symbol scale: (-) 0-0.5; (+) 0.5-1.5; (++) 1.5-2.5; (+++) 2.5-3.5; (++++) 3.5-4.5; (+++++) 4.5-5.0. See list of abbreviations.

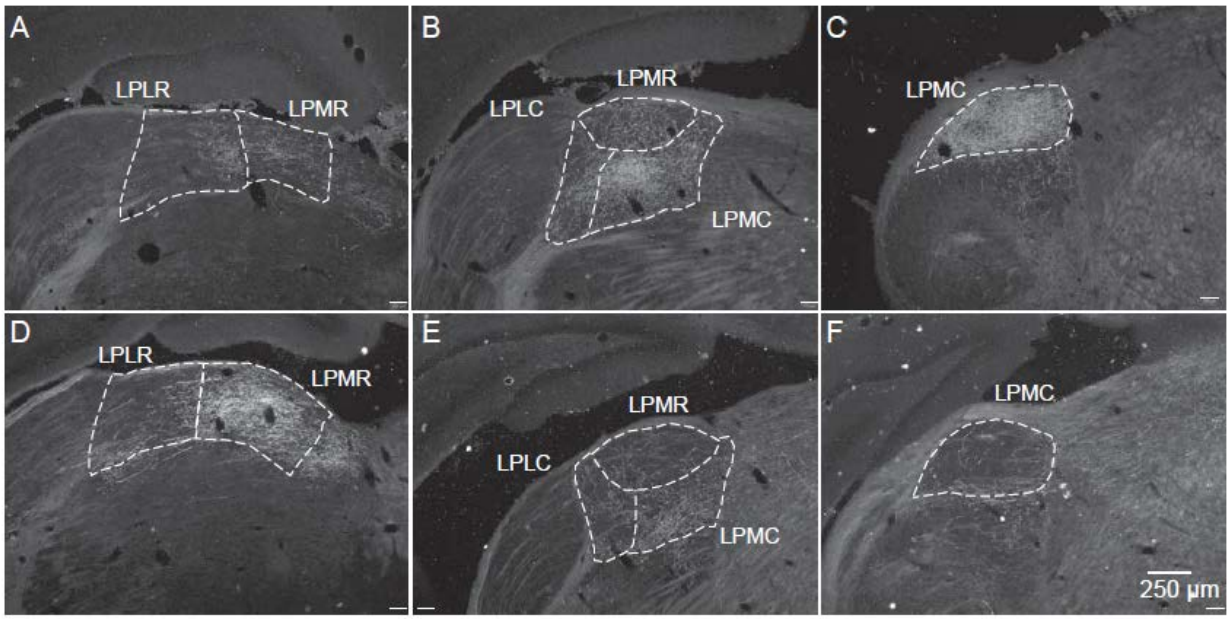


Figure 6. Anterograde labeling in the LP arising from injections in the POR. A-C, representative case 83 is shown to demonstrate labeling pattern of a rostral POR injection site. A greater density of labeled fibers is seen in caudal LP, specifically in LPMC. D-F, representative case 40 is shown to demonstrate the labeling pattern of a caudal POR injection site. A greater density of labeled fibers is seen in rostral LP, specifically in the LPMR. Distance from Bregma is about -4.1 in A,D; -4.6 in B,E; and -5.5 in C,F. Scale bar shown is 250 µm.

### *Projections from LP to the PPC*

The detailed injection sites are described in Table 2 and locations are shown in Figure 3A. The labeling pattern of cases 13-053 and 13-091, whose injection sites were mainly in LPLR, were similar. Both these two cases showed labeling fibers across entire PPC. The heaviest density of labeled fibers was observed in PtPC, especially in the deep layers (Table 7, Figure 7). There was moderate density of labeled fibers in the other subdivisions. In addition, the caudal portions of the PtPD and PtPR had more labeled fibers than those in the rostral portions. The other two cases, cases 13-089 and 13-090, whose injection sites are also located in LPLR resulted in different labeling patterns. Case 13-089 showed a greater density of labeled fibers across all PPC regions than the other cases. The heaviest density was found in PtPD and PtPR, especially in the caudal portions of these two regions (5.4-5.6 mm caudal to bregma). The case 13-090 with injection site in the most rostral LPLC showed a greater density in rostral portions (MPtA and LPtA) and less labeled fibers in the caudal portions (PtPD, PtPR, and PtPC).

One case, case 13-052, had an injection site located mostly in the LPMR but with some involvement in LPLR and displayed a strong fiber labeling in the PtPD and PtPR, whereas other PPC subdivisions (MPtA, LPtA and PtPC) had moderate density of labelled fibers. The densest labeling fibers were in the deep layers (Table 7, Figure 8). Another case, 13-054, whose target injection site was located in caudal portion of the LPMR and parts of the LPMC, showed heaviest density of labeled fibers in the PtPC, followed by the PtPD and PtPR (Table 6, Figure 9). This case also had moderate labeling fibers shown in the rostral portions of the PPC (MPtA and LPtA).

Similar labeling patterns were found in PtLp regions as used in Swanson (1992). In case 13-053, 13-089, 13-090 and 13-091 with injection sites mainly within LPLR displayed labeled fibers throughout all PtLp subdivisions. Specifically, in cases 13-053 and 13-091, greater density of labeled fibers in was observed in the caudal portion of the PtLp than in the dorsal portion (Table 7, Figure 7). In case 13-089, both dorsal and caudal portions of the PtLp displayed dense labeling fibers. In case 13-090, whose injection site was also located in the LPLR, showed a different labeling pattern and gets more LP projections in the dorsal portion of the PtLp. Case 13-052, whose injection site mainly in the LPMR and LPLR, had heavier density of labeled fibers in the dorsal portion of the PtLp and moderate density in the caudal portion of the PtLp (Table7, Figure 8). Case 13-054, whose injection site was located in the caudal portion of the LPMR and part of the LPMC, showed dense labeling throughout all PtLp regions, especially in the DPtLp and the most posterior portion of the CPtLp (Table 7, Figure 9).

Table 7. LP input to PPC: Density of anterogradely labeled fibers in PPC

| | LP Injection Sites | | | | | |
|---|---|---|---|---|---|---|
| Target Region | C13-052 LPMR/LPLR | C13-054 LPMR/LPMC | C13-053 LPLR | C13-089 LPLR | C13-090 LPLR | C13-091 LPLR |
| **PPC**[†] | | | | | | |
| MPtA | ++ | ++ | ++ | +++ | +++ | + |
| LPtA | ++ | ++ | ++ | +++ | ++++ | ++ |
| PtPD | ++++ | ++++ | ++ | ++++ | ++ | ++ |
| PtPR | ++++ | ++++ | ++ | ++++ | +++ | +++ |
| PtPC | ++ | +++++ | +++++ | +++ | + | ++++ |
| **PtLp**[††] | | | | | | |
| DPtLp | ++++ | +++++ | ++ | +++ | ++++ | ++ |
| CPtLp | ++ | ++++ | ++++ | +++ | ++ | +++ |

Densities are shown using a quantitative scale of 0-5 to capture the density of anterograde labeled fibers in the region of interest. The averages were then translated into the following symbol scale: (-) 0-0.5; (+) 0.5-1.5; (++) 1.5-2.5; (+++) 2.5-3.5; (++++) 3.5-4.5; (+++++) 4.5-5.0. [†]Paxinos and Watson (1995). [††]Nomenclature from Swanson (1992). See list of abbreviations.

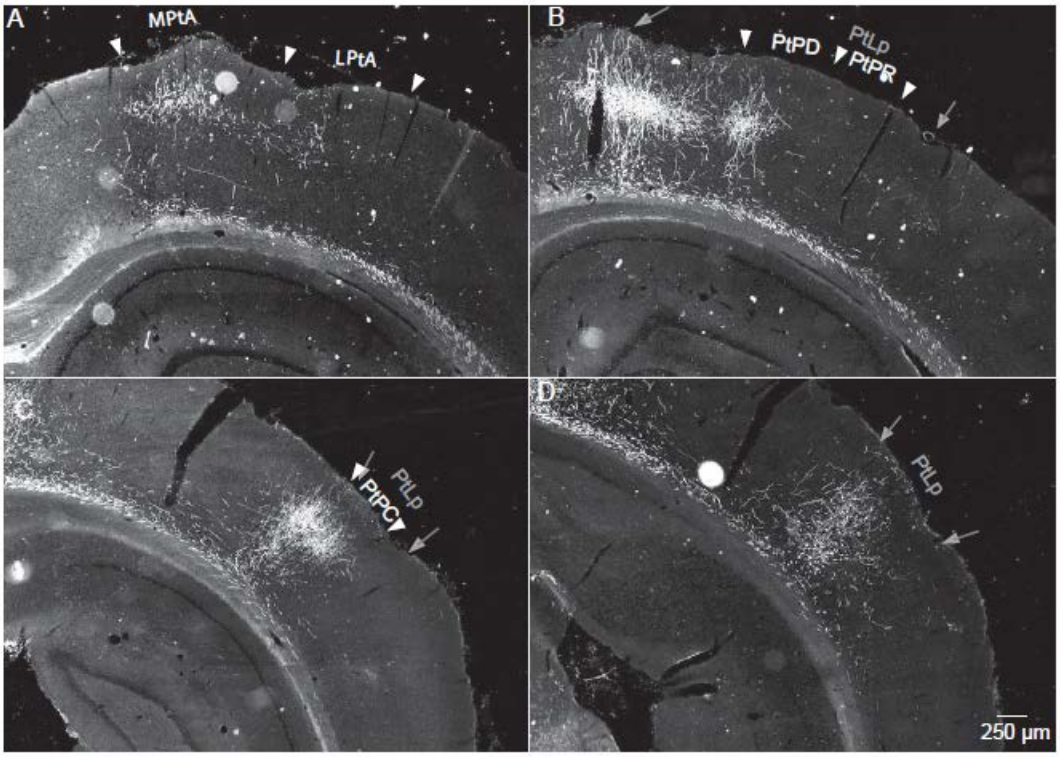


Figure 7. Anterograde labeling in the PPC arising from injections in the LP (case 13-053). This case whose injection site was located in LPLR showed poor labeling throughout the dorsal portions of the PPC, however, denser labeling was observed in more caudal sections. Distance from bregma is about -3.8mm in A; -4.8 mm in B; -5.7 mm in C; -6.4 mm in D. Scale bar shown is 250 µm.

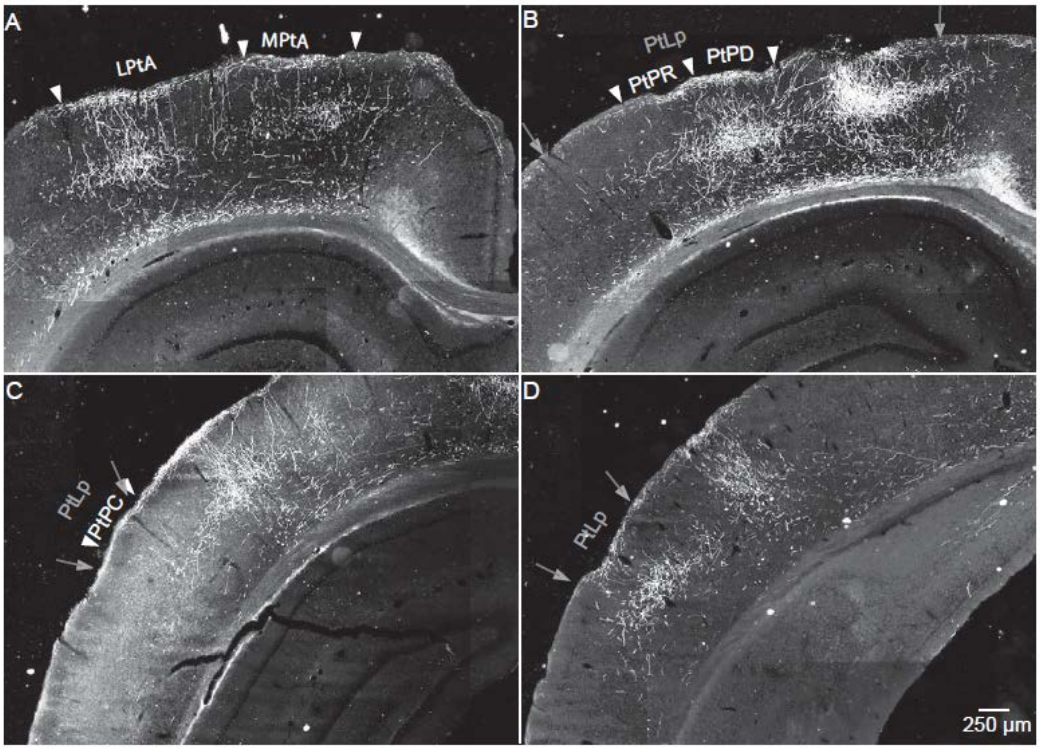


Figure 8. Anterograde labeling in the PPC arising from injections in the LP (case 13-052). This case whose injection site was located in the LPMR and LPLR showed the densest labeling in the PtPD and PtPR, which are dorsal portions of the PtLp and much weaker labeling patterns in other subregions of the PPC. Distance from bregma is about -3.6 mm in A; -4.3 mm in B; -5.7 mm in C; -6.5 mm in D. Scale bar shown is 250 µm.

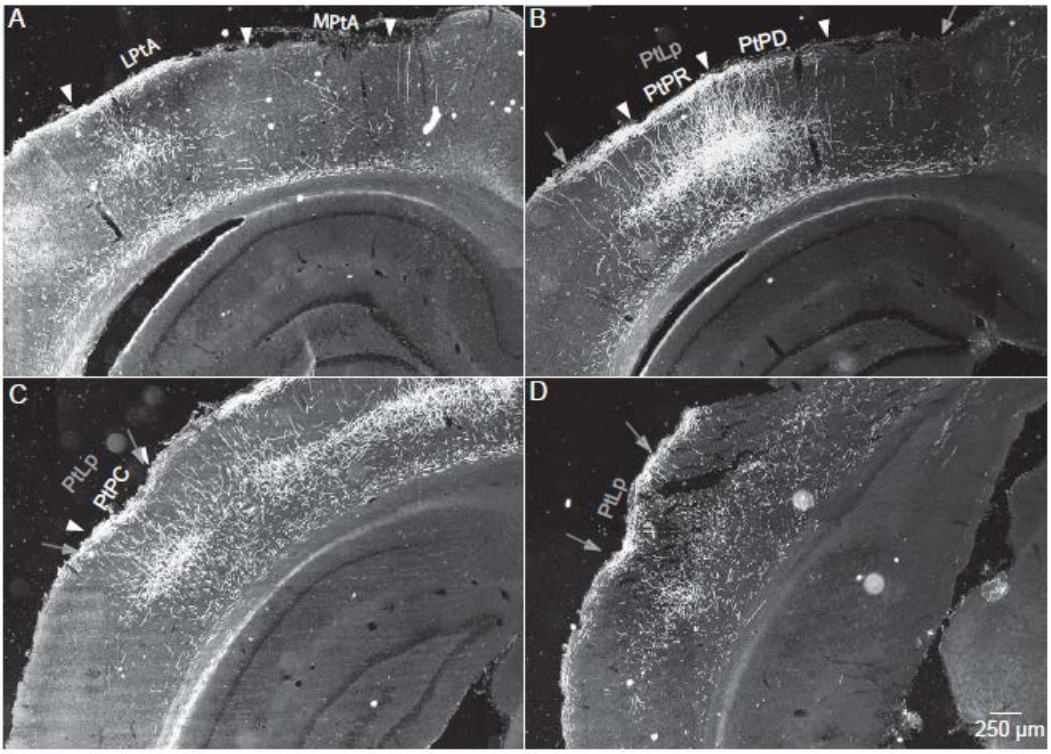


Figure 9. Anterograde labeling in the PPC arising from injections in the LP (case 13-054). This case whose injection site was located in the caudal part of LPMR and most rostral part of LPMC showed dense labeling throughout the PPC, except the most rostral portion of the PPC (MPtA and LPtA). Distance from bregma is about -3.6 mm in A; -4.2 mm in B; -5.7 mm in C; -6.6 mm in D. Scale bar shown is 250 µm.

### *Projections from the PPC to POR*

Retrograde tracer injections in POR resulted in fluorescently labeled cells in parietal association cortex in all cases, regardless of injection locations in the POR (Table 8). The detailed injection location and size of these injections are provided in Table 2 and Figure 3B. The density of labeled cells in the subdivision of the PPC varied based on the injection site in the POR. In general, more rostral portions of the POR received projections from more lateral and caudal portions of PPC (PtPD, PtPR, PtPC, and CPtLp) compared to the projections from medial dorsal portions of it (MPtA, LPtA, and DPtLp). Compared two rostral POR injections, a more ventral POR injection (case 102) showed a greater density of labeled cells in more caudal portions (Table 8, Figure 10) than the other

rostral POR injection case (case 97). The injection site in the middle POR, case 98, displayed a similar labeling pattern to the other two rostral cases having greatest density of labeled cells in the caudal portions, especially in layer II-III. In addition, case 98 also showed heavy densities of labeled cells in the PtPD and PtPR, which is about the DPtLp (Table 8, Figure 11).

For the cases with injection locations in more caudal POR (cases 95, 99 and 100), different patterns of labeling were observed. Cases 95 and 99 showed the heaviest density of labeled cells in the PtPC and the most caudal sections of the CPtLp. Comparing these two cases, case 95, with an injection restricted to layers III-VI, displayed greater densities of labeled cells in MPtA and LPtA than case 99. Case 99, whose injection site was more dorsal and injection was distributed across layer I-V, had the heaviest density of labeled cells in the PtPC (Table 8, Figure 12). In terms of the PtLp (Swanson, 1992), the POR received more projections from the caudal portion of the PtLp compared to the projections from the dorsal portion of it. The other caudal POR injection, case 100, had a poor labeling pattern throughout the PtLp, however, it seemed still receiving more projections from the most caudal sections of the CPtLp.

Table 8. PPC input to POR: Density of retrogradely labeled cells in the PPC

| | POR Injection Sites and Laminar Location | | | | | |
|---|---|---|---|---|---|---|
| Target Region | C102 V | C97 V | C98 I-VI | C95 III-VI | C100 I-VI | C99 I-V |
| **PPC**† | | | | | | |
| MptA | 11 | 37 | 27 | 50 | 48 | 2 |
| LPtA | 7 | 9 | 6 | 21 | 5 | 1 |
| PtPD | 118 | 90 | 73 | 64 | 24 | 40 |
| PtPR | 139 | 109 | 62 | 33 | 52 | 27 |
| PtPC | 334 | 167 | 87 | 106 | 27 | 87 |
| **PtLp**†† | | | | | | |
| DPtLp | 66 | 83 | 58 | 42 | 56 | 7 |
| CPtLp | 346 | 87 | 101 | 107 | 153 | 58 |

For each injection site the density of labeled cells (cells/mm$^3$) is shown for each PPC subdivions. The laminar location of the injection site in the POR is shown for each case. †Paxinos and Watson (1995). ††Nomenclature from Swanson (1992). See list of abbreviations.

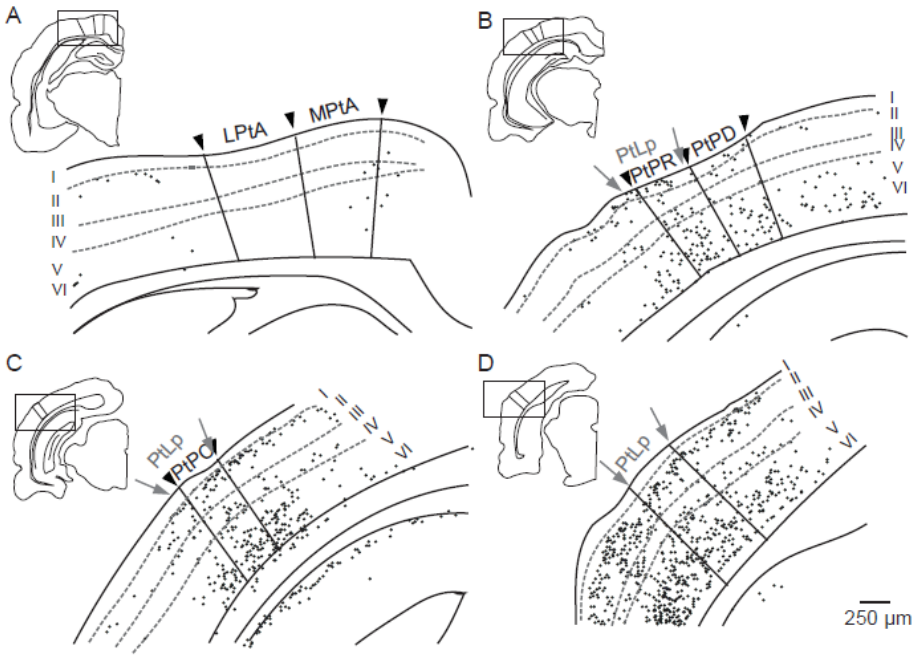


Figure 10. Schematic of the retrograde labeled cells in the PPC arising from injections in the POR. A-D, Representative case 102 whose injection site was located in the deep layers of rostral POR shows weak to moderate labeling in the dorsal portions of the PPC. Denser labeled cells were found in the more caudal sections. Estimated distance from bregma is -3.7 mm in A; -4.7 mm in B; -5.8 mm in C; -6.7 mm in D. Scale bar shown is 250 µm.

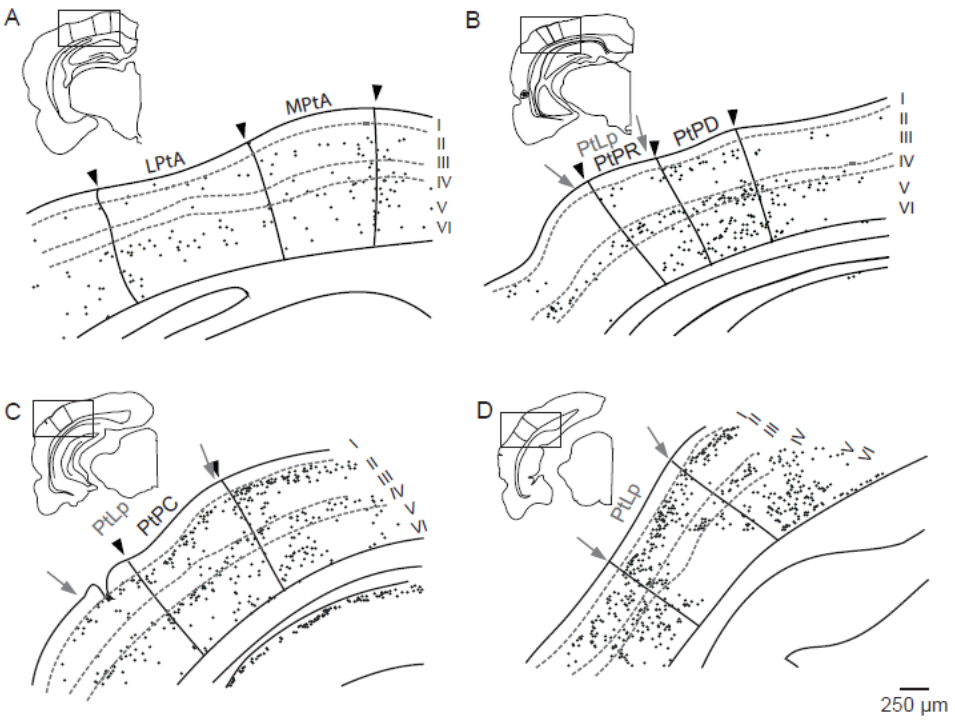


Figure 11. Schematic of the retrograde labeled cells in the PPC arising from injections in the POR. A-D, Representative case 98 whose injection site was located in all layers of mid rostra-caudal POR. Labeled cells were seen throughout entire parietal association cortex, with heavier labeling in the more caudal sections. Estimated distance from bregma is -3.6 mm in A; -4.8 mm in B; -5.8 mm in C; -6.7 mm in D. Scale bar shown is 250 µm.

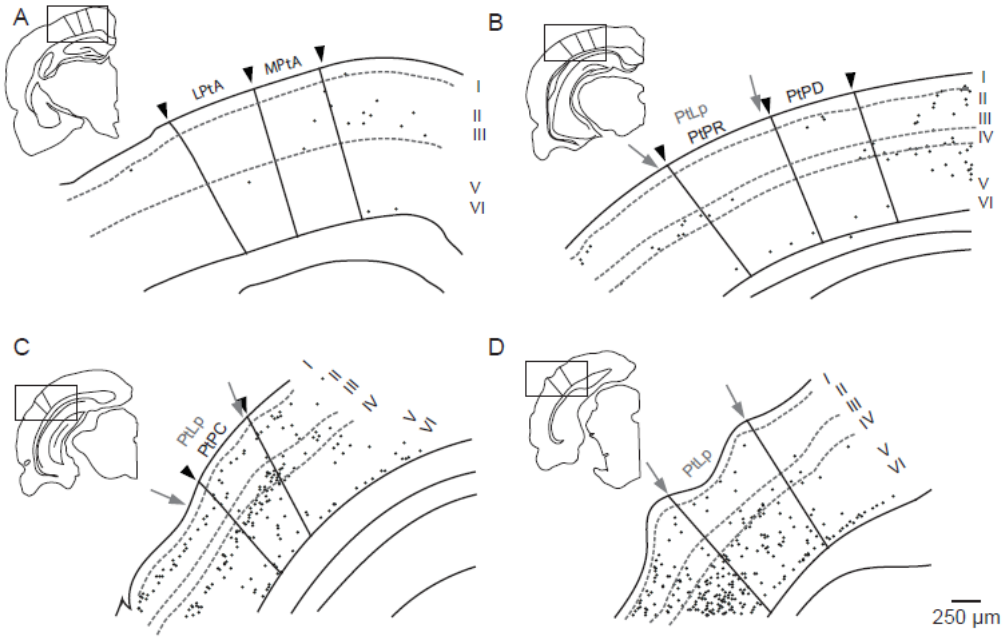


Figure 12. Schematic of the retrograde labeled cells in the PPC arising from injections in the POR. A-D, Representative case 99, whose injections site was located in layer I-V of caudal POR resulted in moderate to denser labeling in the caudal portions of the parietal association cortex and weak labeling in the dorsal portions. Estimated distance from bregma is -3.7 mm in A; -4.8 mm in B; -5.8 mm in C; -6.7 mm in D. Scale bar shown is 250 µm.

Table 9 shows the percentages of labeled cells in each PPC subdivision resulting from the six POR injection sites. This table provides a different view in that it shows the distribution of labeled cells across different subdivisions of the PPC. In terms of the PPC subdivisions from Paxinos and Watson (2005), all cases showed higher percentages of labeled cells in the lateral and caudal portions of the PPC (PtPD, PtPR and PtPC). Similar patterns were observed in the PtLp subvisions from Swanson (1992). Except for case 97 and 100, which had almost equal percentage of labeled cells in both DPtLp and CPtLp, all other cases showed higher percentage of labeled cells in CPtLp than the DPtLp.

Table 9. PPC input to POR: Percentage of retrogradely labeled cells in the PPC

| | | POR Injection Sites and Laminar Location | | | | | |
|---|---|---|---|---|---|---|---|
| Target Region | Mean | C102 V | C97 V | C98 I-VI | C95 III-VI | C100 I-VI | C99 I-V |
| **PPC**[†] | | | | | | | |
| MPtA | 13.51 | 2.74 | 12.63 | 17.15 | 14.43 | 36.48 | 0.63 |
| LPtA | 8.99 | 2.05 | 9.95 | 14.43 | 11.93 | 5.03 | 0.31 |
| PtPD | 36.16 | 39.73 | 39.62 | 28.04 | 44.11 | 16.98 | 47.73 |
| PtPR | 26.52 | 35.62 | 26.99 | 20.60 | 18.04 | 36.48 | 31.92 |
| PtPC | 14.81 | 19.86 | 10.81 | 19.78 | 11.49 | 5.03 | 19.41 |
| **PtLp**[††] | | | | | | | |
| DPtLp | 38.72 | 30.77 | 54.34 | 43.97 | 35.37 | 51.78 | 8.59 |
| CPtLp | 61.28 | 69.23 | 45.66 | 56.03 | 64.63 | 48.22 | 91.41 |

Total number of estimated cells were calculated by first correcting the number of cells for each case, by multiplying by its correction factor. The correction factor was calculated based off of the total number of subcortical cells labeled, averaged across each case. The corrected numbers of cells were then multiplied by 10 (given that we used a 1:10 series for analysis) to estimate the total number of cells in each region, which was then divided by the estimated total number of labeled cells in the PPC to yield the following percentages. [†]Paxinos and Watson (1995). [††]Nomenclature from Swanson (1992).

**Projections from POR to the PPC**

All POR anterograde injection sites resulted in labeling in the PPC, regardless of the rostrocaudal location of the POR injection. The density of labeling in the subdivisions of PPC did vary depending on the injection sites in POR. The detailed location and size

of POR injection has shown in Table 2 and Figure 3C. The quantified results from all subdivisions of the PPC showed in Table 10.

Although all anterograde injections in rostral or caudal POR resulted in labeled fibers in all PPC regions (Paxinos & Watson, 2005) the caudal POR injections (case 40) displayed a heavier density of labeled fibers comparing to the rostral POR injections (Table 10, Figure 13). The obvious heaviest density of labeled fibers was found in PtPD and PtPR. The next heaviest density of labeled fibers was seen in the more caudal sections. The rostral POR injections (cases 39 and 83) resulted in a less density of labeled fibers throughout the PPC, except the caudal portions (Figure 14). An injection in more dorsal POR (case 134) also resulted in labeled fibers in all PPC regions and did not display specific distinction among different subdivisions.

In terms of the PtLp region (Swanson, 1992), the POR anterograde injections resulted in labeled fibers in entire PtLp. The caudal POR injections showed a greater density of labeled fibers than the rostral POR injections. In general, the rostral POR injections displayed heavier density of labeled fibers in CPtLp (case 83 and 39; Figure 14) and the caudal POR injections displayed more labeled fibers in DPtLp (case 40; Figure 13). One injection in dorsal POR (case 134) showed a little more labeled fibers in DPtLP compared to labeled fibers in CPtLP.

In summary, the more rostral POR projects to more caudal PPC, and the caudal POR projects to dorsal PPC. In addition, the more posterior caudal sections of the PtLp (6.2-6.9 mm caudal to bregma) get the densest inputs from rostral POR (case 39 and 83).

Table 10. POR input to PPC: Density of anterogradely labeled fibers in the PPC

| | POR Injection Sites | | | |
|---|---|---|---|---|
| Target Region | 83 V-VI | 39 I-IV | 134 I-VI | 40 III-VI |
| **PPC**[†] | | | | |
| MPtA | ++ | + | ++ | ++ |
| LPtA | ++ | + | ++ | ++ |
| PtPD | ++ | + | ++ | ++++ |
| PtPR | ++ | + | ++ | ++++ |
| PtPC | +++ | ++ | ++ | ++ |
| **PtLp**[††] | | | | |
| DPtLp | ++ | + | +++ | ++++ |
| CPtLp | +++ | +++ | ++ | +++ |

Densities are shown using a quantitative scale of 0-5 to capture the density of anterograde labeled fibers in the region of interest. The averages were then translated into the following symbol scale: (-) 0-0.5; (+) 0.5-1.5; (++) 1.5-2.5; (+++) 2.5-3.5; (++++) 3.5-4.5; (+++++) 4.5-5.0. [†]Paxinos and Watson (1995). [††]Nomenclature from Swanson (1992). See list of abbreviations.

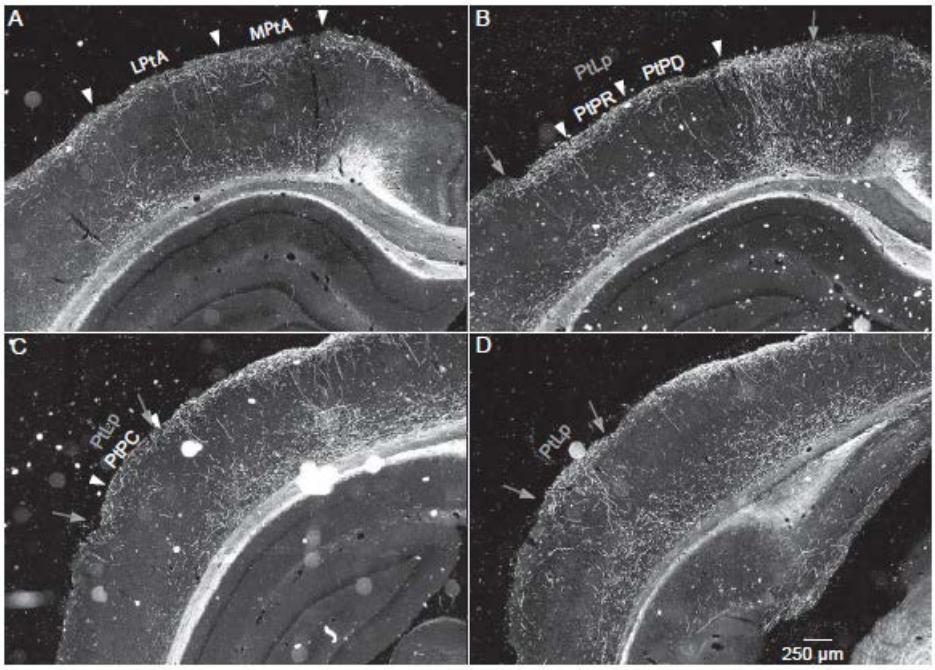


Figure 13. Anterograde labeling in the parietal association cortex arising from the injection in the cPOR (case 40). This case displayed heaviest labeling in the PtPD and PtPR, which are the dorsal portion of the PtLp. Moderate labeling patterns were observed in other portions throughout the entire parietal association cortex. Distance from Bregma is about -3.7 mm in A; -4.3 mm in B; -5.8mm in C; -6.5 mm in D. Scale bar shown is 250 µm.

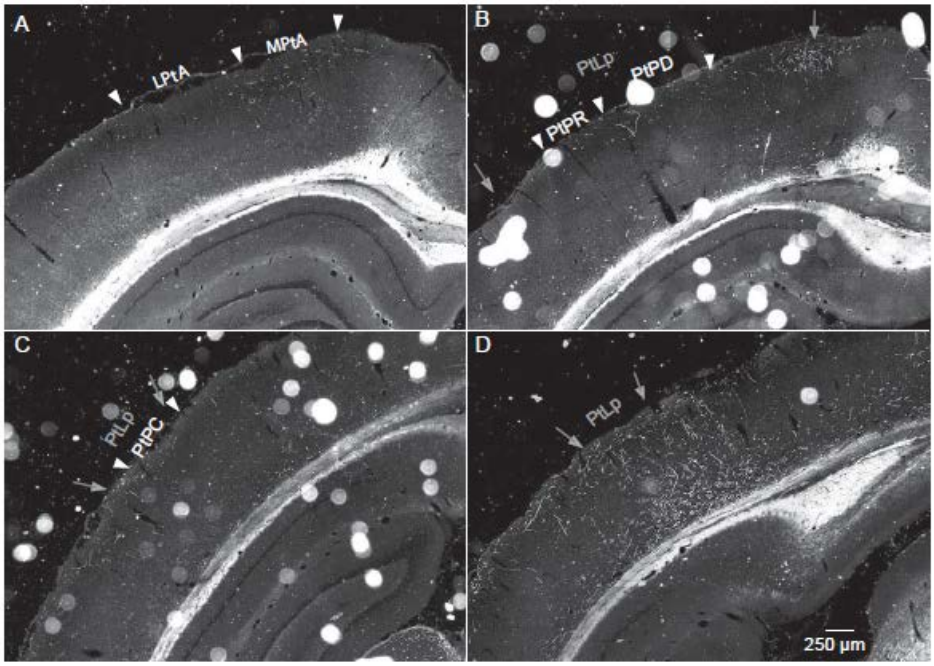


Figure 14. Anterograde labeling in the parietal association cortex arising from the injection in the rPOR (case 39). This case showed poorly labeling in the dorsal sections and denser labeling was observed in more caudal sections. Distance from Bregma is about -3.7 mm in A; -4.3 mm in B; -5.8mm in C; -6.5 mm in D. Scale bar shown is 250 µm.

## Discussion

In the present study, anterograde and retrograde tracer injections revealed a discrete topography of the connections among LP, POR and PPC. Figure 15 is a wiring diagram to show the relative strength of connectivity among various subdivisions of LP, POR and PPC. All the parietal connections in the study were compared the parietal regions from two well-known brain atlases (Paxinos & Watson, 2005; Swanson, 1992). To summarize, first, all subdivisions of the LP project to both PPC and POR, especially the deep layers. We observed that the LP projects preferentially to more caudal portions of the POR and PPC, whereas the rostral portions of the POR and PPC still have moderate LP inputs. In addition, the medial subnuclei of the LP (LPMR and LPMC) appear to project more heavily to the POR than do the lateral subnuclei (LPLR and LPLC). Our data are consistent with the interpretation that the LP projects to layer IV of the POR and the PPC, which is typical of thalamocortical projections. Second, the POR receives heavy inputs from the PPC. Specifically, the caudal portions of the PPC provide heavier inputs to the POR, although the POR still connects with dorsal portions of the PPC. Third, the POR also has return projections to the LP and PPC. Rostral POR appears to provide a stronger input to caudal LP, whereas caudal POR provides a stronger input to rostral LP. The caudal POR also has stronger projections to the parietal regions.

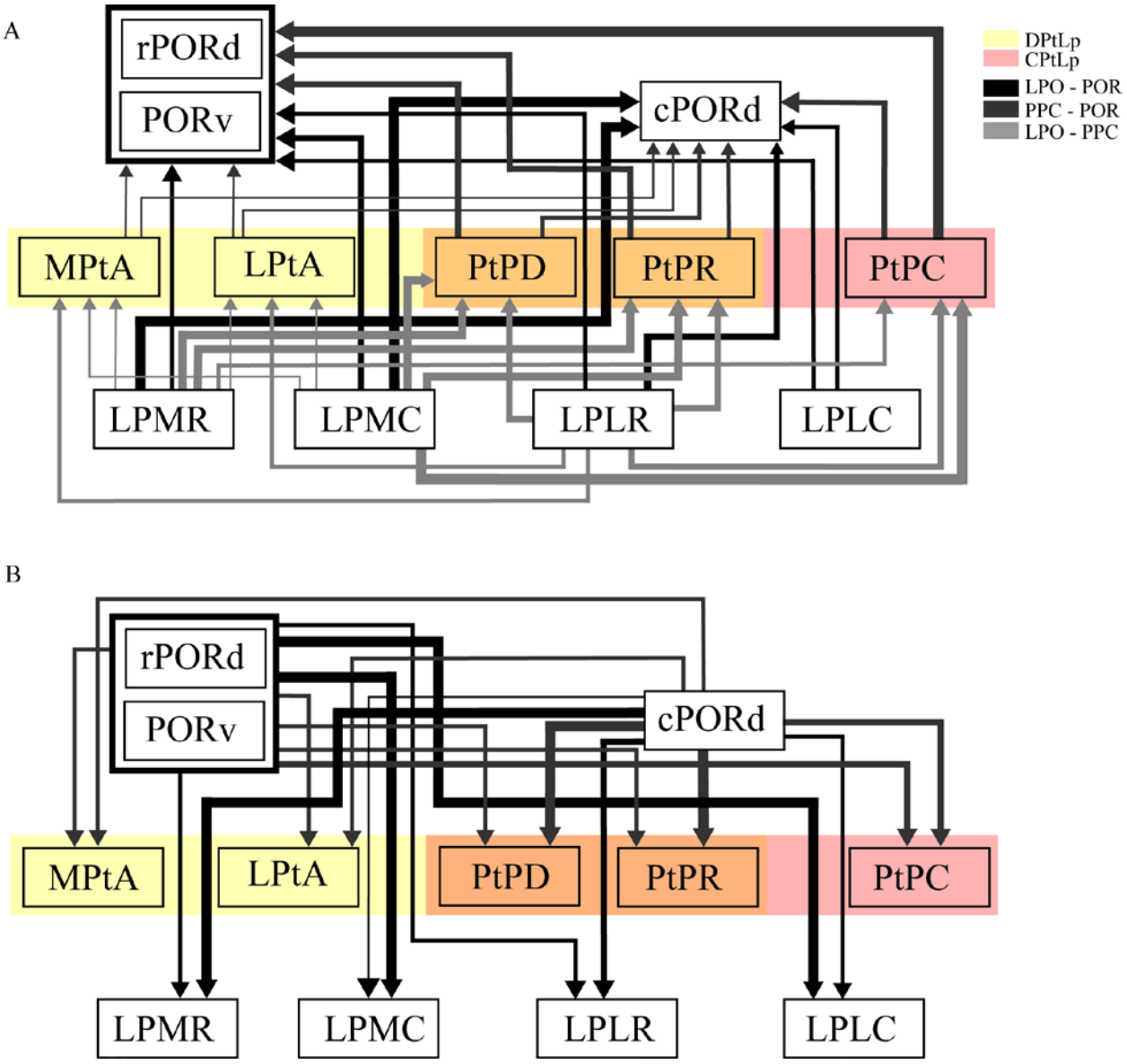


Figure 15. Summary of the connectivity of lateral posterior nucleus of thalamus (LP), postrhinal cortex (POR), and posterior parietal cortex (PPC). A. A summary diagram of projections from LP and PPC. B. A summary diagram of projections from the POR. Note, stronger connections are represented by thicker lines and weaker connections are indicated by the thinner lines. Connections between the LP and POR showed in black; connections between the LP and PPC showed in light gray; connections between the PPC and POR showed in dark gray. See list of abbreviations.

**Comparison with previous studies of the rat**

This study expands the present literature and provides a comprehensive view regarding the connections among LP, POR and the PPC. The LP connections with the POR have not been described in detail until recently (Nakamura et al., 2015). Previous work by Takahashi (1985) demonstrated the LP can be divided into four subnuclei on the basis of its cortical connectivity. Specifically, the LPMR receives input from primary and secondary visual cortex. The LPMC receives bilateral projections from the superior colliculus (SC), but not from the occipital cortex. The two lateral subnuclei, LPLR and LPLC, are also considered distinct from the SC inputs. The LPLR is the rostral part of the lateral subnuclei, which receives projections from the visual cortex, and the LPLC is the caudal part of the lateral subnuclei, which receives projections from the SC. Our results showed that the medial subnuclei of the LP exhibit the most robust interconnectivity with the POR, and the lateral subnuclei of the LP have weaker connections with POR. In addition, both LPMR and LPMC project more heavily to the caudal POR, compared to the projections to the rostral POR. These results are consistent with previous study (Nakamura et al., 2015), which also showed the heavier projections to the POR from the medial LP than the lateral LP. Our findings provide advanced evidence to show the projections from subnuclei of the LP to different subdivisions of POR. The return projections from the POR to the LP showed different patterns in rostral nuclei (LPMR and LPLR) and caudal nuclei (LPLR and LPLC). The rostral nuclei receive heavier inputs from the caudal POR whereas the caudal nuclei receive most POR projections from the rostral portion.

The connections between the LP and PPC have been reported in previous studies (Bucci, Conley, & Gallagher, 1999; Chandler et al., 1992; Hughes, 1977; Kamishina et al., 2009; Reep et al., 1994). Our findings are in line with these studies that confirmed that the LP projects to the PPC. One limitation of the previous studies is that most results from these studies focus in the dorsal portions of the PPC. Although two recent studies have reported the anatomical connection between the thalamus and subdivisions of parietal cortex (Olsen & Witter, 2016; Wilber et al., 2014), the topographic connections between the LP and the caudal portion of the PtLp in Swanson (1992) have not been fully described. Our results from the various series of anterograde tracer injections in different subnuclei of the LP showed that both medial and lateral subnuclei projects to entire PPC including the regions of parietal association cortex in Paxinos and Watson atlas and PtLp in Swanson atlas. These results extend previous literature regarding connectivity between the LP and the PPC and provide more detailed evidence showing a robust connectivity from the LP to the caudal portion of the parietal association cortex (Paxinos & Watson, 2005) , even extended to the most caudal portion of the PtLp (Swanson, 1992).

Our results of the anterograde and retrograde tracer injections in the POR have shown the reciprocal connectivity between the POR and the PPC. Previous studies have been reported that the PPC, in particular the caudal portion, substantially connects with the POR (Burwell & Amaral, 1998a; Furtak et al., 2007). The present study further examined the detailed connections among various subdivisions of the POR and the PPC. The results are consistent with previous studies showing the reciprocal connections between the POR and the PPC. In addition, both rostral and caudal POR receives much heavier inputs from the caudal portion of the PPC. The inputs from the rostral POR

preferentially project to the PtPC and the most caudal sections of the PtLp, whereas projections of the caudal POR preferentially terminate in the caudal portions of the PtPD and PtPR, which are about the caudal portions of the DPtLp.

**Comparison with the previous studies in the monkey.**

The monkey pulvinar, PHC, and PPC have been confirmed as functional and connectional homologous structures of the rodent LP, POR and PPC (Burwell et al., 1995; Kamishina et al., 2009; Reep et al., 1994). The monkey pulvinar, PHC, and PPC exhibit substantial interconnectivity (Baleydier & Mauguiere, 1977, 1985, 1987; Cavada & Goldman-Rakic, 1989; Suzuki & Amaral, 1994). The monkey medial pulvinar in reciprocally connected PHC areas TF and TH (Baleydier & Mauguiere, 1985). Here, we observed heavy inputs from the medial LP to the POR as well as return projections from the POR to the LP. Our observations in the rat also provide evidence for LP connections with the PPC as well as POR connections with the PPC. The pulvinar also provides substantial thalamic input to entire PPC in the rhesus monkey PPC (Baleydier & Mauguiere, 1977, 1987; Mesulam, Van Hoesen, Pandya, & Geschwind, 1977). Additionally, the monkey PHC, particular in area TF, heavily interconnects with area 7 and lateral intraparietal area (LIP) of the PPC (Cavada & Goldman-Rakic, 1989; Suzuki & Amaral, 1994). Our findings that the interconnections of the rat LP, POR and PPC parallel the interconnections of the monkey pulvinar, PHC, and PPC provide further evidence for functional and connectional homology across these brain structures in the rat and monkey.

**Functional considerations**

Evidence from human and monkey studies implicate the pulvinar, PHC and PPC in the circuitry that supports directed attention (Kravitz et al., 2011; Petersen & Posner, 2012; Petersen, Robinson, & Morris, 1987; Yi & Chun, 2005). Several lines of evidence from our results and previous anatomical, behavioral and electrophysiological studies suggest that the LP, POR and PPC in the rat may also play important roles in visuospatial attention. First, LP and visual association regions both project heavily to the POR and PPC suggesting that visual information is further processed by the POR and PPC (Burwell, 2000; Reep et al., 1994). Second, the PPC projections to the POR may support a role for the POR in attentional monitoring for changes in the current spatial context (Bucci & Burwell, 2004; Furtak et al., 2012). Third, like the PPC and PHC in primates, both PPC and POR connect heavily with frontal regions (Burwell & Amaral, 1998a; Reep et al., 1994), which contribute to a network for attention control.

In the primate brain, separate attentional systems have been proposed for processing top-down and bottom-up attention, respectively (Corbetta, Patel, & Shulman, 2008). By this view, the dorsal parieto-frontal pathway, which connects the dorsal parietal cortex and frontal eye field, mediates the top-down attention, whereas the ventral parieto-frontal pathway including the connections between ventral parietal cortex and ventral frontal cortex contributes to bottom-up attention (Corbetta & Shulman, 2002). Whether or not such a functional dissociation exists for the rat PPC is an open question.

**Conclusion**

The present study described the detailed interconnections of the LP, POR and PPC in rats and provided a strong case for the homology of these brain structures across rats and primates. Subsequent chapters will exploit the rat model to address three main

areas of inquiry: 1) the role of the rat PPC in visuospatial attention, 2) the issue of whether there is functional differentiation in the rat PPC similar to that described for the primate PPC, and 3) how the LP, POR and PPC interact in the service of visuospatial attention.

## References


Agster, K. L., & Burwell, R. D. (2009). Cortical efferents of the perirhinal, postrhinal, and entorhinal cortices of the rat. *Hippocampus, 19*(12), 1159-1186.

Agster, K. L., & Burwell, R. D. (2013). Hippocampal and subicular efferents and afferents of the perirhinal, postrhinal, and entorhinal cortices of the rat. *Behavioural Brain Research, 254*, 50-64.

Agster, K. L., Tomás Pereira, I., Saddoris, M. P., & Burwell, R. D. (2016). Subcortical connections of the perirhinal, postrhinal, and entorhinal cortices of the rat. II. efferents. *Hippocampus*, n/a-n/a.

Baleydier, C., & Mauguiere, F. (1977). Pulvinar-latero posterior afferents to cortical area 7 in monkeys demonstrated by horseradish peroxidase tracing technique. *Experimental Brain Research, 27*(5), 501-507.

Baleydier, C., & Mauguiere, F. (1985). Anatomical evidence for medial pulvinar connections with the posterior cingulate cortex, the retrosplenial area, and the posterior parahippocampal gyrus in monkeys. *The Journal of Comparative Neurology, 232*(2), 219-228.

Baleydier, C., & Mauguiere, F. (1987). Network organization of the connectivity between parietal area 7, posterior cingulate cortex and medial pulvinar nucleus: a double fluorescent tracer study in monkey. *Experimental Brain Research, 66*(2), 385-393.

Bucci, D. J. (2009). Posterior parietal cortex: An interface between attention and learning? *Neurobiology of Learning and Memory, 91*(2), 114-120.

Bucci, D. J., & Burwell, R. D. (2004). Deficits in attentional orienting following damage to the perirhinal or postrhinal cortices. *Behavioral Neuroscience, 118*(5), 1117-1122.

Bucci, D. J., Conley, M., & Gallagher, M. (1999). Thalamic and basal forebrain cholinergic connections of the rat posterior parietal cortex. *NeuroReport, 10*(5), 941-945.

Burwell, R. D. (2000). The parahippocampal region: Corticocortical connectivity. *Annals of the New York Academy of Sciences, 911*(1), 25-42.

Burwell, R. D. (2001). Borders and cytoarchitecture of the perirhinal and postrhinal cortices in the rat. *The Journal of Comparative Neurology, 437*(1), 17-41.

Burwell, R. D., & Amaral, D. G. (1998a). Cortical afferents of the perirhinal, postrhinal, and entorhinal cortices of the rat. *The Journal of Comparative Neurology, 398*(2), 179-205.

Burwell, R. D., & Amaral, D. G. (1998b). Perirhinal and postrhinal cortices of the rat: Interconnectivity and connections with the entorhinal cortex. *The Journal of Comparative Neurology, 391*(3), 293-321.

Burwell, R. D., Witter, M. P., & Amaral, D. G. (1995). Perirhinal and postrhinal cortices of the rat: A review of the neuroanatomical literature and comparison with findings from the monkey brain. *Hippocampus, 5*(5), 390-408.

Cavada, C., & Goldman-Rakic, P. S. (1989). Posterior parietal cortex in rhesus monkey: I. Parcellation of areas based on distinctive limbic and sensory corticocortical connections. *The Journal of Comparative Neurology, 287*(4), 393-421.

Chandler, H. C., King, V., Corwin, J. V., & Reep, R. L. (1992). Thalamocortical connections of rat posterior parietal cortex. *Neuroscience Letters, 143*(1-2), 237-242.

Colby, C. L., & Goldberg, M. E. (1999). Space and attention in parietal cortex. *Annual Review of Neuroscience, 22*(1), 319-349.

Corbetta, M., Patel, G., & Shulman, G. L. (2008). The Reorienting System of the Human Brain: From Environment to Theory of Mind. *Neuron, 58*(3), 306-324.

Corbetta, M., & Shulman, G. L. (2002). Control of goal-directed and stimulus-driven attention in the brain. *Nature Reviews Neuroscience, 3*(3), 201-215.

Furtak, S., Ahmed, O., & Burwell, R. D. (2012). Single neuron activity and theta modulation in postrhinal cortex during visual object discrimination. *Neuron, 76*(5), 976-988.

Furtak, S., Wei, S. M., Agster, K. L., & Burwell, R. D. (2007). Functional neuroanatomy of the parahippocampal region in the rat: The perirhinal and postrhinal cortices. *Hippocampus, 17*(9), 709-722.

Hughes, H. C. (1977). Anatomical and neurobehavioral investigations concerning the thalamo-cortical organization of the rat's visual system. *The Journal of Comparative Neurology, 175*(3), 311-335.

Kamishina, H., Conte, W. L., Patel, S. S., Tai, R. J., Corwin, J. V., & Reep, R. L. (2009). Cortical connections of the rat lateral posterior thalamic nucleus. *Brain Research, 1264*(0), 39-56.

Kravitz, D. J., Saleem, K. S., Baker, C. I., & Mishkin, M. (2011). A new neural framework for visuospatial processing. *Nature Reviews Neuroscience, 12*(4), 217-230.

Mesulam, M.-M., Van Hoesen, G. W., Pandya, D. N., & Geschwind, N. (1977). Limbic and sensory connections of the inferior parietal lobule (area PG) in the rhesus monkey: A study with a new method for horseradish peroxidase histochemistry. *Brain Research, 136*(3), 393-414.

Nakamura, H., Hioki, H., Furuta, T., & Kaneko, T. (2015). Different cortical projections from three subdivisions of the rat lateral posterior thalamic nucleus: a single-neuron tracing study with viral vectors. *European Journal of Neuroscience, 41*(10), 1294-1310.

Olsen, G. M., & Witter, M. P. (2016). The posterior parietal cortex of the rat: architectural delineation and thalamic differentiation. *Journal of Comparative Neurology*, n/a-n/a.

Paxinos, G., & Watson, C. (2005). *The rat brain in stereotaxic coordinates*: Amsterdam;. Elsevier Academic Press.

Petersen, S. E., & Posner, M. I. (2012). The attention system of the human brain: 20 years after. *Annual Review of Neuroscience, 35*(1), 73-89.

Petersen, S. E., Robinson, D. L., & Morris, J. D. (1987). Contributions of the pulvinar to visual spatial attention. *Neuropsychologia, 25*(1), 97-105.

Posner, M. I., & Dehaene, S. (1994). Attentional networks. *Trends in Neurosciences, 17*(2), 75-79.

Reep, R. L., Chandler, H. C., King, V., & Corwin, J. V. (1994). Rat posterior parietal cortex: topography of corticocortical and thalamic connections. *Experimental Brain Research, 100*(1), 67-84.

Suzuki, W. L., & Amaral, D. G. (1994). Perirhinal and parahippocampal cortices of the macaque monkey: Cortical afferents. *The Journal of Comparative Neurology, 350*(4), 497-533.

Swanson, L. W. (1992). Brain maps: Structure of the rat brain: Elsevier (Amsterdam and New York).

Takahashi, T. (1985). The organization of the lateral thalamus of the hooded rat. *The Journal of Comparative Neurology, 231*(3), 281-309.

Tomás Pereira, I., Agster, K. L., & Burwell, R. D. (2016). Subcortical connections of the perirhinal, postrhinal, and entorhinal cortices of the rat. I. afferents. *Hippocampus*, n/a-n/a.

Wilber, A. A., Clark, B. J., Demecha, A. J., Mesina, L., Vos, J. M., & McNaughton, B. L. (2014). Cortical connectivity maps reveal anatomically distinct areas in the parietal cortex of the rat. *Frontiers in Neural Circuits, 8*, 146.

Yi, D. J., & Chun, M. M. (2005). Attentional modulation of learning-related repetition attenuation effects in human parahippocampal cortex. *The Journal of Neuroscience, 25*(14), 3593-3600.

# CHAPTER 4

# NEURONAL CORRELATES IN RAT POSTERIOR PARIETAL CORTEX AND THE LATERAL POSTERIOR THALAMIC NUCLEUS DURING PERFORMANCE ON A VISUOSPATIAL ATTENTION TASK

**Abstract**

The posterior parietal cortex (PPC) is known to be important for visuospatial attention. In rats, this region receives input from visual cortex and from the lateral posterior nucleus of thalamus (LPO), the functional homolog of the primate pulvinar. The LPO and pulvinar are also implicated in attention. In primates, the pulvinar differentially projects to two subdivisions of the PPC. Recent studies showed functional differentiation of these PPC subdivisions, with one region supporting top-down attention and the other supporting bottom-up attention (Cabeza, 2008). The rodent PPC can also be subdivided into dorsal and caudal subdivisions based on connectional differences. Whether these subdivisions exhibit a similar functional differentiation, however, remains unknown. Our previous work showed that neuronal activity in dorsal PPC correlated with multiple phases of a visuospatial attention (VSA) task, including onset of the visual stimuli, decision-making, task-relevant location, and behavioral outcome (Yang, Jacobson, and Burwell, under revision). To further understand the roles of the PPC subdivisions and the LPO in visuospatial attention, we simultaneously recorded neuronal activity in all three structures in male Long-Evans rats during performance on the VSA task. The task was designed to involve both goal-directed, top-down attention (engaged when the rat is maintaining attention to the location in which stimuli might appear) and stimulus-driven bottom-up attention (engaged with the onset of stimuli). In the VSA task, rats monitored three locations for the brief appearance of a target stimulus. An approach to the correct target location was followed by a liquid reward. For analysis, each trial was divided into behavioral epochs including stimulus onset, selection behavior, and reward. Using wireless recording methods (32-channel TBSI headstage in combination with a Plexon

MAP system), we recorded neuronal activity of five rats during performance on the VSA task. We isolated 78 cells in the dorsal PPC, 119 cells in the caudal PPC, and 94 cells in the LPO. Our results show that neurons in the LPO and PPC signal stimulus onset and selection behavior consistent with the interpretation that the LPO and PPC subdivisions are engaged in both top-down and bottom-up visuospatial attention. Our data further support the view that the rodent CPPC is preferentially engaged in bottom-up attention process, similar to the ventral PPC in the primate brain. This suggested that subdivisions of rat PPC, similar to primate PPC, have functional differentiation in visuospatial attention. We also observed LPO and PPC units responded to allocentric and egocentric task-relevant locations.

## Introduction

In prior experiments, we observed neuronal correlates of attention in the PPC in rats performing the VSA task. Most electrophysiology studies of the PPC, including our first recording experiment, focused on the dorsal portion of the PPC (Nitz, 2009, 2012; Wilber, Clark, Forster, Tatsuno, & McNaughton, 2014). We found that the dorsal PPC (DPPC) cells signaled stimulus onset, selection behavior, and task-relevant spatial locations. These results provide evidence for the involvement of the PPC in visuospatial attention. Human and monkey studies have shown that subregions of the primate PPC are functionally differentiated: the dorsal portion of PPC is involved in top-down attention, which is directed to specific information in the environment according to a subject's goal. The ventral PPC is involved in bottom-up attention, which is engaged when external stimuli grab attention automatically (Corbetta, Kincade, Ollinger, McAvoy, & Shulman,

2000; Shomstein, 2012). Whether or not such a differentiation exists in the rodent PPC is still an open question. To our knowledge, there are no electrophysiological studies of the caudal PPC (CPPC) in the rat.

Previous studies and our results confirmed anatomical connections between subregions of the PPC and the LPO (Chandler, King, Corwin, & Reep, 1992; Reep, Chandler, King, & Corwin, 1994). In the rat, like primate brain, both DPPC and caudal CPPC receive strong inputs from LPO, but not much is known about how these regions interact during activities that require visuospatial attention. Recent studies and our anatomical data suggest that the rodent LPO is the functional homolog of the primate pulvinar. This view is mostly based on connectional homology (Kamishina et al., 2009; Mason & Groos, 1981; Reep & Corwin, 2009). The primate pulvinar is implicated in visual attention (Saalmann, Pinsk, Wang, Li, & Kastner, 2012; Smith, Cotton, Bruno, & Moutsiana, 2009). Thus, the rat LPO-PPC circuitry provides a good model for the primate pulvinar-PPC circuitry and the role of these regions in visuospatial attention.

Based on previous studies, our guiding hypothesis is that the rat PPC receives primary sensory inputs through its LPO afferents and provides attentional signals to efferent areas, such as the postrhinal cortex and prefrontal cortex. To further investigate our hypothesis that the attentional functions of PPC might rely on LPO input, we simultaneously recorded neuronal activity in the rat LPO, DPPC and CPPC during performance on a visuaospatial attention task. We also modified the visuospatial attention task from our previous study in order to improve behavioral performance. Specifically, we changed the shape of the maze, from a fan-shaped enclosure to a bowtie-shaped enclosure. In this bowtie maze, animals could start trials from one side to the other side

automatically. This new apparatus enhanced the total number of trials within one session, reduced the number of omitted trials, and allowed disambiguation of egocentric and allocentric correlates.

## Methods

### *Subjects*

Subjects were five male Long-Evan rats (Charles Rivers Laboratories, Wilmington, MA). They were individually housed in a temperature-regulated colony maintained on a 12:12 h light:dark cycle. Experiments were carried out in the light phase. All procedures followed the NIH guidelines and were approved by the Brown University animal care and use committee.

### *Apparatus*

Our task uses the Floor Projection Maze, an apparatus that exploits the natural tendency of rats to attend to items located on or close to the ground and permits automated control over visual stimuli (Furtak et al., 2009; Jacobson, Ho, Kent, Yang, & Burwell, 2014) . Essentially, the Floor Projection Maze is a horizontal rear projection screen positioned to allow back-projection of visual stimuli and to serve as a floor to any shaped arena (Figure 1A). The apparatus has a clear Plexiglas subfloor (147.32 cm × 111.80 cm) with a (1.25 cm thick) covered by Dual Vision Fabric (Da-Lite Screen Company, Warsaw, IN), a unity gain flexible fabric designed for rear screen projection. A thin sheet (Plexiglas 0.32 cm) covers the fabric for protection. Visual stimuli were projected onto the unity gain fabric from below the subfloor using an LCD projector (WT610 projector, NEC Corporation). In this experiment, the enclosure was a bowtie shaped region for presentation of stimuli. Food reward (milk with various flavors) was

delivered by two automated pumps (Med Associates, Inc, St. Albans, VT) to stainless steel food ports located at middle region of the maze. Auditory stimuli were controlled by an automated auditory stimulus generator (ANL926, Med Associates, Inc.) and delivered through a speaker located above the maze.

The Floor Projection Maze was interfaced with three Windows PC systems, for location tracking, behavioral control, and neuronal data acquisition. A CinePlex Behavioral Research System (CinePlex Studio and CinePlex Editor) v3.4.1 with a single camera and two additional CinePlex modules, CinePlex Tracking and CinePlex Basic Behavior was used for tracking animal's location during behavioral performance. The position of the rat was recorded by tracking the centroid of the contour of the rat using the CinePlex Tracking module. Position data are analyzed online in the CinePlex Basic Behavior module and also saved in a Plexon data file for further offline analysis. Based on the location of the rat, this system presented stimuli, collected behavioral data, and controlled delivery of reward. A Multichannel Acquisition Processor (MAP, Plexon Inc) and SortClient (Plexon, Inc) recorded real-time neuronal activity and behaviorally relevant event timestamps for later analysis. The MAP system was interfaced with the Med Associates system (DIG-713A SuperPort TTL Input Module and a DIG-726 SuperPort TTL Output module).

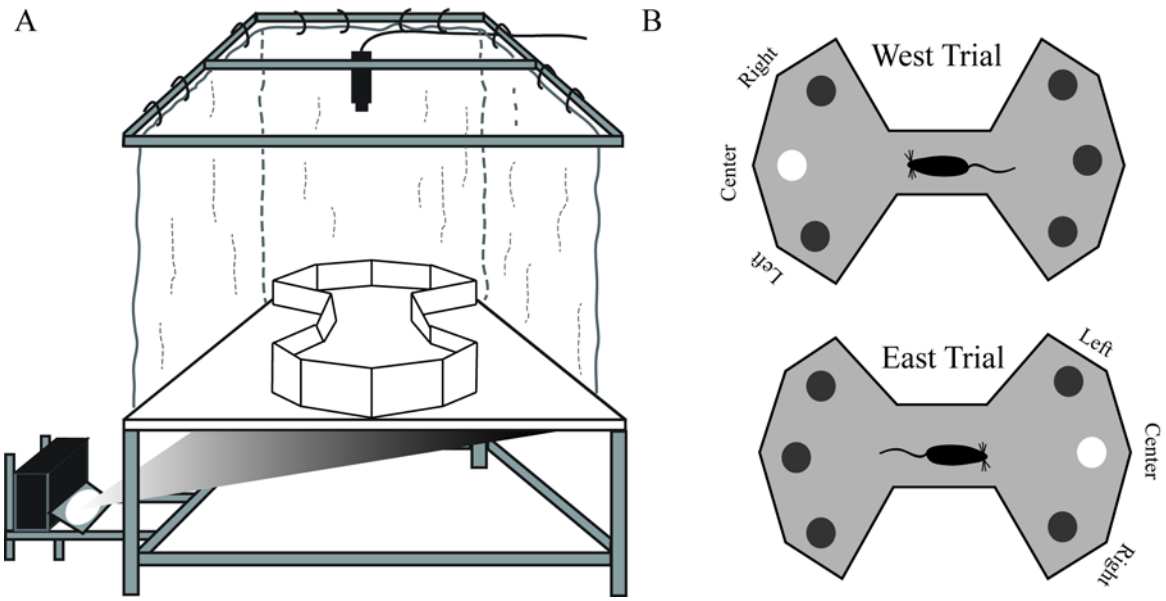


Figure 1. The Visuospatial Attention (VSA) task. A. Schematic of the Floor Projection Maze with the bowtie-shaped enclosure used for the task. B. Topdown view of west vs. east trials. Trials were initiated when the rat stopped in the ready position (middle of the maze) and faced to one side of the maze (either west or east). After a variable period, the target location was briefly illuminated. The animal made a selection by approaching one of the three locations in the same side, and then returned to the food port for a food reward. After the animal consumed the reward, a new trial from the alternative side would be triggered immediately.

***Behavioral training***

Rats were put on food schedules to maintain body weight at 85-90% of free feeding weight. After handling for at least 7 days, rats were habituated to the behavioral room for 10 min/day for three days. Rats were then shaped and trained in the VSA task. In the shaping sessions, rats first were trained in a 30 minute session to approach a visual target stimulus for a food reward (a drop of flavored milk). In the initial shaping sessions, we adopted an errorless shaping procedure such that when the rat moved toward one of the three locations in one side of the maze, the visual stimulus at that location would illuminate and a tone would signal a correct choice. A new trial on the other side of the maze would be initiated after the rat entered reward area. After this initial shaping phase, rats were trained to stop in the ready position zone located in the middle of the bowtie shaped maze facing the stimulus presenting area. After a variable delay, a visual stimulus

would illuminate in one of three randomly chosen locations. There was a short response window for rats to approach the location of the visual stimulus. Approach to the correct location was signaled by a brief tone and presentation of a drop of flavored milk as a food reward. If the rat approached an incorrect location, no reward was given, the trial was terminated, and a new trial would begin immediately. Rats were gradually trained in a series of steps culminating in the final parameters of the task. The duration for rats to stay in the ready position was gradually increased from 0.1 seconds to 1.6 seconds. Visual stimulus duration was gradually decreased from 20 seconds to 0.5 seconds. The response time window was decreased from 20 seconds to 5 seconds. In the final task, rats were required to stay in the ready position for stimulus onset for a variable interval (1.2-1.6 seconds) (Figure 1B).

The behavioral performance criterion for the end of training was 70% accuracy on the VSA task (chance is 33.33%). Behavior was well controlled on correct trials. Rats in this study required 2-3 months of training to reach behavioral criterion on the final stage of the task. Hyperdrives were implanted after a rat reached behavioral criterion for 5 to 7 consecutive days.

***Surgery***

Animals were premedicated with diazepam (2-5 mg/kg; i.p.), glycopyrrolate (0.05 mg/kg; s.c.), carprofen (5 mg/kg; s.c.), and butorphanol tartrate (0.5 mg/kg; s.c.) to counteract respiratory effects of anesthesia, to control pain, and to decrease risk of seizures. They were brought to a surgical level of anesthesia with isofluorane (1.0 – 2.5%). Using a stereotaxic apparatus (Kopf, Tujunga, CA), rats were unilaterally implanted with a custom hyperdrive into the LPO (AP – 3.9 mm, ML ± 1.8 mm, DV –

4.0 mm), dorsal PPC (AP – 4.2 mm, ML ± 2.0 mm, DV – 0.1mm), and caudal PPC (AP – 5.2 mm, ML ± 4.5mm, DV – 2.0 mm). The hyperdrive had fifteen microdrives, each consisting of a drivable screw with guide tubing containing one stereotrode. Stereotrodes were made of two 12 μm twisted, formvar-insulated nichrome wires (A-M systems, Sequim, WA). A full turn of the screw advanced the stereotrode by 350 μm. Two silver ground wires were wrapped around anchor screws in the skull. The hyperdrive was secured to the skull by the ground screws, small anchor screws, grip cement (Dentsply Caulk, Milford, DE), and dental cement (Coltene/Whaledent Inc., Cuyahoga Falls, OH).

***Histology***

After the last recording session, the rats were deeply anesthetized with an overdose of Beuthanasia-D (100 mg/kg, i.p.) and the final recording site was marked with an electrolytic lesion. The rats were then perfused with normal saline, followed by 4% formalin. The brains were post-fixed for 24 hours in 4% formalin and then transferred to a 30% sucrose solution until the time for sectioning. The brains were sectioned at 40 μm and stained for Nissl material with thionin.

***Electrophysiology***

Neuronal activity recorded from stereotrodes, was amplified with a 2X gain 31-channel wireless head stage (Triangle BioSystems Inc., Durham, NC). Signals were passed through a high-gain amplifier (total = 10000X, MAP system, Plexon, Inc., Dallas, TX). Single-unit activity was filtered between 0.8 - 6 Hz. The signal was then digitized at 40 kHz for single-unit activity. These signals were extracted through real-time thresholding (Sort Client, Plexon, Inc). The final waveforms were stored with timestamps of relevant events and position information for later analysis.

***Single neuron activity analysis***

Spikes associated with putative individual cells were isolated offline based on waveform characteristics and using a variety of partially-automated and manual techniques (Offline Sorter, Plexon, Inc.). The result was a dataset for each cell containing timestamps corresponding to spike times and behaviorally relevant event markers. These datasets were further analyzed using Neuroexplorer (NEX, Nex Technologies, Madision, AL) and SPSS.

Each cell was analyzed for behavioral correlates using factorial analysis of variance (fANOVA). We analyzed five epochs from each completed trial: pre-stimulus and post-stimulus epochs were the 500 msec periods immediately before and after stimulus onset; pre-selection and post-selection epochs were the 500 msec periods immediately before and after the rat selected a target by approaching the location; and the reward-approach epoch was the first 500 msec after the animal entered the food reward area. The selection time event was the moment the rat entered a zone just in front of the location in which the target stimulus had appeared. Entry of the ready position of the other side of bowtie maze triggered the next trial. Rats invariably approached and checked the food port even after incorrect trials.

Firing rate was the dependent variable for the fANOVAs. For each neuron, we first computed the mean firing rate (spikes/sec) for each epoch on each trial. In the first set of analyses, the between-trial variable was outcome (correct response vs. incorrect response), and the two within-trial variables were stimulus onset (pre-stimulus vs. post-stimulus) and selection time (pre-selection vs. post-selection). Outcome was analyzed for the reward-approach epoch.

In a second set of analyses, we examined neural correlates associated with the location of the target stimulus. Based on the location of stimulus presentation, we pooled trials in which the target stimulus was at the same side of the maze (east vs. west) for analyzing allocentric location correlates. We then pooled trials in which the target stimulus was at the same egocentric location (left, right, and center) for analyzing egocentric location correlates. Only correct trials were used in this series of analyses. Thus, the between trial variable was allocentric location or egocentric location. Sessions were analyzed for location only if there were at least three correct trials on each side. Allocentric location was analyzed separately for the post-stimulus, pre-selection, post-selection, and reward epochs. The pre-stimulus epochs was not analyzed for trial location because there was no information about the allocentric location. Egocentric location was analyzed for the post-stimulus, preselection, and post-selection epochs without pre-stimulus and reward epochs.

To further understand changes of neuronal activity over time, a sliding window analysis was employed. We focused on the neuronal activity during the stimulus presentation period. For each neuron, we took a 100ms window of time, beginning at stimulus onset and compare the mean firing rate of this 100ms bin to the neuron's mean firing rate during pre-stimulus epoch by using paired t-test. We then advanced the window by 20ms and analyzed the next 100ms window of time, and continued until the end of the stimulus presentation. Significance of a cell was determined by at least two continuous bin showing statistical significant differences ($p < 0.05$).

## Results

### *Histology*

Examination of Nissl-stained coronal brain sections from each of the five animals indicated electrode tips were located in LPO between 3.5-4.4 mm posterior to bregma and between 1.5-3.5 mm lateral to the midline, DPPC between 4.0-4.6 mm posterior to bregma and between 2.0-4.0 mm lateral to the midline, and CPPC between 5.2-6.0 mm posterior to bregma and between 6.0-7.0 mm lateral to the midline (Figure 2). One stereotrode was located in an adjacent brain region, but cells from adjacent areas were analyzed.

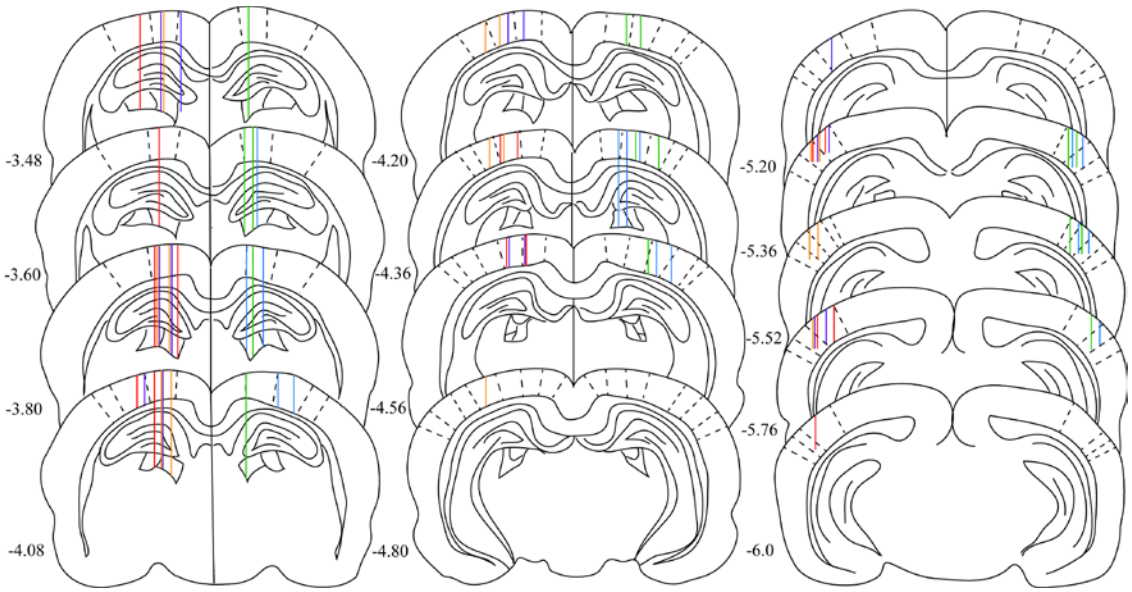


Figure 2. Estimated locations of implanted stereotrode. Various color indicated stereotrodes from different animals. Same color indicated stereotrodes from the same animal.

### *LPO, DPPC, and CPPC cells signaled stimulus onset and predicted behavioral outcome*

All five animals yielded isolated units. A total of 94 LPO cells, 78 DPPC cells, and 119 CPPC cells that have good quality waveforms and were well clustered were used

in following analyses. Each cell was recorded for a single session. The majority of these criterion cells, 70 (74.46%) in the LPO; 65 (83.33%) in the DPPC; 94 (78.99%) in the CPPC, exhibited behavioral correlate(s) during at least one of the task epochs as indicated by significant main effects or interactions of stimulus onset, target selection time, location, or outcome.

To investigate whether LPO and PPC cells signaled attention to visual stimuli, we first analyzed neuronal responses to stimulus onset by comparing firing rates for the 500 ms before vs 500 ms after the onset of the 500 ms illumination of the target stimulus for correct vs incorrect trials. Of all cells, 27 (28.72%) LPO cells, 22 (28.21%) DPPC cells, and 53 (44.54%) CPPC cells showed some form of selectivity for stimulus onset. The CPPC had a significant larger proportion cells exhibited selectivity for stimulus onset, comparing to cells in LPO and DPPC ($\chi^2_{(2)} = 7.96$, $p = 0.02$). Of these cells, 18 LPO cells (19.15%), 12 DPPC cells (15.38%), and 39 CPPC cells (32.77%) showed significant increases or decreases in firing rate associated with stimulus onset, alone (Table 1). For example, the LPO cell and DPPC cell shown in Figure 3A and 3B fired more during the pre-stimulus epoch than the post-stimulus epoch. The CPPC cell shown in Figure 3C fired more during the post-stimulus epoch than the pre-stimulus epoch. Five (5.32%) LPO cells, 7 (8.97%) DPPC cells, and 8 (6.72%) CPPC cells fired differentially depending on whether the animal was about to make a correct selection. Four (4.96%) LPO cells, 3 (3.85 %) DPPC cells and 6 (5.04%) CPPC cells exhibited a main effect of outcome alone. Thus, a total of 9 (9.57%) LPO cells, 10 (12.82%) DPPC cells, and 14 (11.76%) CPPC cells fired differentially depending on the subsequent outcome of the trial.

***LPO, DPPC and CPPC cells signaled target selection and behavioral outcome***

The activity of LPO, DPPC, and CPPC cells correlated with target selection. Eighteen (19.15%) LPO cells, 9 (11.54%) DPPC cells and 23 (19.33%) CPPC cells signaled selection by firing more during either pre-selection or post-selection epoch (Table 1 and Figure 3D-F). Eight (8.51%) LPO cells, eight (10.26%) DPPC cells, and eight (6.72%) CPPC cells signaled both selection and outcome. Of these cells, one DPPC cells and five CPPC cells displayed main effects of both selection and outcome without a significant interaction; the rest of these cells exhibited an interaction effect showing differential firing patterns depending on whether the animal made a correct vs. an incorrect selection. Six (6.38%) LPO cells, three (3.85%) DPPC cells, and seven (5.88%) CPPC cells responded to outcome alone during the peri-selection interval. Thus, 26 (27.66%) LPO cells, 17 (21.79%) DPPC cells and 31 (26.05%) CPPC cells differentiated pre- and post-selection epochs. Fourteen (14.89 %) LPO cells, 11 (14.10%) DPPC cells, and 15 (12.60%) CPPC cells displayed differential firing patterns related to behavioral outcome.

For the reward-approach epoch, in which the animal had just entered food area after selecting a target location, 19 (20.21%) LPO cells, 20 (25.64%) DPPC cells, and 28 (23.53%) CPPC cells displayed selectivity for different outcomes in the reward-approach epoch (Table 1). A representative cell from the LPO, DPPC and CPPC, shown in Figure 2G, fired more in correct trials than incorrect trials. Figure 2H and 2I displayed a DPPC cell and a CPPC cell that fired more in incorrect trials than correct trials.

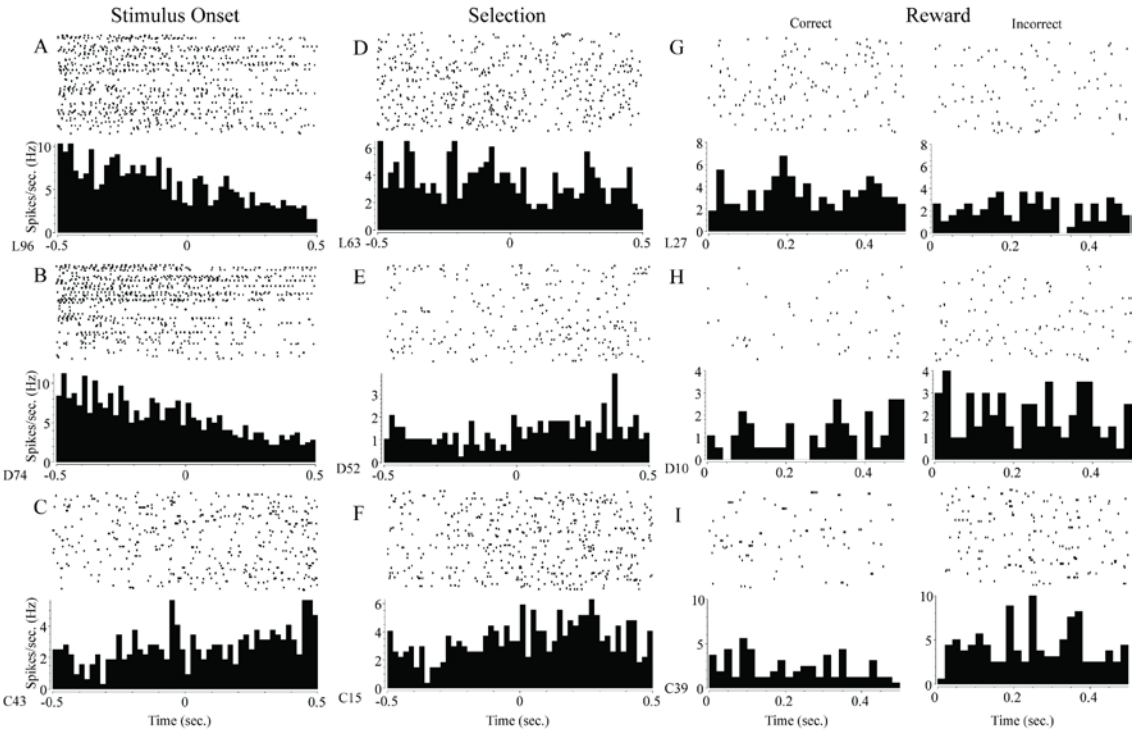


Figure 3. Example neuronal correlates for LPO, DPPC, and CPPC cells. Perievent ratster plots and histograms are shown for example cells with behaviorally relevant firing patterns. For the stimulus epoch, time 0 is stimulus onset (A, B, C). For the selection epoch, time 0 is selection (D, E, F). For the reward epoch, time 0 is when the animal entered the reward area (G, H, I). Example cells shown in upper panels were recorded from the LPO (A, D, G); cells in middle panels were recorded from the DPPC (B, E, H); cells in lower panels were recorded from the CPPC (C, F, I).

***LPO, DPPC and CPPC cells signaled allocentric and egocentric location.***

We previously reported that DPPC cells displayed selectivity for the location of the target stimulus, as demonstrated by differential firing patterns on left vs. right trials. In the present study, we had the opportunity to examine the role of subregions of the PPC and its thalamic associate, the LPO, in the processing of allocentric and egocentric information. Only correct trials were analyzed because behavior was better controlled on correct trials. We analyzed the post-stimulus, pre-selection, and post-selection epochs because spatial location was relevant during these epochs. Reward epoch was also analyzed for allocentric location correlates. As expected, location selectivity was evident in all analyzed epochs (Table 1). Based on the location of stimulus presentation, we

pooled trials in which the target stimulus was in the same side of the maze (east vs. west) for analyzing allocentric location correlates. We then pooled trials in which the target stimulus was at the same egocentric location (left, right, and center) for analyzing egocentric location correlates.

Regarding allocentric location correlates, we observed significant differences in east vs west trials for 19 (20.21%) LPO cells in the in the post-stimulus epoch, 14 (14.89%) cells in the pre-selection epoch, 4 (4.26%) cells in the post-selection epoch, and 13 (13.83%) cells in the reward epoch. Similar allocentric location correlates were also observed in the DPPC and CPPC. For allocentric correlates in the the DPPC we observed significant east vs. west correlats for 23 (29.49%) cells in the post-stimulus epoch, 12 (15.38%) cells in the pre-selection epoch, 8 (10.26%) cells in the post-selection epoch, and 15 (19.23%) cells in the reward epochd. In the CPPC, we observed east-west allocentric selectivity in 28 (23.53%) cells in the post-stimulus epoch, 20 (16.81%) cells in the pre-selection epoch, 12 (10.08%) cells in the post-selection epoch and 23 (19.33%) cells in the reward epoch . A total of 37 (39.36%) LPO cells, 43 (55.13%) DPPC cells, and 59 (49.58%) CPPC cells differentiated east and west trials in at least one behavioral epoch.

Regarding egocentric location correlates we observed significant differences for left vs. right trials in the LPO for eight (8.51%) cells in the post-stimulus epoch, five (5.32%) cells in the pre-selection epoch, and 19 (20.21%) cells in the post-selection epoch showed a significant difference in firing rate among left, center, and right trials. In the DPPC, we observed egocentric correlates in five (6.41%) cells in the post-stimulus epoch, 11 (14.10%) cells in the pre-selection epoch, and 10 (12.82%) cells in the post-

selection epoch exhibited the egocentric location selectivity. In the CPPC, we observed egocentric correlates in 11 (9.24%) cells in the post-stimulus epoch, 10 (8.40%) cells in the pre-selection epoch, and 13 (10.92%) cells in the post-selection epoch showed differential firing rate to different egocentric location. A total of 29 (30.85%) LPO cells, 22 (28.21%) DPPC cells, and 30 (25.21%) CPPC cells differentiated left, center and right trials in at least one behavioral epoch.

***Sliding window analysis of neuronal activity during peri-stimulus epochs***

Compared to the LPO and DPPC, the CPPC exhibited a significantly larger proportion cells showing selectivity of stimulus onset. To characterize changes in neuronal activity over time in LPO, DPPC and CPPC during peri-stimulus epochs, we also used a sliding window analysis. For each neuron, we used a 100 ms sliding, beginning at stimulus onset and advancing by 20 ms to the end of the stimulus presentation. Each window was compared with the neuron's mean firing rate during pre-stimulus epoch using a paired t-test. The results showed that the firing rates of 30 (31.91%) LPO cells, 32 (41.03%) DPPC cells, and 102 (85.71%) CPPC cells were significantly different ($p < 0.05$) between pre-stimulus & post-stimulus epochs in at least two continuous sliding windows. Compared to the LPO and DPPC, the CPPC had a significantly larger proportion of cells showing differential firing rate before and after stimulus onset ($\chi^2_{(2)} = 71.98$, $p < 0.01$). We also observed that about half of CPPC cells (49.58%) displayed significantly different firing rates between pre-stimulus & post-stimulus epochs in the first two time bins immediately after stimulus onset. The proportion of cells showing this difference was lower in the LPO and DPPC (Figure 4).

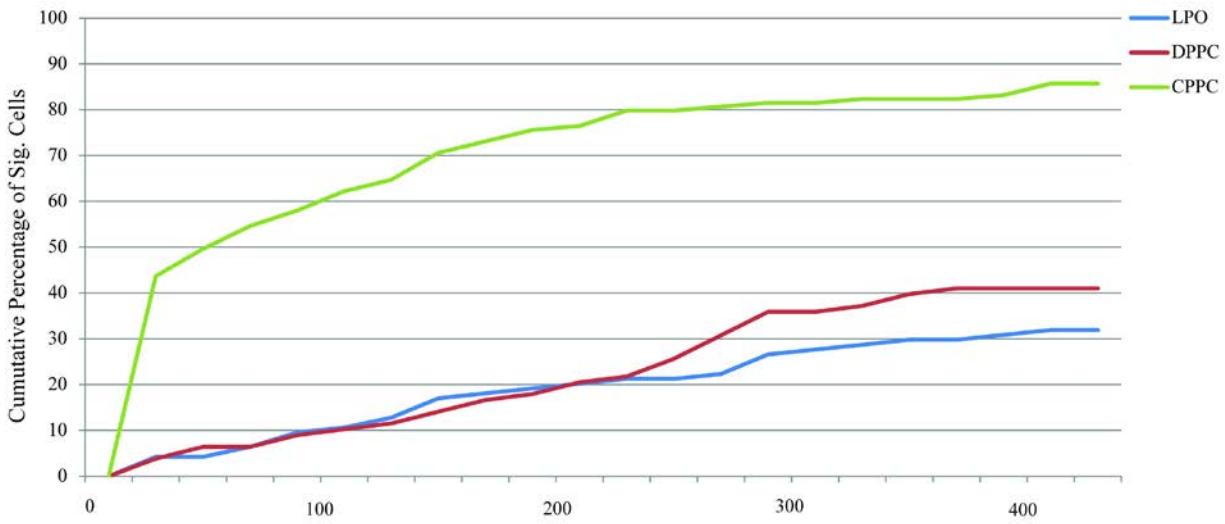


Figure 4. Cumulative percentage of cells that exhibited significant difference between PreStimulus and PostStimulus epochs in at least two continuous sliding windows. Blue, red and green lines indicate cumulative percentage of significant cells in LPO, DPPC and CPPC, respectively.

Table 1. Numbers and percentage of selective cells.

| **Epoch (criterion cells)** | **Correlate** | **LPO Cells (%)** | **DPPC Cells (%)** | **CPPC Cells (%)** |
|---|---|---|---|---|
| Peri-Stimulus | Stimulus Only | 18 (19.15) | 12 (15.38) | *#39 (32.77) |
| | Stimulus and Outcome | 5 (5.32) | 7 (8.97) | 8 (6.72) |
| | Outcome Only | 4 (4.26) | 3 (3.85) | 6 (5.04) |
| Total | | 27 (28.72) | 22 (28.21) | *#53 (44.54) |
| Peri-Selection | Selection Only | 18 (19.15) | 9 (11.54) | 23 (19.33) |
| | Selection and Outcome | 8 (8.51) | 8 (10.26) | 8 (6.72) |
| | Outcome Only | 6 (6.38) | 3 (3.85) | 7 (5.88) |
| Total | | 32 (34.04) | 20 (25.64) | 38 (31.93) |
| Reward-Approach | Outcome | 19 (20.21) | 20 (25.64) | 28 (23.53) |
| Post-stimulus | Allo-Location | 19 (20.21) | 23 (29.49) | 28 (23.53) |
| Pre-selection | Allo-Location | 14 (14.89) | 12 (15.38) | 20 (16.81) |
| Post-selection | Allo-Location | 4 (4.26) | 8 (10.26) | 12 (10.08) |
| Reward | Allo-Location | 13 (13.83) | 15 (19.23) | 23 (19.33) |
| Total | | 37 (39.36) | *43 (55.13) | 59 (49.58) |
| Post-stimulus | Ego-Location | 8 (8.51) | 5 (6.41) | 11 (9.24) |
| Pre-selection | Ego-Location | 5 (5.32) | 11 (14.10) | 10 (8.40) |
| Post-selection | Ego-Location | 19 (20.21) | 10 (12.82) | 13 (10.92) |
| Total | | 29 (30.85) | 22 (28.21) | 30 (25.21) |

* Significantly higher number of selective cells in CPPC than DPPC ($p < 0.05$).
# Significantly higher number of selective cells in CPPC than LPO ($p < 0.05$).

## Discussion

We used our novel VSA task to study functional differentiation in PPC subdivisions and corticothalamic interactions with the LPO. In this series of experiment, we simultaneously recorded neuronal activity in the rat LPO, DPPC and CPPC as animals performed the VSA task. As we predicted, our results showed that the LPO and subregions of the PPC engaged in the visuospatial attention. First, cells from all three brain regions signaled stimulus onset. Compared to DPPC and LPO, however, the CPPC had a significantly larger proportion of cells showing stimulus relevant selectivity. About half CPPC cells showed differential firing patterns immediately after stimulus onset. Second, cells in the LPO, DPPC and CPPC responded to selection behavior and reward; we observed no significant differences among the three areas. Third, cells in all three regions displayed differential firing patterns to task-relevant locations. To analyze allocentric correlates in the VSA task, we pooled same side trials (east and west). To analyze egocentric correlates, we pooled same response trials (left, center and right). Cells in all three brain areas showed allocentric location correlates or egocentric location correlates. Roughly half the DPPC (55.13%) and CPPC (49.58%) cells displayed allocentric location selectivity on the VSA task.

Our observation of DPPC neuronal correlates was consistent with our data in the previous experiment showing that the DPPC cells signaled stimulus onset, stimulus selection, and task-relevant locations during the VSA task. To our knowledge, ours is the first study to examine behavioral correlates of cells in the rat CPPC. Based on our guiding hypothesis, we predicted that functional differentiation in subregions of the rat PPC would be similar to those in the primate PPC. In primates, the dorsal portion of PPC

is involved in top-down attention, which is directed to specific information in the environment according to a subject's goal. The ventral PPC is involved in bottom-up attention, which is engaged when external stimuli grab attention automatically (Corbetta et al., 2000; Shomstein, 2012). We observed that cells in both DPPC and CPPC responded to stimulus onset. The CPPC, however, had a significantly larger proportion of cells showing this type of selectivity. Also, half of CPPC cells displayed differential firing patterns between pre-stimulus and post-stimulus epochs immediately after stimulus onset. Our results support the view that the rodent CPPC is preferentially engaged in bottom-up attention process, similar to the ventral PPC in the primate brain.

We also observed that a large proportion of LPO cells displayed differential firing pattern between pre- and post-stimulus epochs. Previous studies anatomical studies provided evidence that the rat LPO is a connectional homologue area of primate pulvinar, however, electrophysiological evidence for homology between the LPO and pulvinar is lacking. The pulvinar in primates has been considered as a part of attention circuitry (Arend et al., 2008; Grieve, Acuna, & Cudeiro, 2000). Although detailed mechanisms still need to be clarified, our results providesthe first piece of evidence that the rat LPO is also involved in visuospatial attention.

Our results showed that the LPO, DPPC and CPPC had more than 25% of cells displaying selectivity around peri-selection epochs. During peri-selection epochs, animals first selected a target location to approach, after selection, they knew the outcome of the selection (correct or incorrect). These data suggest that the LPO is not a primary sensory thalamic nucleus like lateral geniculate nucleus, which is considered visual thalamus. In contrast, the LPO with its connection to cortical association areas, such as PPC, is in

good position to process and integrate information in the service of visuospatial attention. We also confirmed the CPPC is similar to DPPC in that it engages in selection behavior when animals perform a visuospatial attention task. We further observed that there were about 20-25% cells in the LPO, DPPC and CPPC displaying differential firing rates between correct and incorrect trials during reward epoch. This finding is consistent with a monkey study reporting that inactivation of the pulvinar impaired reward-based selection without impairing perception or memory (Wilke, Kagan, & Andersen, 2013). This study suggested that the reward expectation signaled by the pulvinar might be able to modulate activity in cortical areas, such as PPC and prefrontal cortex. Our results support this view by providing evidence for the interaction between LPO and PPC subregions in the VSA task.

Although the LPO and PPC are thought to be important brain structures for visuospatial attention, only a few electrophysiological studies have examined the role of DPPC in spatial processing, and there are no such studies of the LPO and CPPC. We observed that cells in the LPO, DPPC and CPPC showed task-relevant allocentric and/or egocentric location selectivity. A few studies have shown task-relevant spatial correlates in rat DPPC (Nitz, 2012, 2014; Whitlock, 2014; Wilber et al., 2014). One of these studies reported that the DPPC responded to both allocentric- and egocentric spatial locations (Wilber et al., 2014). We also found that DPPC cells respond to both allocentric- and egocentric spatial locations in rats performing the VSA task. We also showed, however, that neurons in the LPO and CPPC respond to task-relevant allocentric and egocentric locations. To our knowledge, these results are first evidence to reveal attentional

correlates in these anatomically connected brain structures by recording them simultaneously.

The present study was one of a series aimed at understanding the behavioral function of the PPC in visuospatial attention. Here, we showed evidence from simultaneous recordings of cells in the LPO, DPPC and CPPC in freely moving rats performing a task with high visuospatial attentional demands. These data indicated that, first, the functions of the LPO go beyond those of a sensory thalamic nucleus to process attentional information similar to the functions of the primate pulvinar. Second, in the rat brain, similar to primate brain, the LPO, DPPC and CPP have anatomical connections as well as behavioral interactions in visuospatial attention. Furthermore, the rat PPC is subdivided in similar to primate PPC, such that the caudal portion is be more relevant to bottom-up attention. The direction of information flow between the LPO and PPC within the visuospatial attention circuit is still an open question. Our follow-up study uses optogenetic approaches to address how the LPO interacts with the PPC in the service of attention.

## References


Arend, I., Machado, L., Ward, R., McGrath, M., Ro, T., & Rafal, R. D. (2008). Chapter 5.15 - The role of the human pulvinar in visual attention and action: evidence from temporal-order judgment, saccade decision, and antisaccade tasks. *Progress in Brain Research*, 475-483.

Chandler, H. C., King, V., Corwin, J. V., & Reep, R. L. (1992). Thalamocortical connections of rat posterior parietal cortex. *Neuroscience Letters, 143*(1-2), 237-242.

Corbetta, M., Kincade, J. M., Ollinger, J. M., McAvoy, M. P., & Shulman, G. L. (2000). Voluntary orienting is dissociated from target detection in human posterior parietal cortex. *Nature Neuroscience, 3*(3), 292-297.

Furtak, S. C., Cho, C. E., Kerr, K. M., Barredo, J. L., Alleyne, J. E., Patterson, Y. R., & Burwell, R. D. (2009). The Floor Projection Maze: A novel behavioral apparatus for presenting visual stimuli to rats. *Journal of Neuroscience Methods, 181*(1), 82-88.

Grieve, K. L., Acuna, C., & Cudeiro, J. (2000). The primate pulvinar nuclei: vision and action. *Trends in Neurosciences, 23*(1), 35-39.

Jacobson, T. K., Ho, J. W., Kent, B. W., Yang, F. C., & Burwell, R. D. (2014). Automated visual cognitive tasks for recording neural activity using a Floor Projection Maze. *Journal of Visual Experimentation*.

Kamishina, H., Conte, W. L., Patel, S. S., Tai, R. J., Corwin, J. V., & Reep, R. L. (2009). Cortical connections of the rat lateral posterior thalamic nucleus. *Brain Research, 1264*, 39-56. doi:doi: 10.1016/j.brainres.2009.01.024

Mason, R. & Groos, G. A. (1981). Cortico-recipient and tecto-recipient visual zones in the rat's lateral posterior (pulvinar) nucleus: An anatomical study, *Neuroscience Letters,25,* 107-112.

Nitz, D. (2009). Parietal cortex, navigation, and the construction of arbitrary reference frames for spatial information. *Neurobiology of Learning and Memory, 91*, 179-185.

Nitz, D. (2012). Spaces within spaces: rat parietal cortex neurons register position across three reference frames. *Nature Neuroscience, 15*(10), 1365-1367.

Nitz, D. (2014). The posterior parietal cortex: Interface between maps of external spaces and the generation of action sequences. In D. Derdikman & J. J. Knierim (Eds.), *Space,Time and Memory in the Hippocampal Formation* (pp. 27-54): Springer Vienna.

Reep, R. L., Chandler, H. C., King, V., & Corwin, J. V. (1994). Rat posterior parietal cortex: topography of corticocortical and thalamic connections. *Experimental Brain Research, 100*(1), 67-84.

Reep, R. L., & Corwin, J. V. (2009). Posterior parietal cortex as part of a neural network for directed attention in rats. *Neurobiology of Learning and Memory, 91*(2), 104-113.

Saalmann, Y. B., Pinsk, M. A., Wang, L., Li, X., & Kastner, S. (2012). The pulvinar regulates information transmission between cortical areas based on attention demands. *Science, 337*(6095), 753-756.

Shomstein, S. (2012). Cognitive Functions of the Posterior Parietal Cortex: Top-down and bottom-up attentional control. *Frontiers in Integrative Neuroscience, 6*.

Smith, A. T., Cotton, P. L., Bruno, A., & Moutsiana, C. (2009). Dissociating vision and visual attention in the human pulvinar. *Journal of Neurophysiology, 101*(2), 917-925.

Whitlock, J. R. (2014). Navigating actions through the rodent parietal cortex. *Frontiers in Human Neuroscience, 8*.

Wilber, A. A., Clark, B. J., Forster, T. C., Tatsuno, M., & McNaughton, B. L. (2014). Interaction of egocentric and world-centered reference frames in the rat posterior parietal cortex. *The Journal of Neuroscience, 34*(16), 5431-5446.

Wilke, M., Kagan, I., & Andersen, R. A. (2013). Effects of pulvinar inactivation on spatial decision-making between equal and asymmetric reward options. *Journal of Cognitive Neuroscience, 25*(8), 1270-1283.

# CHAPTER 5

# INACTIVATION EFFECT OF THE LATERAL POSTERIOR THALAMIC NUCLEUS ON NEURONAL CORRELATES IN RAT POSTERIOR PARIETAL CORTEX DURING PERFORMANCE ON A VISUOSPATIAL ATTENTION TASK

**Abstract**

The posterior parietal cortex (PPC) receives input from visual cortex and from the lateral posterior nucleus of thalamus (LPO), the functional homolog of the primate pulvinar. Like the PPC, the LPO and pulvinar are also implicated in attention. In primates, the pulvinar differentially projects to two subdivisions of the PPC. Our previous results (Chapter 4 of this thesis) showed that neuronal activity in the DPPC and CPPC is consistent with top-down and bottom-up attentional functions, respectively. We also observed that the neuronal activity in LPO and parietal subdivisions correlated with multiple phases of a visuospatial attention (VSA) task, including onset of the visual stimuli, decision-making, task-relevant location, and behavioral outcome. To understand how posterior parietal activity depends on the LPO, we simultaneously recorded neuronal activity in the LPO, DPPC, and CPPC in male Long-Evans rats during performance on the VSA task. On some trials, LPO activity was optogenetically inhibited. We recorded neuronal activity in six rats performing the VSA task. We isolated 318 cells in the DPPC, 225 cells in the CPPC, and 474 cells in the LPO. We report that the LPO and PPC cells signaled stimulus onset and selection behavior consistent with the interpretation that the LPO and PPC are engaged in both top-down and bottom-up visuospatial attention. We also observed that LPO and PPC cells responded to allocentric and egocentric task-relevant locations. Preliminary analyses showed that behavioral correlates of LPO and PPC neurons disappeared or changed during optogenetic inhibition of LPO activity supporting our hypothesis that the parietal activity depends on the LPO inputs when visuospatial attentional demands are high.

## Introduction

The findings reported in Chapters 2-4 link the anatomical connections between the LPO and PPC to their functional interactions. These results are in line with some primate studies supporting a view that primate pulvinar, a homologue of rat LPO, is engaged in visuospatial attention and regulates neuronal activity in cortical areas (Petersen et al., 1987; Purushothaman et al., 2012; Saalmann & Kastner, 2011; Saalmann et al., 2012; Zhou et al., 2016). A recent monkey study reported that unilateral pulvinar inactivation did not significantly influence accuracy of goal directed behavior. However, the inactivation resulted in strong bias of visually guided selection toward the side ipsilateral to the inactivation resulting in a form of visual attentional neglect (Wilke, Turchi, Smith, Mishkin, & Leopold, 2010). Another study further reported that attention-relevant activity in the monkey pulvinar interacted with in the secondary visual area, V4. Inactivation of the pulvinar resulted in a reduction of attentional modulation on both cell firing rate and brain oscillations in V4 (Zhou et al., 2016). Other evidence showed increased thalamocortical coherence in monkeys performing a visuospatial attention task (Saalmann et al., 2012). Coherence was increased between the pulvinar and higher order visual areas, V4 and TEO. These findings, especially the inactivation studies, support a view that the pulvinar is not only crucial for attention, but also that the pulvinar modulates attention-related neuronal activity in cortical areas. To our knowledge, there are no rodent studies of attention in which LPO-PPC interactions were manipulated.

We hypothesized that the attentional functions of the PPC including the functional differentiation between the DPPC and CPPC rely on sensory inputs provided by the LPO.

To address this hypothesis, we injected Halorhodopsin (NpHR) in the LPO in order to suppress the LPO and the LPO inputs to the PPC during performance on the VSA task in the two-sided bowtie maze. All behavioral procedures and setup in this experiment were similar to the previous experiment reported in Chapter 4 except that we added trials with optical suppression of the LPO to all recording sessions. The optogenetic manipulation required modification to the microdrive. We used a larger microdrive with the addition of a polymer optical fiber integrated with the bundle of recording electrodes inplanted into the LPO. Our prediction was that suppression of the LPO would influence neuronal correlates in the PPC during the VSA task possibly causing attentional neglect in the visual hemifield contralateral to the LPO suppression.

## Methods

### *Subjects*

Subjects were six male Long-Evan rats (Charles Rivers Laboratories, Wilmington, MA). They were individually housed in a temperature-regulated colony maintained on a 12:12 h light:dark cycle. Experiments were carried out in the light phase. All procedures followed the NIH guidelines and were approved by the Brown University animal care and use committee.

### *Viral vectors*

For viral transduction in the LPO, pAAV-hSyn-eNpHR 3.0-EYFP plasmid with an inhibitory halorhodopsin (NpHR)-EYFP fusion gene driven by a synapsin 1 promoter packaged into an adeno-associated viral vector (AAV9) at the University of Pennsylvania Vector Core was used. Plasmid maps are available at www.optogenetics.org. Viral titers were 2.04 e13 GC/mL.

***Apparatus***

Our task uses the Floor Projection Maze, an apparatus that exploits the natural tendency of rats to attend to items located on or close to the ground and permits automated control over visual stimuli (Furtak et al., 2009; Jacobson, Ho, Kent, Yang, & Burwell, 2014) . Essentially, the Floor Projection Maze is a horizontal rear projection screen positioned to allow back-projection of visual stimuli and to serve as a floor to any shaped arena (Figure 1A). The apparatus has a clear Plexiglas subfloor (147.3 cm x 111.8 cm) with a (1.25 cm thick) covered by Dual Vision Fabric (Da-Lite Screen Company, Warsaw, IN), a unity gain flexible fabric designed for rear screen projection. A thin sheet (Plexiglas 0.6 cm) covers the fabric for protection. Visual stimuli were projected onto the unity gain fabric from below the subfloor using an LCD projector (WT610 projector, NEC Corporation). In this experiment, the enclosure was a bowtie shaped region for presentation of stimuli. Food reward (milk with various flavors) was delivered by two automated pumps (Med Associates, Inc, St. Albans, VT) to stainless steel food ports located at middle region of the maze. Auditory stimuli were controlled by an automated auditory stimulus generator (ANL926, Med Associates, Inc.) and delivered through a speaker located above the maze.

The Floor Projection Maze was interfaced with three Windows PC systems, for location tracking, behavioral control, and neuronal data acquisition. A CinePlex Behavioral Research System (CinePlex Studio and CinePlex Editor) v3.4.1 with a single camera and two additional CinePlex modules, CinePlex Tracking and CinePlex Basic Behavior was used for tracking animal's location during behavioral performance. The position of the rat was recorded by tracking the centroid of the contour of the rat using

the CinePlex Tracking module. Position data are analyzed online in the CinePlex Basic Behavior module and also saved in a Plexon data file for further offline analysis. Based on the location of the rat, this system presented stimuli, collected behavioral data, and controlled delivery of reward. A OmniPlex Neural Data Acquisition System (Plexon, Inc) and SortClient (Plexon, Inc) recorded real-time neuronal activity and behaviorally relevant event timestamps for later analysis. The OminiPlex system was interfaced with the Med Associates system (DIG-716B SmartCTL, DIG-713A SuperPort TTL Inuput module and DIG-726 SuperPort TTL Output module).

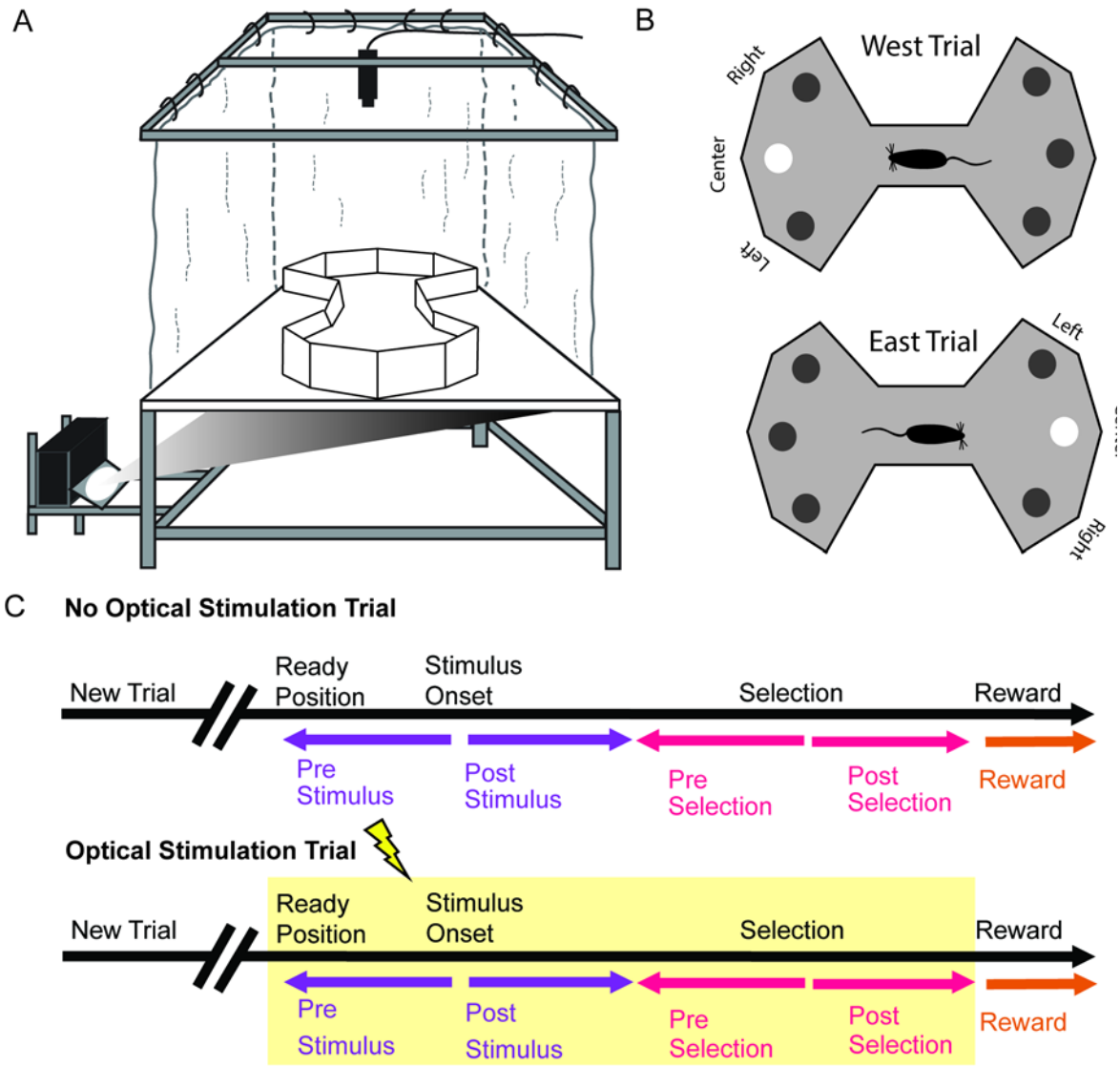


Figure 1. The Visuospatial Attention (VSA) task. A. Schematic of the Floor Projection Maze with the bowtie-shaped enclosure used for the task. B. Topdown view of west vs. east trials. Trials were initiated when the rat stopped in the ready position (middle of the maze) and faced to one side of the maze (either west or east). After a variable period, the target location was briefly illuminated. The animal made a selection by approaching one of the three locations in the same side, and then returned to the food port for a food reward. After the animal consumed the reward, a new trial from the alternative side would be triggered immediately. C. Trials with and without optical suppression. Optical suppression was added randomly to trials. The duration of suppression started when the rat entered ready position initiating a new trial and ended when the rat entered the reward zone terminating the trial.

### *Optical Suppression*

LPO neurons were stimulated optogenetically at 40 Hz with 15 ms pulse width. LPO was transduced with the light sensitive inhibitory protein halorhodopsin for optical suppression. For optical suppression, we used multimode fiber (Paradigm optics; core

diameter 240 microns, 0.5 NA). The fibers were pulled using a laser-based pipette puller (P-97; Sutter Instruments) and attached to a ferrule before inserted into the microdrive. All pulled fibers were tested before use and only fibers delivering light with at least 80% efficiency were used in the experiment. Light suppression was delivered by a PlexBright Optogenetic Stimulation System (Plexon, Inc) through a 4 channel optogenetic controller with a software (Radiant, Plexon, Inc.). The light suppression and connecting cable were tested before each session.

***Behavioral training***

Rats were put on food schedules to maintain body weight at 85-90% of free feeding weight. After handling for at least 7 days, rats were habituated to the behavioral room for 10 min/day for three days. Rats were then shaped and trained in the VSA task. In the shaping sessions, rats first were trained in a 30 minute session to approach a visual target stimulus for a food reward (a drop of flavored milk). In the initial shaping sessions, we adopted an errorless shaping procedure such that when the rat moved toward one of the three locations in one side of the maze, the visual stimulus at that location would illuminate and a tone would signal a correct choice. A new trial on the other side of the maze would be initiated after the rat entered reward area. After this initial shaping phase, rats were trained to stop in the ready position zone located in the middle of the bowtie shaped maze facing the stimulus presenting area. After a variable delay, a visual stimulus would illuminate in one of three randomly chosen locations. There was a short response window for rats to approach the location of the visual stimulus. Approach to the correct location was signaled by a brief tone and presentation of a drop of flavored milk as a food reward. If the rat approached an incorrect location, no reward was given, the trial was

terminated, and a new trial would begin immediately. Rats were gradually trained in a series of steps culminating in the final parameters of the task. The duration for rats to stay in the ready position was gradually increased from 0.1 seconds to 1.6 seconds. Visual stimulus duration was gradually decreased from 20 seconds to 0.5 seconds. The response time window was decreased from 20 seconds to 5 seconds. In the final task, rats were required to stay in the ready position for stimulus onset for a variable interval (1.2-1.6 seconds) (Figure 1B).

The behavioral performance criterion for the end of training was 70% accuracy on the VSA task (chance is 33.33%). Behavior was well controlled on correct trials. Rats in this study required 2-3 months of training to reach the behavioral criterion on the final stage of the task. A surgery for implanting the hyperdrive was done after a rat reached behavioral criterion for 5 to 7 consecutive days.

For recording sessions after implanting surgery, optical suppressions were added randomly to trials for whole session. The duration of optical suppression started when the rat entered ready position initiating a new trial and ended when the rat entered the reward zone terminating the trial. So, for one recording session, there were both trials with and without optical suppression.

***Surgery***

Animals were premedicated with diazepam (2-5 mg/kg; i.p.), glycopyrrolate (0.05 mg/kg; s.c.), carprofen (5 mg/kg; s.c.), and butorphanol tartrate (0.5 mg/kg; s.c.) to counteract respiratory effects of anesthesia, to control pain, and to decrease risk of seizures. They were brought to a surgical level of anesthesia with isofluorane (1.0 – 2.5%). Using a stereotaxic apparatus (Kopf, Tujunga, CA), rats were unilaterally

implanted with a custom hyperdrive into the LPO (AP –3.9 mm, ML ± 2.0 mm, DV–4.0mm), dorsal PPC (AP – 4.2 mm, ML ± 3.0mm, DV -0.1mm), and caudal PPC (AP – 5.5 mm, ML ± 4.5 mm, DV -2.0 mm). The hyperdrive had fourteen microdrives for recording neuronal activity and two fibers for optical suppression. Each microdrive consisted a drivable screw with guide tubing containing on stereotrode. Stereotrodes were made of two 12 μm twisted, formvar-insulated nichrome wires (A-M systems, Sequim, WA). A full turn of the screw advanced the stereotrode by 350 μm. Two silver ground wires were wrapped around anchor screws in the skull. The hyperdrive was secured to the skull by the ground screws, small anchor screws, grip cement (Dentsply Caulk, Milford, DE), and dental cement (Coltene/Whaledent Inc., Cuyahoga Falls, OH).

***Histology***

After the last recording session, the rats were deeply anesthetized with an overdose of Beuthanasia-D (100 mg/kg, i.p.) and the final recording site was marked with an electrolytic lesion. The rats were then perfused with normal saline, followed by 4% formalin. The brains were post-fixed for 24 hours in 4% formalin and then transferred to a 30% sucrose solution until the time for sectioning. The brains were sectioned at 40 μm. One set stained with Nissl material using thionin for examining electrode implanting sites. Another set stained for DAPI (VECTASHIELD, Vector Laboratories) to see the NpHR expression in the LPO.

***Electrophysiology***

Neuronal activity recorded from stereotrodes, was amplified with a gain of 20 at the head stage (HST/32V-G20, Plexon, Inc., Dallas, TX). Signals were passed through a high-gain amplifier (total = 10000X, Omniplex system, Plexon, Inc., Dallas, TX). Single-

unit activity was filtered between 0.8 - 6 Hz. The signal was then digitized at 40 kHz for single-unit activity. These signals were extracted through real-time thresholding (Sort Client, Plexon, Inc). The final waveforms were stored with timestamps of relevant events and position information for later anal Single neuron activity analysis

***Single neuron activity analysis***

Spikes associated with putative individual cells were isolated offline based on waveform characteristics and using a variety of partially-automated and manual techniques (Offline Sorter, Plexon, Inc.). The result was a dataset for each cell containing timestamps corresponding to spike times and behaviorally relevant event markers. These datasets were further analyzed using Neuroexplorer (NEX, Nex Technologies, Madision, AL) and SPSS.

Each cell was first analyzed for changes in firing rates due to suppression of LPO. We calculated mean firing rates from suppression and no-suppression trials and compared differences using a t-test. Then, each cell was analyzed for behavioral correlates using factorial analysis of variance (fANOVA). We analyzed five epochs from each completed trial: pre-stimulus and post-stimulus epochs were the 500 msec periods immediately before and after stimulus onset; pre-selection and post-selection epochs were the 500 msec periods immediately before and after the rat selected a target by approaching the location; and the reward-approach epoch was the first 500 msec after the animal entered the food reward area. The selection time event was the moment the rat entered a zone just in front of the location in which the target stimulus had appeared. Entry of the ready position of the other side of bowtie maze triggered the next trial. Rats invariably approached and checked the food port even after incorrect trials.

Firing rate was the dependent variable for the fANOVAs. For each neuron, we first computed the mean firing rate (spikes/sec) for each epoch on each trial. In the first set of analyses, the between-trial variable was outcome (correct response vs. incorrect response), and the two within-trial variables were stimulus onset (pre-stimulus vs. post-stimulus) and selection time (pre-selection vs. post-selection). Outcome was analyzed for the reward-approach epoch. Only trials with no optical suppression were used in this analysis.

In a second set of analyses, we examined neural correlates associated with the location of the target stimulus. Only trials with no optical suppression were used in this set of analyses. Based on the location of stimulus presentation, we pooled trials in which the target stimulus was at the same side of the maze (east vs. west) for analyzing allocentric location correlates. We then pooled trials in which the target stimulus was at the same egocentric location (left, right, and center) for analyzing egocentric location correlates. We also included outcome (correct vs. incorrect) as a factor because we have observed cells in all three brain regions showing outcome correlates. A fANOVA was computed on each cell from all target regions. Thus, between trial variables were choice location (left vs. right) and outcome (correct vs. incorrect). Location cells were cells that showed a main effect of location or an interaction with location.Thus, the between trial variables were choice location (either allocentric location or egocentric location) and outcome (correct vs. incorrect). Location cells were cells that showed a main effect of location or an interaction with location. Allocentric location was analyzed separately for the post-stimulus, pre-selection, post-selection, and reward epochs. The pre-stimulus epochs was not analyzed for trial location because there was no information about the

allocentric location. Egocentric location was analyzed for the post-stimulus, preselection, and post-selection epochs without pre-stimulus and reward epochs.

## Results

### *Histology*

Examination of Nissl-stained coronal brain sections from each of the six animals indicated electrode tips were located in LPO between 3.48-4.2 mm posterior to bregma and between 1.5-3.0 mm lateral to the midline; DPPC between 3.8-4.36 mm posterior to bregma and between 2.0-5.0 mm lateral to the midline; CPPC between 5.2-6.0 mm posterior to bregma and between 6.0-7.0 mm lateral to the midline (Figure 2). Few stereotrodes were located in the adjacent brain regions including posterior thalamic nucleus (PO) and visual cortex.

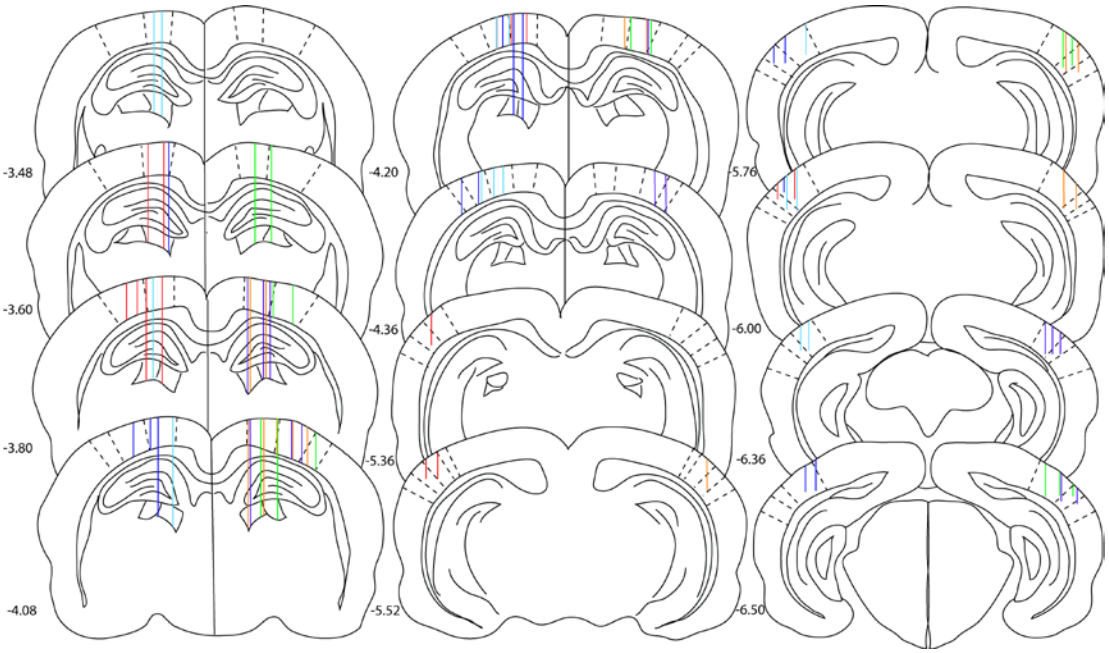


Figure 2. Estimated locations of implanted stereotrode. Various color indicated stereotrodes from different animals. Same color indicated stereotrodes from the same animal.

NpHR expressions were located within the LPO for all subjects. Figure 3 shows an example of an optic fiber implant in the left LPO. All five animals yielded isolated

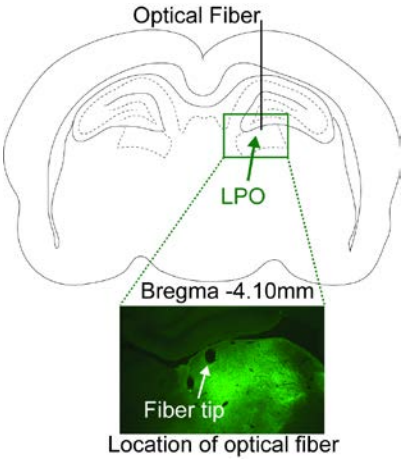


Figure 3. Optical fiber target in the lateral posterior nucleus of thalamus (LPO).

units. A total of 474 LPO cells, 318 DPPC cells, and 225 CPPC cells that have good qualities were used in following analyses. We also recorded 64 cells in the PO and 65 cells in the visual cortex. Each cell was recorded for a single session. The majority of these criterion cells, 438 (92.41%) in the LPO; 281 (88.36%) in the DPPC; 205 (91.11%) in the CPPC, exhibited behavioral correlate(s) during at least one of the task epochs as indicated by main effects or interactions of stimulus onset, target selection time, location, or outcome. To investigate neuronal correlates of all cells, we first analyzed neuronal responses to stimulus onset by comparing firing rates for the 500 ms before vs 500 ms after the onset of the 500 ms illumination of the target stimulus for correct vs incorrect trials. Of all cells, 130 (27.43 %) LPO cells, 68 (21.38 %) DPPC cells, and 65 (28.89 %) CPPC cells showed some form of selectivity for stimulus onset. Of these cells, 78 LPO cells (16.46 %), 34 DPPC cells (10.69 %), and 24 CPPC cells (10.67%) showed significant increases or decreases in firing rate associated with stimulus onset, alone (Table 1). For example, example cells from LPO, DPPC and CPPC shown in Figure 4A-C fired more during the post-stimulus epoch than the pre-stimulus epoch. Thiry-five (7.38 %) LPO cells, 16 (5.03 %) DPPC cells, and 32 (14.22 %) CPPC cells fired differentially depending on whether the animal was about to make a correct selection. Seventeen (3.59 %) LPO cells, 18 (5.66 %) DPPC cells and 9 (4.00 %) CPPC cells exhibited a main effect

of outcome alone. Thus, a total of 52 (10.97 %) LPO cells, 34 (10.69 %) DPPC cells, and 41 (18.22 %) CPPC cells fired differentially depending on the subsequent outcome of the trial.

Of all cells, 113 (23.84%) LPO cells, 50 (15.72%) DPPC cells, and 56 (24.89%) CPPC cells showed some form of selectivity for stimulus (including cells with stimulus-only correlates and cells with both stimulus and outcome correlates). The LPO and CPP both had significantly larger proportion cells exhibiting selectivity for stimulus onset, comparing to cells in the DPPC ($\chi^2_{(1)} = 7.67$, $p = 0.01$; $\chi^2_{(1)} = 7.05$, $p = 0.01$). No difference was found in LPO and CPPC.

***LPO, DPPC and CPPC cells signaled target selection and behavioral outcome***

For this set of analysis, we only used trials without optical suppression. Similar to our previous findings, the activity of LPO, DPPC, and CPPC cells correlated with target selection. One hundred and sixty (33.76 %) LPO cells, 122 (38.36%) DPPC cells and 98 (43.56 %) CPPC cells signaled selection by firing more during either pre-selection or post-selection epoch (Table 1 and Figure 4D-F). Thirty (6.33 %) LPO cells, 24 (7.55 %) DPPC cells, and 20 (8.89 %) CPPC cells signaled both selection and outcome. Twenty-one (4.43 %) LPO cells, 10 (3.14 %) DPPC cells, and 6 (2.67 %) CPPC cells responded to outcome alone during the peri-selection interval. Thus, 190 (40.08%) LPO cells, 146 (45.91 %) DPPC cells and 118 (52.44 %) CPPC cells differentiated pre- and post-selection epochs. Fifty-one (10.76 %) LPO cells, 34 (10.69 %) DPPC cells, and 26 (11.56 %) CPPC cells displayed differential firing patterns related to behavioral outcome.

Of all cells, 190 (40.08%) LPO cells, 146 (45.91%) DPPC cells, and 118 (52.44%) CPPC cells showed some form of selectivity for selection (including cells with selection-only correlates and cells with both selection and outcome correlates). The CPPC had significantly larger proportion cells exhibiting selectivity for selection, comparing to cells in the LPO ($\chi^2_{(1)} = 9.457$, $p < 0.01$). No difference was found between LPO and DPPC or between DPPC and CPPC.

For the reward-approach epoch, in which the animal had just entered food area after selecting a target location, 59 (12.45 %) LPO cells, 38 (11.95 %) DPPC cells, and 22 (9.78 %) CPPC cells displayed selectivity for different outcomes in the reward-approach epoch (Table 1, Figure 4G-I). Two representative cells from the LPO and DPPC, shown in Figure 4G-H, fired more in incorrect trials than correct trials. Figure 4I displayed a CPPC cell that fired more in correct trials than incorrect trials during the reward- approach epoch.

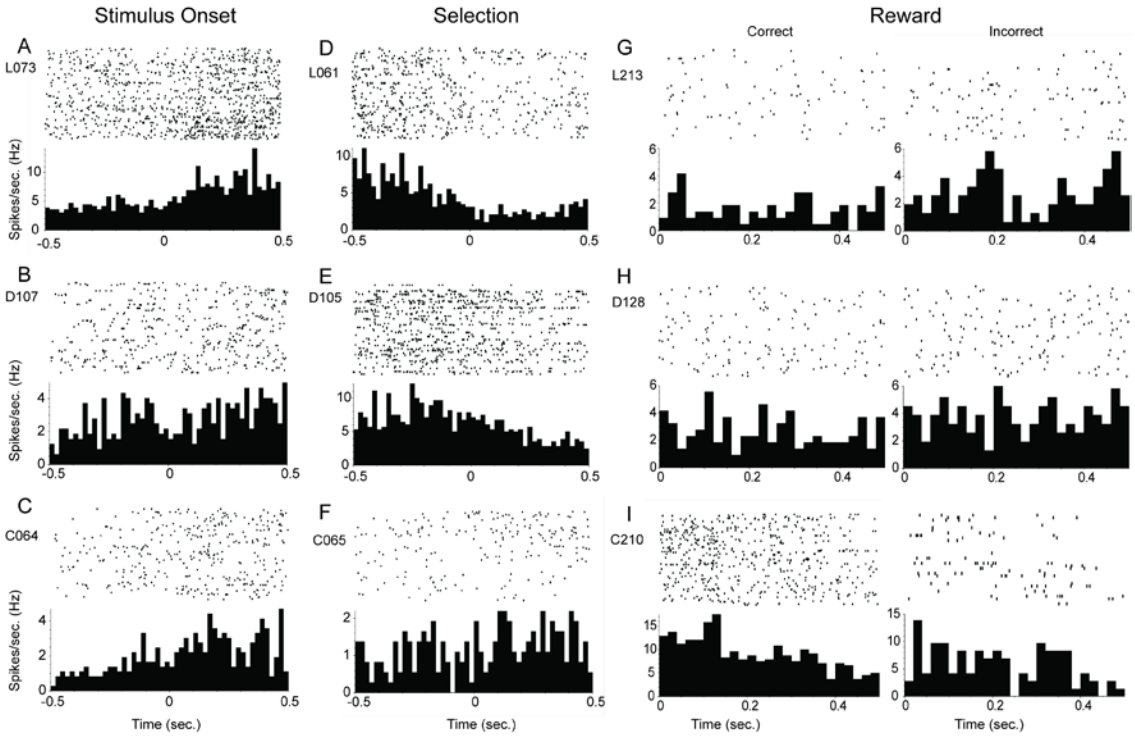

Figure 4. Example neuronal correlates for LPO, DPPC, and CPPC cells. Perievent ratster plots and

histograms are shown for example cells with behaviorally relevant firing patterns. For the stimulus epoch, time 0 is stimulus onset (A, B, C). For the selection epoch, time 0 is selection (D, E, F). For the reward epoch, time 0 is when the animal entered the reward area (G, H, I). Example cells shown in upper panels were recorded from the LPO (A, D, G); cells in middle panels were recorded from the DPPC (B, E, H); cells in lower panels were recorded from the CPPC (C, F, I).

***LPO, DPPC and CPPC cells signaled allocentric and egocentric location.***

We have found previously that LPO, DPPC and CPPC cells displayed selectivity for the allocentric and egocentric location of the target stimulus. In this series of analysis, we further investigated neuronal correlates of location with behavioral outcomes of the VSA task. We analyzed the post-stimulus, pre-selection, and post-selection epochs because spatial location was relevant during these epochs. Reward epoch was also analyzed for allocentric location correlate. For this set of analysis, we only used trials without optical suppression. As expected, trial location selectivity was evident in all analyzed epochs (Table 2-3). Based on the location of stimulus presentation, we pooled trials in which the target stimulus was at the same side of the maze (east vs. west) for analyzing allocentric location correlates (Table 2). We then pooled trials in which the target stimulus was at the same egocentric location (left, right, and center) for analyzing egocentric location correlates (Table 3).

Table 1. Numbers and percentage of selective cells.

| **Epoch (criterion, cells)** | **Correlate** | **LPO 474 (%)** | **DPPC 318 (%)** | **CPPC 225 (%)** |
|---|---|---|---|---|
| Peri-Stimulus | Stimulus Only | 78(16.46) | 34 (10.69) | 24 (10.67) |
| | Stimulus and Outcome | 35(7.38) | 16 (5.03) | 32 (14.22) |
| | [Stimulus Only+ Both] | *113 (23.84) | 50 (15.72) | + 56 (24.89) |
| | Outcome Only | 17(3.59) | 18 (5.66) | 9 (4) |
| Total | | 130(27.43) | 68 (21.38) | 65 (28.89) |
| Peri-Selection | Selection Only | 160 (33.76) | 122 (38.36) | 98 (43.56) |
| | Selection and Outcome | 30 (6.33) | 24 (7.55) | 20 (8.89) |
| | [Selection Only + Both] | 190 (40.08) | 146 (45.91) | # 118 (52.44) |
| | Outcome Only | 21 (4.43) | 10 (3.14) | 6 (2.67) |
| Total | | 211 (44.51) | 156 (49.06) | 124 (55.11) |
| Reward-Approach | Outcome | 59 (12.45) | 38 (11.95) | 22 (9.78) |
| Total | Selectivity | 305 (64.35) | 117 (36.79) | 157 (69.78) |

* Significantly higher number of selective cells in LPO than DPPC ($p < 0.05$). + Significantly higher number of selective cells in CPPC than DPPC ($p < 0.05$). # Significantly higher number of selective cells in CPPC than LPO ($p < 0.05$).

For allocentric location correlates in the LPO, 50 (10.55%) cells in the post-stimulus epoch, 58 (12.24 %) cells in the pre-selection epoch, 60 (12.66 %) cells in the post-selection epoch, and 99 (20.89%) cells in the reward epoch showed a significant difference in firing rate between east and west side trails. Thirty-seven (7.80%) cells in the post-stimulus epoch, 25 (5.27 %) cells in the pre-selection epoch, 31 (6.54 %) cells in the post-selection epoch, and 44 (9.28 %) cells in the reward epoch responded to both allocentric location and outcome. Twenty-two (4.64 %) cells in the post-stimulus epoch, 20 (4.22 %) cells in the pre-selection epoch, 23 (4.85 %) cells in the post-selection epoch, and 28 (5.19 %) cells in the reward epoch signaled differentially to correct and incorrect outcomes. Figure 5A-B showed two LPO cells that had allocentric correlates to west or east trials during pre-selection epoch.

Similar allocentric location correlates were also observed in the PPC subregions. In the DPPC, 37 (11.64 %) cells in the post-stimulus epoch, 51 (16.04 %) cells in the pre-selection epoch, 37 (11.64 %) cells in the post-selection epoch, and 52 (16.35 %) cells in the reward epoch showed a significant difference in firing rate between east and west side trails. Twenty-seven (8.50 %) cells in the post-stimulus epoch, 20 (6.29 %) cells in the pre-selection epoch, 22 (6.92 %) cells in the post-selection epoch, and 24 (7.55 %) cells in the reward epoch responded to both allocentric location and outcome. Ten (3.14 %) cells in the post-stimulus epoch, 8 (2.52 %) cells in the pre-selection epoch, 16 (5.03 %) cells in the post-selection epoch, and 18 (5.67 %) cells in the reward epoch signaled differentially to correct and incorrect outcomes. In the CPPC, 22 (9.78 %) cells in the post-stimulus epoch, 23 (10.22 %) cells in the pre-selection epoch, 25 (11.11 %) cells in

the post-selection epoch, and 48 (21.33 %) cells in the reward epoch showed a significant difference in firing rate between east and west side trails. Twenty (8.89 %) cells in the post-stimulus epoch, 16 (7.11 %) cells in the pre-selection epoch, 24 (10.67 %) cells in the post-selection epoch, and 23 (10.22 %) cells in the reward epoch responded to both allocentric location and outcome. Three (1.33 %) cells in the post-stimulus epoch, 9 (4.00 %) cells in the pre-selection epoch, 14 (6.22 %) cells in the post-selection epoch, and 12 (5.33 %) cells in the reward epoch signaled differentially to correct and incorrect outcomes. Figure 5C-F showed two DPPC cells and two CPPC cells that had allocentric correlates to west or east trials during pre-selection epoch.

In summary, a total of 319 (67.29 %) LPO cells, 195 (61.32 %) DPPC cells, and 160 (71.11 %) CPPC cells displayed selectivity in this analysis.

Table 2. Number and percentage of selective cells for allocentric location correlates.

| **Epoch (criterion cells)** | **Correlate** | **LPO 474 (%)** | **DPPC 318 (%)** | **CPPC 225 (%)** |
|---|---|---|---|---|
| PostStimulus | Allocentric Only | 50 (10.55) | 37 (11.64) | 22 (9.78) |
| | Allocentric and Outcome | 37 (7.80) | 27 (8.50) | 20 (8.89) |
| | Outcome Only | 22 (4.64) | 10 (3.14) | 3 (1.33) |
| Total | | 109 (23.00) | 74 (23.27) | 45 (20) |
| PreSelection | Allocentric Only | 58 (12.24) | 51 (16.04) | 23 (10.22) |
| | Allocentric and Outcome | 25 (5.27) | 20 (6.29) | 16 (7.11) |
| | Outcome Only | 20 (4.22) | 8 (2.52) | 9 (4.00) |
| Total | | 103 (21.73) | 79 (24.84) | 48 (21.33) |
| PostSelection | Allocentric Only | 60 (12.66) | 37 (11.64) | 25 (11.11) |
| | Allocentric and Outcome | 31 (6.54) | 22 (6.92) | 24 (10.67) |
| | Outcome Only | 23 (4.85) | 16 (5.03) | 14 (6.22) |
| Total | | 114 (24.05) | 75 (23.58) | 63 (28.00) |
| Reward | Allocentric Only | 99 (20.89) | 52 (16.35) | 48 (21.33) |
| | Allocentric and Outcome | 44 (9.28) | 24 (7.55) | 23 (10.22) |
| | Outcome Only | 28 (5.91) | 18 (5.67) | 12 (5.33) |
| Total | | 171 (36.08) | 94 (29.56) | 83 (36.89) |
| Total | Selective | 319 (67.29) | 195 (61.32) | 160 (71.11) |

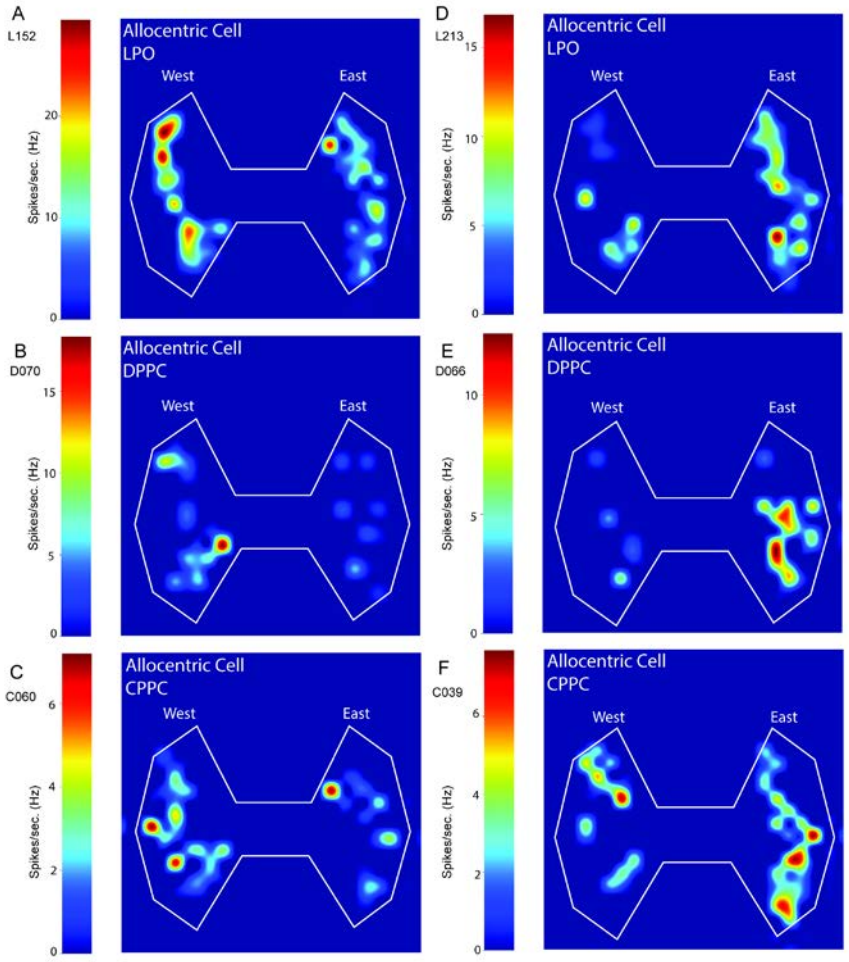


Figure 5. Example cells with allocentric location correlates in LPO, DPPC and CPPC. Firing fields are shown. Cells in left panel (A-C) fired more on west trials during the pre-selection epoch. Cells in right panel (D-F) fired more on east trials during the pre-selection epoch. The cells in A and D were recorded from LPO; the cells in B and E were recorded from DPPC; the cells in C and F were recorded from CPPC.

For egocentric location correlates in the LPO, 16 (3.38%) cells in the post-stimulus epoch, 65 (13.71 %) cells in the pre-selection epoch, and 81 (17.09 %) cells in the post-selection epoch showed a significant difference in firing rate for different egocentric locations. Twenty-nine (6.12%) cells in the post-stimulus epoch, 46 (9.70 %) cells in the pre-selection epoch, and 42 (8.86 %) cells in the post-selection epoch responded to both egocentric location and outcome. Twenty-two (4.64 %) cells in the post-stimulus epoch, 14 (2.95 %) cells in the pre-selection epoch, and 9 (1.90 %) cells in

the post-selection epoch signaled differentially to correct and incorrect outcomes. Figure 6A and 6D showed two LPO cells that had egocentric correlates during pre-selection epoch when animals were about to make a selection. The cell in Figure 6A only fired more on left trials and the cell in Figure 6B only fired more on right trials.

Similar egocentric location correlates were also observed in the PPC subregions. In the DPPC, 16 (5.03 %) cells in the post-stimulus epoch, 53 (16.67 %) cells in the pre-selection epoch, and 59 (18.55 %) cells in the post-selection epoch signaled differentially for egocentric locations. Twenty-nine (9.12 %) cells in the post-stimulus epoch, 25 (7.86 %) cells in the pre-selection epoch, and 38 (11.95 %) cells in the post-selection epoch responded to both egocentric location and outcome. Twelve (3.77 %) cells in the post-stimulus epoch, six (1.89 %) cells in the pre-selection epoch, and 8 (2.52 %) cells in the post-selection epoch signaled differentially to correct and incorrect outcomes. Two DPPC cells shown in Figure 6B and 6E displayed egocentric correlates during pre-selection epoch. The cell in Figure 6B had higher firing rate on left trials and the cell in Figure 6E fired more on right trials.

In the CPPC, 15 (6.67 %) cells in the post-stimulus epoch, 38 (16.89 %) cells in the pre-selection epoch, and 33 (14.67 %) cells in the post-selection epoch showed a significant difference in firing rate for different egocentric locations. Twenty-two (9.78 %) cells in the post-stimulus epoch, 16 (7.11 %) cells in the pre-selection epoch, and 30 (13.33 %) cells in the post-selection epoch responded to both egocentric location and outcome. Seven (3.11 %) cells in the post-stimulus epoch, 6 (2.67 %) cells in the pre-selection epoch, and 5 (2.22 %) cells in the post-selection epoch signaled differentially to correct and incorrect outcomes. Figure 6C and 6F showed two CPPC cells with

egocentric correlates during pre-selection epoch. The cell in Figure 6C only fired on central trials and the cell in Figure 6F only fired on right trials.

In summary, a total of 242 (51.05 %) LPO cells, 175 (55.03 %) DPPC cells, and 128 (56.88 %) CPPC cells displayed selectivity in this analysis.

Table 3. Number and percentage of selective cells for egocentric location correlates.

| **Epoch (criterion cells)** | **Correlate** | **LPO 474 (%)** | **DPPC 318 (%)** | **CPPC 225 (%)** |
|---|---|---|---|---|
| PostStimulus | Egocentric Only | 16 (3.38) | 16 (5.03) | 15 (6.67) |
| | Egocentric and Outcome | 29 (6.12) | 29 (9.12) | 22 (9.78) |
| | Outcome Only | 22 (4.64) | 12 (3.77) | 7 (3.11) |
| Total | | 67 (14.14) | 57 (17.92) | 44 (19.56) |
| PreSelection | Egocentric Only | 65 (13.71) | 53 (16.67) | 38 (16.89) |
| | Egocentric and Outcome | 46 (9.70) | 25 (7.86) | 16 (7.11) |
| | Outcome Only | 14 (2.95) | 6 (1.89) | 6 (2.67) |
| Total | | 125 (26.37) | 84 (26.42) | 60 (26.67) |
| PostSelection | Egocentric Only | 81 (17.09) | 59 (18.55) | 33 (14.67) |
| | Egocentric and Outcome | 42 (8.86) | 38 (11.95) | 30 (13.33) |
| | Outcome Only | 9 (1.90) | 8 (2.52) | 5 (2.22) |
| Total | | 132 (27.85) | 105 (33.02) | 68 (30.22) |
| Total | Selective | 242 (51.05) | 175 (55.03) | 128 (56.88) |

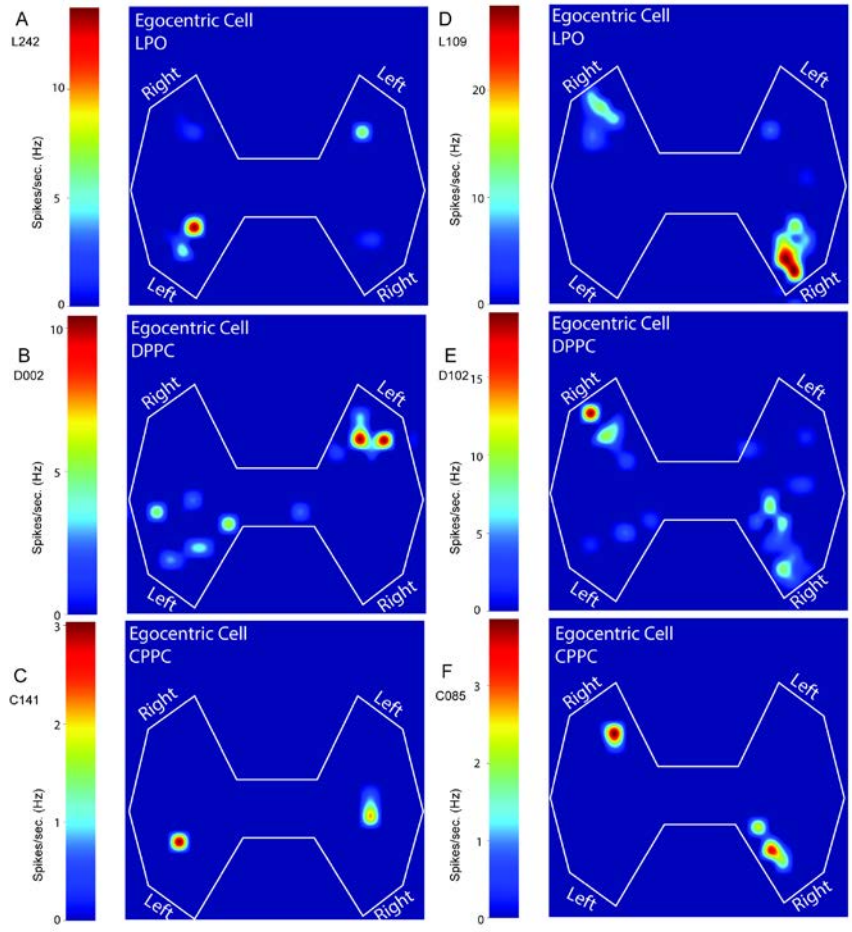


Figure 6. Example cells with egocentric location correlates in LPO, DPPC and CPPC. Firing fields are shown. Two LPO cells (A and D) fired more on only left trials or right trials regardless the side of the maze. Two DPPC cells (B and E) also fired more on only left trials or right trials. A CPPC cells shown in C fired more on the central trials. Another CPPC cells shown in F had higher firing rate only on the right trials.

### *Optical suppression altered neuronal correlates in the LPO, DPPC and CPPC*

We first asked the question of whether firing rates in LPO, DPPC, and CPPC were significantly different with between suppression and no-suppression trials. On suppression trials, the LED was on from arrival at the ready position to arrival at the reward position. Each cell was tested to determine whether firing rates were significantly different between suppression and no suppression trials in this window. A total of 10.97%, 10.06%, and 12.89% cells in LPO, DPPC and CPPC, respectively, showed

significant different firing rates between suppression and no suppression trials. In the LPO, of total cells displaying significant changes in firing rates, 54% increased firing and 46% decreased firing. In the DPPC, of total cells displaying significant changes in firing rates, 56% increased firing and 44% decreased firing. Finally, in the CPPC, of total cells showing significant changes in firing rates, 38% increased firing and 62% decreased firing. Because firing rates of principle cells are overall low and some cells fire preferentially only in certain time windows and only in some trial types, the effects of optical suppression on firing rates may not be the best indicator of changes in the network.

To understand the effect of optical suppression, we applied exact the same analysis that we used for stimulus and selection epochs. Instead of using trials without optical suppression, we only used trials with optical suppression for this set of analysis. We expected to see that the optical suppression should be able to shut down a cell's function, which means the behavioral selectivity of selective cells would be influenced by optical suppression. As expected, majority of selective cells in the LPO, DPPC and CPPC were affected by the optical suppression. Although most of non-selective cell stayed non-selective after optical suppression, however, we also observed a relative small proportion of non-selective cells became selective to animal's behavior.

For neuronal correlates of stimulus onset in the LPO, we found that, out of 130 selective cells, 71 cells (54.62%) lost original selectivity. In the rest of 59 cells with behavioral selectivity, 33 cells still displayed same selectivity after optical suppression and 26 cells changed to a different selectivity. For those non-selective cells in no suppression conditions (n= 344), 58 cells (16.86%) displayed behavioral selectivity after optical suppression. Most of non-selective cells (n=286) stayed non-selective after

optical suppression. We also observed similar results in the DPPC and CPPC. In the DPPC, out of 68 selective cells, 57 cells (83.82%) lost original selectivity. In the rest of 11 cells with behavioral selectivity, 8 cells still displayed same selectivity after optical suppression and only 3 cells changed to a different selectivity. For those non-selective cells in no suppression conditions (n= 250), 34 cells (13.60 %) displayed behavioral selectivity after optical suppression. Most of non-selective cells (n=216) stayed non-selective after optical suppression. In the CPPC, out of 65 selective cells, 43 cells (66.15%) lost original selectivity. In the rest of 22 cells with behavioral selectivity, 12 cells still displayed same selectivity after optical suppression and 10 cells changed to a different selectivity. For those non-selective cells in no suppression conditions (n= 160), 34 cells (15.62 %) displayed behavioral selectivity after optical suppression. Most of non-selective cells (n=135) stayed non-selective after optical suppression. In summary, 32.70% of total LPO cells (n=155 out of 474 cells), 29.56% of total DPPC cells (n=94 out of 318 cells) and 34.67% CPPC cells (n=78 out of 225 cells) were influenced by optical suppression. Figure 7 showed a summary for the distribution of all cells in the LPO, DPPC and CPPC for this analysis.

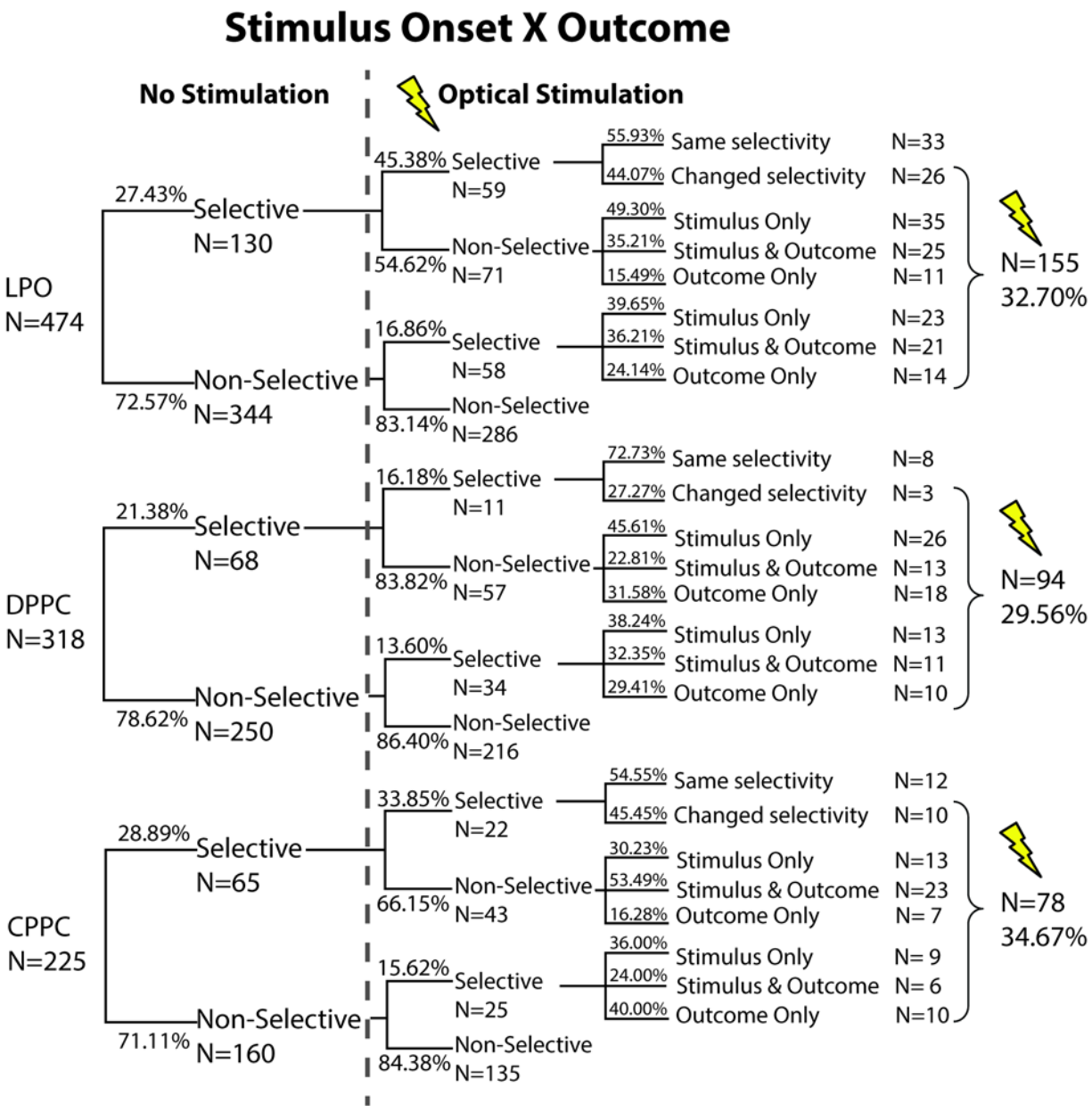


Figure 7. Numbers and percentage of cells affected by optical suppression during pre- and post-stimulus epochs. Upper panel showed the cell changes in the LPO; middle and lower panel displayed changes in the DPPC and CPPC.

For neuronal correlates of selection in the LPO, we found that, out of 211 selective cells, 103 cells (48.82%) lost original selectivity. In the rest of 108 cells with behavioral selectivity, 66 cells still displayed same selectivity after optical suppression and 42 cells changed to a different selectivity. For those non-selective cells in no

suppression conditions (n= 263), 59 cells (22.43%) displayed behavioral selectivity after optical suppression. Most of non-selective cells (n=204) stayed non-selective after optical suppression. We also observed similar results in the DPPC and CPPC. In the DPPC, out of 156 selective cells, 71 cells (45.51%) lost original selectivity. In the rest of 85 cells with behavioral selectivity, 55 cells still displayed same selectivity after optical suppression and 30 cells changed to a different selectivity. For those non-selective cells in no suppression conditions (n= 162), 37 cells (22.84 %) displayed behavioral selectivity after optical suppression. Most of non-selective cells (n=125) stayed non-selective after optical suppression. In the CPPC, out of 124 selective cells, 57 cells (45.97%) lost original selectivity. In the rest of 67 cells with behavioral selectivity, 46 cells still displayed same selectivity after optical suppression and 21 cells changed to a different selectivity. For those non-selective cells in no suppression conditions (n= 101), 28 cells (27.72 %) displayed behavioral selectivity after optical suppression. Most of non-selective cells (n=73) stayed non-selective after optical suppression. In summary, 43.04% of total LPO cells (n=204 out of 474 cells), 43.40% of total DPPC cells (n=138 out of 318 cells) and 47.11% CPPC cells (n=106 out of 225 cells) were influenced by optical suppression. Figure 8 showed a summary for the distribution of all cells in the LPO, DPPC and CPPC for this analysis.

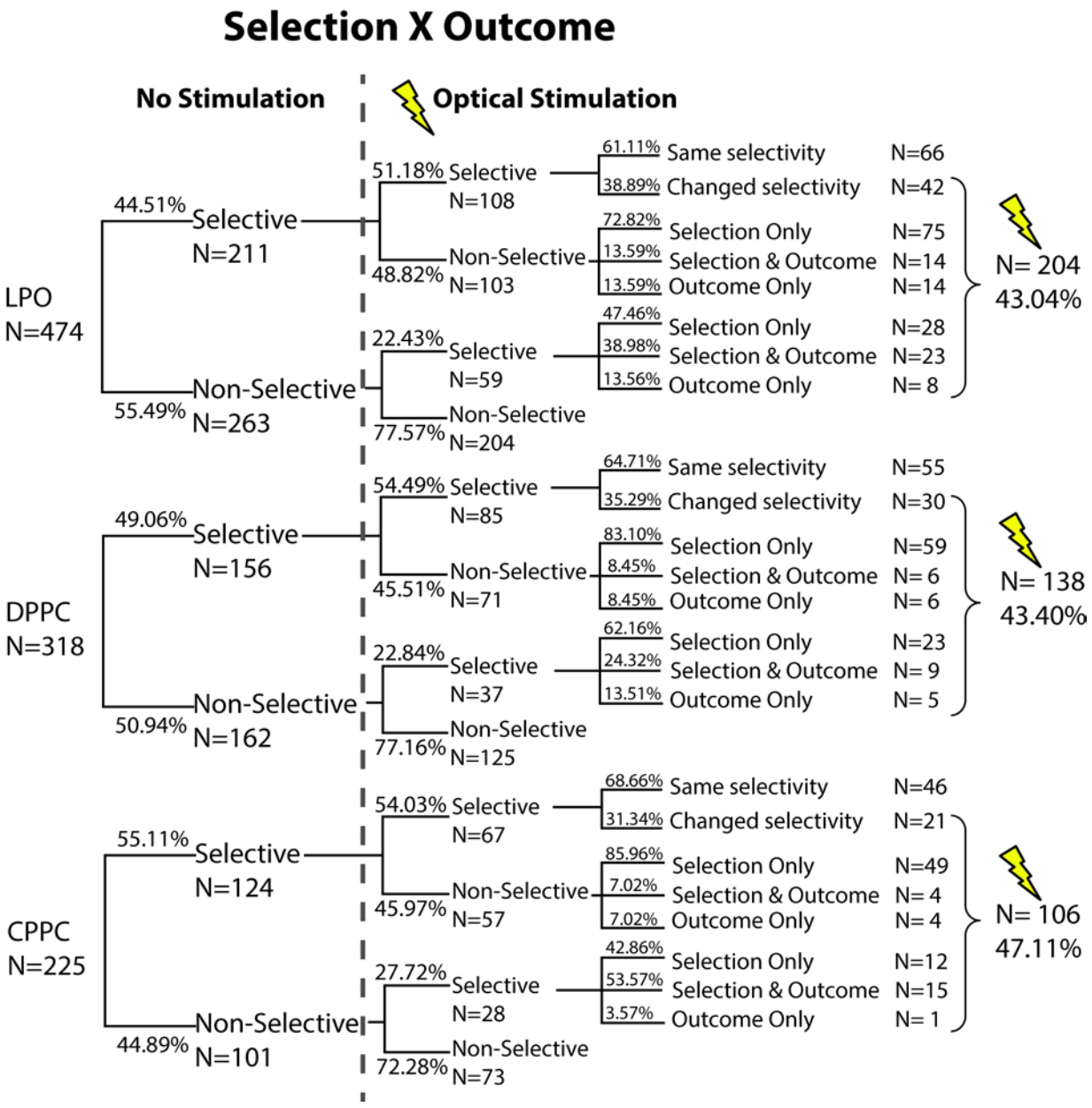


Figure 8. Numbers and percentage of cells affected by optical suppression during pre- and post-selection epochs. Upper panel showed the cell changes in the LPO; middle and lower panel displayed changes in the DPPC and CPPC.

## Discussion

In this study, we used our novel VSA task to address the hypothesis that neuronal activity in the PPC depends on the sensory input from the LPO. We recorded neuronal activity in the LPO, DPPC and CPPC simultaneously when animals performed the VSA

task. In some trials we used optical suppression to inactivate LPO activity. We first used only trials without optical suppression for analyzing to replicate our previous study. As we predicted, the results showed that the LPO and both subregions of the PPC responded to different behavioral phases of the VSA task, such as stimulus onset, selection and various task-relevant spatial locations. First, all three brain regions signaled stimulus onset. In addition, compared to the DPPC, both LPO and CPPC had a relatively larger proportion of cells showing stimulus relevant selectivity. This result is consistent with our previous findings suggesting that the LPO and CPPC are more involved in bottom-up attention. Second, cells in the LPO, DPPC and CPPC responded to selection behavior and reward. No significant differences among the three brain areas were observed in selection correlates. Third, cells displaying differential firing patterns to task-relevant locations were found in all three brain areas. Similar to the prior study, we used a bowtie shaped maze allowing us to analyze both allocentric location correlates and egocentric locations. All three brain areas exhibited cells selectivity to allocentric and egocentric frames of reference.

Results from analyzing control trials without optical suppression successfully replicated our previous experiments. There was, however, a significantly larger proportion of cells selective for stimulus onset in CPPC, compared to the DPPC, suggesting that the rat PPC might be similar to primate PPC having functional dissociation in different subregions. Evidence has shown that, in primates, the dorsal portion of PPC is involved in top-down attention, which is directed to specific information in the environment according to a subject's goal. The ventral PPC is involved in bottom-up attention, which is engaged when external stimuli grab attention

automatically (Corbetta, Kincade, Ollinger, McAvoy, & Shulman, 2000; Shomstein, 2012). Our data provided evidence to show that the rat CPPC, similar to ventral PPC in primates, is involved in bottom-up attention more than the DPPC during visuospatial attention process.

The analysis of allocentric location and egocentric location correlates in this dataset differed from the analysis we used for the previous one. We only used correct trials in the previous one because we did not have location coordinates for incorrect trials. Thus, we could not analyze the relationship between task-relevant locations and outcome (correct vs. incorrect). We addressed this issue in the current dataset and added new analyses for assessing neuronal correlates of task-relevant location. Instead of having allocentric or egocentric location correlates, we found that cells in the LPO, DPPC and CPPC not only responded to task-relevant locations, some cells also exhibited differential firing patterns based on different outcomes. Various location correlates were found across different phases of trials including post-stimulus, pre-selection and post-selection. We also observed amount of cells in the LPO and parietal areas differentiating two locations of reward ports during the reward-approach epochs in allocentric location analysis. These results were consistent to previous findings showing task-relevant location correlates in LPO and parietal areas and further provided evidence suggesting that task-relevant spatial correlates in these brain areas could be altered base on attentional demands.

By adding trials with optical suppression into recording session, we further investigate influences in the PPC areas of inactivating the LPO. We analyzed neuronal correlates by using trials with the optical suppression and compared results that we had from control trials without optical suppression. First, for the stimulus onset, we observed

that more than half of selective cells in the LPO (54.62%), DPPC (83.82%) and CPPC (66.15%) lost their original selectivity. Majority (more than 80%) of non-selective cells in the control condition stayed non-selective during optical suppression. We also observed a small proportion of cells changed their original selectivity across three brain regions. In summary, there were 32.70% LPO cells, 29.56% DPPC cells, and 34.67% CPPC cells were influence by optical suppression inactivating in the LPO. Second, we also found similar results for neuronal activity changes when animals made selection during the task. Almost half of selective cells in the LPO (48.82%), DPPC (45.51%) and CPPC (45.97%) lost their original selectivity. Also, more than 70% non-selective cells in the control condition stayed non-selective during optical suppression. A small proportion of cells changed their original selectivity across three brain regions. In summary, there were 43.04% LPO cells, 43.40% DPPC cells and 47.11% CPPC cells had some form of influences by optical inactivation in the LPO.

Our results supported our hypothesis that neuronal activity in the both DPPC and CPPC depends on the LPO inputs. Once the LPO was inactivated by optical suppression, the majority of cells in parietal areas either lost or changed their patterns of selectivity. Our results were consistent with the view that, like the primate pulvinar, the rat LPO provides sensory inputs for the parietal areas and modulates parietal activity during situations with high visuospatial attentional demand. Although anatomical connections between LPO/pulvinar and parietal areas are well-documented (Chandler, King, Corwin, & Reep, 1992; Kamishina et al., 2009; Takahashi, 1985), our findings provide both anatomical and electrophysiological evidence for interactions between the LPO and parietal areas in visuospatial attention.

Although there was a significant inhibiting effect of LPO inactivation on the cells with behavioral selectivity in the LPO, DPPC and CPPC, we did not observe decreasing neuronal activity on most of non-selective cells across three brain areas during optical suppression condition. One possibility is that firing rate of these non-selective cells was fairly low since they supposedly did not fire a lot, so that we could not see a significant inhibition due to the low firing rate. To further confirm this possibility, we calculated the mean firing rate of these non-selective cells within the analyzed behavioral epochs (pre- and post-stimulus; pre-and post-selection). We indeed observed relatively low firing rate for those non-selective cells. In the LPO, mean firing rate of non-selective cells were less than 4Hz during control conditions for all analyzed epochs. We further observed relatively low firing rates of non-selective cells in both DPPC and CPPC. Mean firing rates of these cortical cells were less than 1.5Hz. These results may explain why we did not see suppression in these non-selective cells in the LPO, DPPC and CPPC.

Importantly, we also observed that some non-selective cells became selective in LPO, DPPC, and CPPC during suppression of LPO activity. These results suggest that the LPO is modulating the focus of attention as evident in posterior parietal correlates. In other words, if there the LPO is modulating attention toward one feature of the visual environment over another, LPO suppression might allow visual correlates to emerge, This is consistent with the thalamic gating model theory in primates (Ketz, Jensen, & O'Reilly, 2015; Saalmann & Kastner, 2009). The thalamic gating model proposes that there are first order and higher order nuclei within the visual thalamus for modulating functions of cortical areas. The visual thalamus consists of three nuclei, including lateral geniculate nuclus (LGN), the pulvinar, and the thalamic reticular nucleus (TRN). The

LGN receives direct retinal input and has been considered as the first order nucleus for processing visual information. The pulvinar and TRN receive feedback projections from cortical areas including visual-, parietal, and frontal cortices, and have been thought to function as higher order nuclei in the thalamus. The higher order nuclei not only receive cortical projections, but they also send feedforward projections to cortical areas. These interconnections between higher order thalamic nuclei and cortical areas might be the key to how thalamic modulation is involved translating information for further processing in the cortical areas (Ketz, Jensen, & O'Reilly, 2015; Saalmann & Kastner, 2009).

Although the changes in selectivity are provocative, these interpretations should be made with caution for two reasons. First, interpretations of changes in selectivity are hampered by the nature of the statistical analysis in setting a significance level. The issue is that cells that barely show significance are treated the same as cells that are significant to a very low probability. So for example, in calculated percentages, the 10% of total cells that are barely selective for a particular variable are treated exactly as the 10% of cells that are highly selective and highly predictive of the variable.

It is also possible that the optogenetic manipulation simply adds noise to the system rather than shutting down input to the PPC. If that is the case, then cells that are borderline selective could easily become nonselective and cells that are borderline non-selective could easily become selective. To address this possibility, we examined p-values of all selective cells with statistical significance. The cut-off significance level was $p < 0.05$. As reported in the results, for each brain regions, we did two analyses for stimulus and selection epochs, respectively. For each analysis, we compared cell selectivity between suppression and no-suppression trials. The average p-values from any

type of selective cell are not close to borderline. For the stimulus onset epoch, the average p-values were less than 0.022 in both conditions across all three areas. For the selection epoch, the average p-values were less than 0.020 in both conditions across all three areas.

Specifically, all selective cells that lost selectivity during suppression have low p-values in the no-suppression condition. For these cells in the LPO, average p-values were 0.023 (stimulus) and 0.019 (selection) in no-suppression trials, and 0.462 (stimulus) and 0.422 (selection) in suppression trials. For these cells in the DPPC, average p-values were 0.023 (stimulus) and 0.021 (selection) in no-suppression trials, and 0.471 (stimulus) and 0.389 (selection) in suppression trials. For these cells in the CPPC, average p-values were 0.018 (stimulus) and 0.019 (selection) in no-suppression trials and 0.477 (stimulus) and 0.380 (selection) in suppression trials.

Similar to this, all cells in which selectivity emerged during suppression trials have low p-values in the suppression condition, in general. For these cells in the LPO, average p-values were 0.487 (stimulus) and 0.419 (selection) in no-suppression trials, and 0.022 (stimulus) and 0.024 (selection) in suppression trials. For these cells in the DPPC, average p-values were 0.488 (stimulus) and 0.406 (selection) in no-suppression trials, and 0.022 (stimulus) and 0.020 (selection) in suppression trials. For these cells in the CPPC, average p-values were 0.499 (stimulus) and 0.364 (selection) in no-suppression trials and 0.024 (stimulus) and 0.022 (selection) in suppression trials.

The shifts in average p-values reported above argue against the possibility that adding noise to the system shifted cells that were borderline significant one way or the other. Nevertheless, rather than relying on selectivity of individual cells, a more

powerful approach that avoids these issues would be to conduct population analyses that do not rely on statistical significance testing of individual cells. The value of these approaches is further discussed in Chapter 6.

To our knowledge, there are only a few studies supporting the gating control of thalamus model (Saalmann, Pinsk, Wang, Li, Kastner, 2012; Purushothaman, Marion, Li, & Casagrande, 2012). Our data provide further evidence to show thalamocortical interaction is important in translating visual and spatial information to motor action. Different from the first order nucleus, the modulatory role of the LPO is to filter sensory information by using feedback projection from cortical areas and then, transmitting information relevant to attentional control in the PPC.

This experiment was one of a series experiments to examine behavioral function of the PPC in visuospatial attention. Taken together, results from this experiment were consistent with our previous findings about neuronal activity of the LPO, DPPC and CPPC when animals performed the VSA task. Rather than successfully replicated previous experiment, by adding optical suppression to inactivate the LPO, we were able to observe how the LPO inputs influence neuronal activity in the DPPC and CPPC. Results in this experiment supported our hypothesis that attentional signals in the PPC depend on sensory inputs from LPO. When we used optogenetic methods to suppress LPO inputs to the PPC during performance of the VSA task, not only LPO cells lost original behavioral correlates, as a subsequence, cells with behavioral selectivity in the DPPC and CPPC also lost their behavioral functions due to inactivation of the LPO.

Recent studies have shown that pulvinar in primates has a role in visuospatial attention and could also regulate neuronal activity in cortical areas (Buchsbaum et al.,

2006; Purushothaman et al., 2012; Saalmann et al., 2012). Our results provided a solid evidence showing that the rat LPO might be as important as primate pulvinar in visuospatial attention network. By providing sensory input to parietal areas, the LPO plays a role of attentional source and further regulates parietal activity base on attentional demand. These findings addressed our hypothesis about the dependency between LPO inputs and various parietal areas. This experiment could also confirm that the rat LPO and primate pulvinar are not only anatomical homologue but also share similar behavioral function suggesting that the rat LPO-PPC circuitry may become a good model for investigating the primate pulvinar-PPC circuitry.

## References


Buchsbaum, M. S., Buchsbaum, B. R., Chokron, S., Tang, C., Wei, T. C., & Byne, W. (2006). Thalamocortical circuits: fMRI assessment of the pulvinar and medial dorsal nucleus in normal volunteers. *Neuroscience Letters, 404*(3), 282-287.

Chandler, H. C., King, V., Corwin, J. V., & Reep, R. L. (1992). Thalamocortical connections of rat posterior parietal cortex. *Neuroscience Letters, 143*(1-2), 237-242.

Corbetta, M., Kincade, J. M., Ollinger, J. M., McAvoy, M. P., & Shulman, G. L. (2000). Voluntary orienting is dissociated from target detection in human posterior parietal cortex. *Nature Neuroscience, 3*(3), 292-297.

Furtak, S. C., Cho, C. E., Kerr, K. M., Barredo, J. L., Alleyne, J. E., Patterson, Y. R., & Burwell, R. D. (2009). The Floor Projection Maze: A novel behavioral apparatus for presenting visual stimuli to rats. *Journal of Neuroscience Methods, 181*(1), 82-88.

Jacobson, T. K., Ho, J. W., Kent, B. W., Yang, F. C., & Burwell, R. D. (2014). Automated visual cognitive tasks for recording neural activity using a Floor Projection Maze. *Journal of Visual Experimentation*.

Kamishina, H., Conte, W. L., Patel, S. S., Tai, R. J., Corwin, J. V., & Reep, R. L. (2009). Cortical connections of the rat lateral posterior thalamic nucleus. *Brain Research, 1264*(0), 39-56.

Petersen, S. E., Robinson, D. L., & Morris, J. D. (1987). Contributions of the pulvinar to visual spatial attention. *Neuropsychologia, 25*(1, Part 1), 97-105.

Purushothaman, G., Marion, R., Li, K., & Casagrande, V. A. (2012). Gating and control of primary visual cortex by pulvinar. *Nat Neurosci, 15*(6), 905-912.

Saalmann, Y. B., & Kastner, S. (2011). Cognitive and perceptual functions of the visual thalamus. *Neuron, 71*(2), 209-223.

Saalmann, Y. B., Pinsk, M. A., Wang, L., Li, X., & Kastner, S. (2012). The pulvinar regulates information transmission between cortical areas based on attention demands. *Science, 337*(6095), 753-756.

Shomstein, S. (2012). Cognitive Functions of the Posterior Parietal Cortex: Top-down and bottom-up attentional control. *Frontiers in Integrative Neuroscience, 6*.

Takahashi, T. (1985). The organization of the lateral thalamus of the hooded rat. *The Journal of Comparative Neurology, 231*(3), 281-309.

Wilke, M., Turchi, J., Smith, K., Mishkin, M., & Leopold, D. A. (2010). Pulvinar inactivation disrupts selection of movement plans. *The Journal of Neuroscience, 30*(25), 8650-8659.

Zhou, H., Schafer, Robert J., & Desimone, R. (2016). Pulvinar-cortex interactions in vision and attention. *Neuron, 89*(1), 209-220.

# CHAPTER 6

# CONCLUSIONS

## Abstract

In this series of studies, I used a rodent model of visuospatial attention to examine the anatomy, physiology, and behavioral functions of the posterior parietal cortex (PPC) and its thalamic inputs from the lateral posterior nucleus (LPO). The behavioral task was a novel visuospatial attention (VSA) task that I developed for the Floor Projection Maze from the five choice serial reaction time (5CSRT) task. The VSA task was adapted from the 5CSRT task to restrict information processing demands to the visual and spatial domains. This comprehensive inspection of these brain structures yielded new information about the function of these structures and the circuitry that underlies visuospatial attention. These studies revealed new information about these circuits and established a more complete rodent model of primate visuospatial attention and visually guided actions. In this chapter, I will discuss general methods, provide summaries for each study and as well as a section on future work.

## General Methods

For all three electrophysiology studies in this thesis, we applied the same criteria to isolate single neurons and we used similar statistical approach to analyze neuronal data. I will discuss general methods in this section.

To identify putative individual cells, we used several criteria for isolating cell signals from raw data. When sorting cells offline, cells were isolated based on waveform characteristics, amplitude relative to noise and autocorrelations. These are typical criteria that use to identify isolated cells in most of electrophysiological studies. In our first electrophysiological study, to ensure good quality of analyzed units, we also gave each isolated unit a confidence rating from three raters. Only units rated "Good" quality by at least two of three independent raters were retained for the following analyses.

To analyze neuronal correlates of individual cells, we used analysis of variance (ANOVA) in most of our analyses. The ANOVA based on generalized linear models (GLMs) has been used as a common approach to assess neuronal data from in vivo recording studies (Czanner et al., 2008). The aim of analyzing neural data is to capture the network properties of the neuron, such as changes in rate or timing of action potentials. Firing rates carry most of the information encoded by individual neurons correlated to stimulus presentation or behavioral responses and such firing rate information is available in short periods (Rolls & Treves, 2011). To extract enough information from individual neurons, the ANOVA analysis is usually done on specific behavioral, stimulus, or response window (e.g. 500 ms in our analyses). For each cell, spikes were binned to give a firing rate for a response window for each trial. Then for each cell, we used ANOVA or repeated measures ANOVA to compare firing rates

between various variables. For example, to analyze peri-event effecst in our studies (e.g. peri-stimulus and peri-selection), firing rate was the dependent variable and epoch was the within trial repeated measure that served as the independent variable. Between-trial independent variable were, for example, outcome (correct vs. incorrect), response (left vs. right) or side (east vs. west). In this way we identified cells that were selective for particular properties or combinations of properties, including stimulus onset, time of selection, outcome, response, or side.

Although ANOVA approaches are widely used to determine selectivity of individual cells, there are drawbacks. For example, spike trains recorded *in vivo* tend to be irregular across time and thus are unlikely to meet the assumptions for ANOVA. An approach that addresses this issue is calculate a selectivity index for each cell to avoid the problem of data structure not meeting assumptions of ANOVA. In addition, any method of analyzing selectivity of individual cells does not take into account mutual information across cells, i.e. from the neural population of a brain area (Cunningham & Yu, 2014; Kass, Ventura, & Brown, 2005; Rolls & Treves, 2011). I next describe alternative approaches for determining selectivity of individual neurons and coding of neuronal ensembles.

When a brain area encodes complex behavior, neuronal activity likely involves coordination of responses across neurons. Although it is useful and necessary to understand the behavior of individual cells, population analyses are necessary to understand how a neuronal ensemble can encode particular representations (Cunningham & Yu, 2014). In our first electrophysiological study, we employed a representational similarity analysis (Kriegeskorte, Mur, & Bandettini, 2008; McKenzie et al., 2014) to examine whether PPC ensembles code for task-relevant behavior. We have described

detailed methods in Chapter 2. In brief, we first normalized firing rates of each cell and used these normalized firing rates to construct a population vector for various conditions. Pearson's correlation coefficients were calculated for every pair of population vectors yielding a similarity matrix. We then calculated the average correlations for same and different conditions to look at the difference between conditions. To test for statistical significance, we used a bootstrapping test in which we randomly shuffled the testing conditions 10,000 times and performed the above correlation analyses, obtaining correlation differences in the same way for each resampled data set. We then compared the observed difference from the original data set to the differences calculated from the resampled data. Statistical significance was defined as an observed difference greater than the 95% of the distribution of correlation differences obtained from the bootstrapped datasets. The bootstrap is nonparametric without the assumption of a specific distribution for the data set. The advantage of using these population analyses is that it could be applied in complicated conditions and measure mutual information to the ensemble (Kass et al., 2005).

Another approach that could avoid statistical problem of ANOVAs is to calculate a selectivity index (SI) for each individual cell to indicate dimensionality (Keene et al., 2016; Moody, Wise, di Pellegrino, & Zipser, 1998; Wirth et al., 2003). The SI uses the absolute value of the averaged responses to each condition and takes account of the responses across trials. It is defined as follows:

$$SI = (n - \sum_{i=1}^{n} (\lambda_i \,/\, \lambda\,)) \,/\, (n-1)$$

where n is the number of conditions under study (e.g., 2 in the outcomes which we looked at correct vs. incorrect). $\lambda_i$ is the firing rate of the neuron for ith possible event type and $\lambda$ is the average firing rate of the neuron in the condition. For each neuron, SI = 1 if a cell fired for only one condition. In contrast, SI = 0 if a cell fired equally under all conditions. The bootstrap methods are usually used to test for statistical significance of the SI values for individual cells. To do so, as I described above, the data set is shuffled randomly (e.g. 10,000 times) to compare each observed SI value against a distribution of shuffled SI scores. Cells are defined as significantly selective for particular dimension if $p < 0.05$ for the observed SI value relative to the shuffled distribution. In brief, the SI normalizes the scale of firing rates for every individual neuron and uses the bootstrap method to improve statistical power. This might be another better approach to look at the neuronal correlates of cells in our data set.

In summary, we have applied ANOVAs in all our electrophysiological studies to look at the neuronal correlates of the single unit data. Although the ANOVA might not be a flawless way, it is a common method to analyze neuronal data. To compensate drawbacks of ANOVA, adding a population analysis or to look at the selectivity index would be helpful to extract maximum information for individual cells.

**The role of posterior parietal cortex in visuospatial attention and visually-guided action selection**

Based on our anatomical findings and a few functional studies in primates, we hypothesized that the PPC plays a role in visuospatial attention and in visually guided action selection. Chapter 2 of this thesis reports an electrophysiological study of the rat PPC. We chose the dorsal limb of the rat PPC to be our first recording target site because

this area has been studied in previous rodent studies. To address the hypothesis, we developed a novel visuospatial attention (VSA) task by using the Floor Projection Maze. In study 1, the VSA task was conducted in a fan-shaped maze such the presentation of stimuli were always in the fan-shaped part of the maze and reward was presented in the stem. In this task, rats attended to four locations on the floor of a maze. A randomly chosen location was briefly illuminated. Approach to the correct target location was followed by food reward.

Attention is a cognitive process that comprises complex components. According to the Posner's attention framework, three networks were support attention processing, including alerting-, orienting- and executive networks (Petersen & Posner, 2012; Posner & Dehaene, 1994). Alerting is defined as maintaining alert state; orienting is the selection from sensory input; executive control is to resolve conflicts from multiple responses. A study reported that efficiencies of these three networks were uncorrelated but would interact with each other (Fan, McCandliss, Sommer, Raz, & Posner, 2002). Previous studies also suggested that various brain areas, such as PPC and its connected areas are involved in various attentional networks (Corbetta, Kincade, & Shulman, 2002; Corbetta & Shulman, 2002; Fan et al., 2002; Petersen & Posner, 2012). To investigate the role of the PPC in different components of attention process, we divided animals' behavior regarding their performance of the VSA task into separate epochs, such as stimulus onset, selection and reward-approach, to analyze neuronal correlates of the PPC for various components in visuaospatial attention processing.

Our results showed that neuronal activity in the dorsal PPC (DPPC) exhibited a variety of behavioral correlates when rats performed the VSA task that were consistent

with our hypothesis. Regarding visuospatial attention, we observed correlates associated with monitoring for stimulus onset and detection of a target stimulus. Some of these stimulus onset correlates were also modulated by locations of the target. Regarding visually-guided action selection, a large proportion of cells (about 20%) showed location correlates prior to selection of a target location. We interpret this as evidence that the PPC is involved in visually-guided action selection.

There are drawbacks to constraining analyses to particular epochs. For example, it is highly likely that the windows we analyzed based on manipulation of stimuli and the behavior of the animal do not precisely map onto cognitive processes. A good example has to do with the 500 msec window immediately following stimulus onset. As we showed in Chapter 4, Figure 4 depending on the area, cells behave differently after stimulus onset. Figure 4 shows the cumulative percentage of cells with firing rates that were significantly different from prestimulus baseline plotted against time. In dPPC firing rates of 60% of the cells were significantly different from baseline within 100 msec, whereas in cPPC and LPO only 10% of cells were different from baseline in that 100 msec window. This analysis clarifies populations of cells are participating in multiple processes that are overlapping in time. It would be interesting to conduct the same analyses from stimulus onset through selection time. As the capability to record in larger populations of individual cells in multiple brain areas, it will be necessary to keep pace by developing analyses that capture properties of individual cells as well as how cells interact within and across brain areas.

We also recorded the local field potentials. Interestingly, about a third of PPC cells were phase locked to theta. In addition, theta power increased significantly after an

incorrect choice suggesting that DPPC activity might be relevant to a prediction error signal depending on animal's selection. This is additional evidence for a role in visually guided action selection.

Previous studies showed that PPC neuronal activity changes differentially in response to behavioral outcomes in detection and navigation tasks (Harvey, Coen, & Tank, 2012). Our study extends those findings by showing that PPC neuronal activity correlates with response outcome in a task in which the animal must choose between multiple responses. We also provided new evidence showing that theta coherence in PPC is important during visuospatial attention processing.

**Functional neuroanatomy of the posterior parietal cortex and the lateral posterior nucleus**

Chapter 3 reports and anatomical study in which we examined in detail the topography of the connections among the PPC, postrhinal cortex (POR), and LPO. We examined the connections according to two definitions of the rat PPC. The first was from the most widely used rat stereotaxic brain atlases (Paxinos & Watson, 2005), and the second was from an atlast that includes the caudal extension of the rat PPC (Swanson, 1992). We found that, although all subdivisions of the LPO project to both the PPC and POR, the projections exhibited an interesting topography. Specifically, the more caudal aspects of the PPC and POR received heavy LPO inputs, whereas the rostral aspects received moderate input from the LPO. In addition, subnuclei within the LPO show different patterns of projections. The more medial LPO subnuclei project more heavily to the POR. In addition, our data suggest that the medial and caudal LPO subnuclei provide the heaviest projections to the PPC. Similar to other thalamo-cortical projections,

thalamic inputs from the LPO provide a feedforward input to layer IV of the POR and the PPC. The POR and PPC are reciprocally connected; the POR projects to all parts of the PPC, but the heaviest projection is to CPPC.

Available anatomical evidence, including ours, suggests that the monkey pulvinar, PHC and PPC are connectional homologs of the rat LPO, POR and PPC (Agster, Tomás Pereira, Saddoris, & Burwell, 2016; Burwell, Witter, & Amaral, 1995; Kamishina et al., 2009; Tomás Pereira, Agster, & Burwell, 2016). The PHC (area TF and TH) receive heavy thalamic inputs from the medial pulvinar, which also gets the cortical afferents from the PHC (Baleydier & Mauguiere, 1985). Compared to the monkey studies, we did observe heavy inputs from the medial LP to the POR and the return projections from the POR to the LP. Also, similar to our results from rats, evidence has shown that the pulvinar provides substantial thalamic input to the PPC (Broadmann's area 7) in the rhesus monkey (Baleydier & Mauguiere, 1977; Baleydier & Mauguiere, 1987) and the PHC, particular in area TF, heavily interconnects with area 7 and lateral intraparietal area (LIP) of the PPC (Cavada & Goldman-Rakic, 1989; Suzuki & Amaral, 1994).

To our knowledge, this is the only study to compare the topography of the LPO projections to the POR and the PPC. Our findings suggest that the circuitry underlying visuospatial attention in the rat includes all subnuclei of the LPO, all aspects of the POR, and both subdivisions of the PPC, but there is some topography. For example, the LPO projections arise mainly in the medial and caudal nuclei and the LPO preferentially targets caudal PPC and caudal POR. In addition, the PPC to POR projection arises mainly in the caudal PPC. These patterns of connections suggest medial LPO and caudal PPC/POR may preferentially support bottom-up attention. However, the rostral POR

preferentially targets caudal PPC, and the caudal POR preferentially targets rostral PPC. These crossed projections may serve to balance top-down and bottom-up attention.

**Functional differentiation of posterior parietal subdivisions**

In Chapter 4, I reported the results of simultaneously recordings in DPPC, caudal PPC (CPPC), and the major thalamic input, the LPO, in a modified version of the VSA task. To our knowledge, this is the first rat study to record in the rat caudal PPC and the first to record simultaneously from the PPC and LPO in freely behaving rats. For the VSA task, we used a bowtie-shaped maze allowing animals to alternately start trials from one side to the other to increase the total number of trials within one session. The larger number of trials allowed us to do more detailed analyses of neuronal correlates during the VSA task. In addition, because trials alternated from the east and west sides of the bowtie maze, we could also distinguish correlates of allocentric as well as egocentric spatial locations.

We hypothesized that the rat DPPC, CPPC, and LPO form a circuit for processing visuospatial information in the service of visuospatial attention and visually guided action selection. We found that cells in the LPO, DPPC and CPPC responded to aspects of the selection epoch and task-relevant correlates of the location of the target, such as egocentric and allocentric locations. Neuronal activity across all three brain regions also signaled stimulus onset. We also tested the hypothesis that the rat PPC shows functional differentiation between dorsal- and caudal portions such that DPPC is more important for top-down attention and the CPPC is more important for bottom up attention. We observed that the CPPC, compared to the DPPC, had a significantly larger proportion of cells responded to stimulus onset, consistent with a role in bottom up attention. Also,

using a sliding window analysis more than twice as many CPPC cells as DPPC or LPO cells responded to stimulus onset and six times as many CPPC cells as DPPC and LPO cells responded to stimulus onset within 100 msec. Our findings suggest that DPPC, CPPC, and LPO all participate in visually guided action selection, but that the CPPC is preferentially involved in bottom up attention.

**Circuitry underlying visuospatial attention and visually-guided behavior**

In Chapter 5, I used optogenetic methods to manipulate the LPO while recording simultaneously recording in the same locations and in the same task as the study reported in Chapter 4. The goal was to better understand how the LPO contributes to PPC functions by suppressing its activity on some trials. We hypothesized that the functions of the PPC depend, in part, on input from the LPO, specifically that the LPO might modulate the focus of attention. If this is the case, the suppressing activity in the LPO should alter attentional correlates in the PPC. To address this hypothesis, we virally transduced the LPO with halorhodopsin (NpHR) so that we could optically suppress neuronal activity in the LPO, and thus its input to the PPC, on selected trials during performance of the VSA task. We simultaneously recorded neuronal activity in the LPO, DPPC and CPPC, and each daily recording session included both control trials and LPO suppression trials.

Similar to our previous results, we reported that LPO and PPC cells signaled stimulus onset and selection behavior in the VSA task confirming the engagement of these brain areas in both top-down and bottom-up visuospatial attention as well as action selection. We also observed that cells in the LPO and PPC responded to both allocentric and egocentric task-relevant locations. The primary analysis was designed to detect

changes in the behavioral correlates of cells in each of these brain areas during optogenetic inhibition of the LPO. Our results showed that behavioral correlates of LPO and PPC neurons disappeared or changed because of inactivation in the LPO supporting our hypothesis that the posterior parietal functions depend on the LPO inputs when visuospatial attentional demands are high. LPO suppression altered correlates during stimulus processing and during action selection in all three regions. Interestingly, on suppression trials behavioral correlates emerged for some cells that did not show selectivity on control trials. This is consistent with the interpretation that the LPO might be modulating the focus of attention.

**Conclusions and future directions**

In this thesis, we executed a series of experiments including one anatomical examination and three electrophysiological studies combined with optogenetic manipulation to address the overarching hypothesis that the PPC and its major thalamic input comprise a circuit that supports visuospatial attention and visually guided action selection. Our work was based on the two-streams hypothesis of visual processing in primates (Goodale & Milner, 1992; Goodale & Westwood, 2004) indicating that there are two streams originating from primary visual cortex (Chapter 1 of this thesis; Figure 1). The ventral stream projects to ventral cortical areas, including inferior temporal cortex and ventral temporal cortex, functions for perception. The dorsal stream projects to parietal cortex for processing visually guided actions. The posterior parietal cortex also receives input from the pulvinar in primates and the LPO in the rat. In Chapter 2 I showed that the rat PPC is involved in action selection. In Chapter 3, I showed that the rat LPO-PPC-POR and monkey pulvinar-PPC-PHC circuits show a substantial amount of

connectional homology. In Chapter 4 I showed that the rat PPC shows functional differentiation such that the caudal part (CPPC) supports bottom up attention. I also provided evidence that all three regions (DPPC, CPPC, and LPO) contribute to both visuospatial attention and action selection. In Chapter 5, I further showed that LPO activity modulates processing in both the DPPC and the CPPC.

Recent primate studies have contributed to a thalamic gating model in which the thalamus plays a modulatory role in the gating of cortical activity by coordinating oscillatory activity in cortical regions (Ketz, Jensen, & O'Reilly, 2015). Highly relevant to the current thesis, Saalmann and Kastner (2009) proposed that the visual thalamus and pulvinar modulate the information transmitted to cortical regions in the service of current cognitive and behavioral demands. For example, in a monkey electrophysiology study provided evidence that the pulvinar synchronized neuronal activity in V4 and temporal-occipital areas according to attentional demands (Saalmann, Pinsk, Wang, Li, & Kastner, 2012). In future work, I plan to address questions about whether and how the LPO modulates information transmission in the rat PPC.

For the study reported in Chapter 5, in addition to single unit activity, I also simultaneously recorded local field potentials in the DPPC, CPPC, and LPO. This dataset will allow me to investigate the role of oscillatory activity and oscillatory coherence in this circuit during visuospatial attention and visually-guided actions. Gamma oscillations are thought to reflect local cortical processing and slower oscillations are thought to reflect long range interactions. The model proposed by Ketz et al. (2015) suggested that oscillations in the alpha frequency band depend on posterior parietal cortex and the pulvinar. They further proposed that gamma is modulated by lower frequency bands, for

example alpha in the pulvinar, by cross-frequency coupling. Because I have single unit and local field potential data and because the activity of the LPO was suppressed on some trials, my data will allow me to test most predictions of this model.

In summary, we report that DPPC, CPPC, and the LPO comprise a functional circuit that supports visuospatial attention and action selection. Our evidence suggests that the CPPC is more involved in bottom up attention than the other two regions. This circuit maps on to a homologous circuit in the primate brain comprising dorsal and ventral PPC and the pulvinar. Our evidence is consistent with a gating model of thalamocortical control of corticocortical interactions that relies on oscillatory mechanisms. Future work will utilize existing data to address open questions about oscillatory dynamics and visuospatial information processing in this circuit.

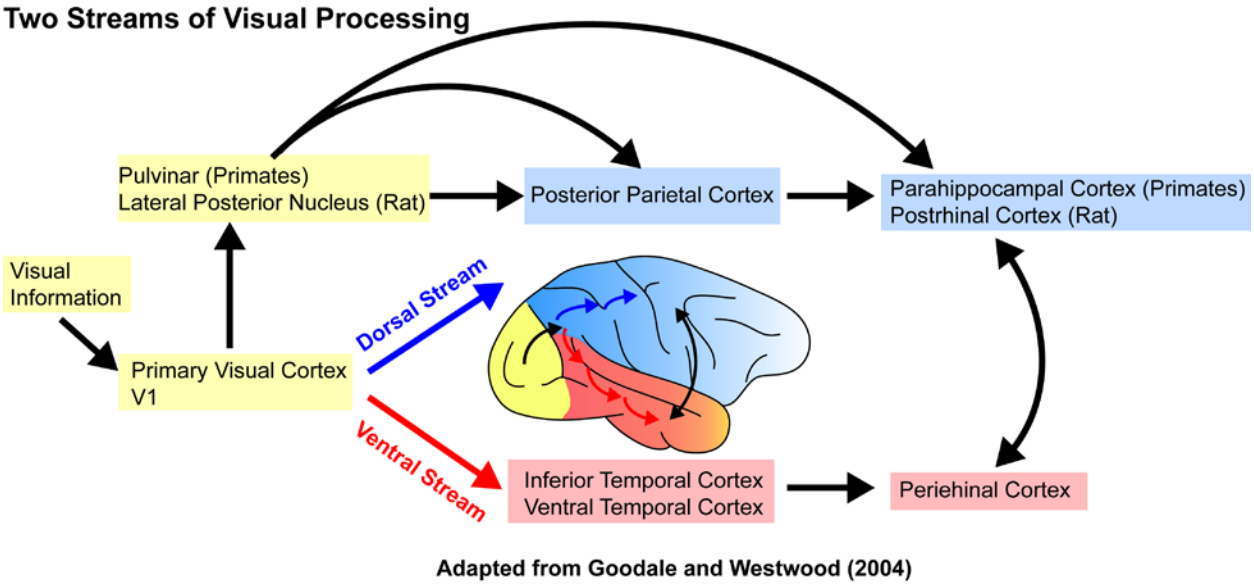


Figure 1. Schematic of visual processing streams. The dorsal and ventral streams (shown in blue and red arrows, respectively) originate from primary visual cortex to the posterior parietal cortex and inferior temporal cortex, respectively. The dorsal stream connects with the parahippocampal cortex in primates and postrhinal cortex in the rat. The ventral stream connects with the perirhinal cortex in both primates and rats. The posterior parietal cortex and parahippocampal/postrhinal cortex also receives thalamic input from the pulvinar nuclus in primates and lateral posterior nucleus in rats. This figure is adapted from Goodale and Westwood (2004).

## References


Agster, K. L., Tomás Pereira, I., Saddoris, M. P., & Burwell, R. D. (2016). Subcortical connections of the perirhinal, postrhinal, and entorhinal cortices of the rat. II. efferents. *Hippocampus*, n/a-n/a.

Baleydier, C., & Mauguiere, F. (1977). *Pulvinar-latero posterior afferents to cortical area 7 in monkeys demonstrated by horseradish peroxidase tracing technique*. Paper presented at the Experimental Brain Research.

Baleydier, C., & Mauguiere, F. (1985). Anatomical evidence for medial pulvinar connections with the posterior cingulate cortex, the retrosplenial area, and the posterior parahippocampal gyrus in monkeys. *The Journal of Comparative Neurology, 232*(2), 219-228.

Baleydier, C., & Mauguiere, F. (1987). Network organization of the connectivity between parietal area 7, posterior cingulate cortex and medial pulvinar nucleus: a double fluorescent tracer study in monkey. *Experimental Brain Research, 66*(2), 385-393.

Burwell, R. D., Witter, M. P., & Amaral, D. G. (1995). Perirhinal and postrhinal cortices of the rat: A review of the neuroanatomical literature and comparison with findings from the monkey brain. *Hippocampus, 5*(5), 390-408.

Cavada, C., & Goldman-Rakic, P. S. (1989). Posterior parietal cortex in rhesus monkey: I. Parcellation of areas based on distinctive limbic and sensory corticocortical connections. *The Journal of Comparative Neurology, 287*(4), 393-421.

Corbetta, M., Kincade, J. M., & Shulman, G. L. (2002). Neural systems for visual orienting and their relationships to spatial working memory *Journal of Cognitive Neuroscience* (Vol. 14, pp. 508-523): MIT Press.

Corbetta, M., & Shulman, G. L. (2002). Control of goal-directed and stimulus-driven attention in the brain. *Nature Reviews Neuroscience, 3*(3), 201-215.

Cunningham, J. P., & Yu, B. M. (2014). Dimensionality reduction for large-scale neural recordings. *Nat Neurosci, 17*(11), 1500-1509.

Czanner, G., Eden, U. T., Wirth, S., Yanike, M., Suzuki, W. A., & Brown, E. N. (2008). Analysis of between-trial and within-trial neural spiking dynamics. *Journal of Neurophysiology, 99*(5), 2672-2693.

Fan, J., McCandliss, B. D., Sommer, T., Raz, A., & Posner, M. I. (2002). Testing the Efficiency and Independence of Attentional Networks. *Journal of Cognitive Neuroscience, 14*(3), 340-347.

Goodale, M. A., & Milner, A. D. (1992). Separate visual pathways for perception and action. *Trends in Neurosciences, 15*(1), 20-25.

Goodale, M. A., & Westwood, D. A. (2004). An evolving view of duplex vision: separate but interacting cortical pathways for perception and action. *Current Opinion in Neurobiology, 14*(2), 203-211.

Harvey, C. D., Coen, P., & Tank, D. W. (2012). Choice-specific sequences in parietal cortex during a virtual-navigation decision task. *Nature, 484*(7392), 62-68. doi:10.1038/nature10918

Kamishina, H., Conte, W. L., Patel, S. S., Tai, R. J., Corwin, J. V., & Reep, R. L. (2009). Cortical connections of the rat lateral posterior thalamic nucleus. *Brain Research, 1264*(0), 39-56.

Kass, R. E., Ventura, V., & Brown, E. N. (2005). Statistical issues in the analysis of neuronal data. *Journal of Neurophysiology, 94*(1), 8-25.

Keene, C. S., Bladon, J., McKenzie, S., Liu, C. D., O'Keefe, J., & Eichenbaum, H. (2016). Complementary Functional Organization of Neuronal Activity Patterns in the Perirhinal, Lateral Entorhinal, and Medial Entorhinal Cortices. *The Journal of Neuroscience, 36*(13), 3660-3675.

Ketz, N. A., Jensen, O., & O'Reilly, R. C. (2015). Thalamic pathways underlying prefrontal cortex–medial temporal lobe oscillatory interactions. *Trends in Neurosciences, 38*(1), 3-12.

Kriegeskorte, N., Mur, M., & Bandettini, P. (2008). Representational Similarity Analysis – Connecting the Branches of Systems Neuroscience. *Frontiers in Systems Neuroscience, 2*, 4.

McKenzie, S., Frank, A. J., Kinsky, N. R., Porter, B., Riviere, P. D., & Eichenbaum, H. (2014). Hippocampal representation of related and opposing memories develop within distinct, hierarchically organized neural schemas. *Neuron, 83*(1), 202-215.

Moody, S. L., Wise, S. P., di Pellegrino, G., & Zipser, D. (1998). A model that accounts for activity in primate frontal cortex during a delayed matching-to-sample task. *The Journal of Neuroscience, 18*(1), 399-410.

Paxinos, G., & Watson, C. (2005). *The rat brain in stereotaxic coordinates*: Amsterdam;. Elsevier Academic Press,.

Petersen, S. E., & Posner, M. I. (2012). *The attention system of the human brain: 20 years after*. Paper presented at the Annual Review of Neuroscience

Posner, M. I., & Dehaene, S. (1994). Attentional networks. *Trends in Neurosciences, 17*(2), 75-79.

Rolls, E. T., & Treves, A. (2011). The neuronal encoding of information in the brain. *Progress in Neurobiology, 95*(3), 448-490.

Saalmann, Y. B., Pinsk, M. A., Wang, L., Li, X., & Kastner, S. (2012). The pulvinar regulates information transmission between cortical areas based on attention demands. *Science, 337*(6095), 753-756.

Suzuki, W. L., & Amaral, D. G. (1994). Perirhinal and parahippocampal cortices of the macaque monkey: Cortical afferents. *The Journal of Comparative Neurology, 350*(4), 497-533.

Swanson, L. W. (1992). Brain maps: Structure of the rat brain: Elsevier (Amsterdam and New York).

Tomás Pereira, I., Agster, K. L., & Burwell, R. D. (2016). Subcortical connections of the perirhinal, postrhinal, and entorhinal cortices of the rat. I. afferents. *Hippocampus*, n/a-n/a.

Wirth, S., Yanike, M., Frank, L. M., Smith, A. C., Brown, E. N., & Suzuki, W. A. (2003). Single neurons in the monkey hippocampus and learning of new associations. *Science, 300*(5625), 1578-1581.